Effect of calcium and iron(III) on membrane fouling under conditions typical of submerged membrane bioreactor treatment of wastewaters

Author:
Xin, Yongjia

Publication Date:
2015

DOI:
https://doi.org/10.26190/unsworks/18500

Effect of calcium and iron(III) on membrane fouling under conditions typical of submerged membrane bioreactor treatment of wastewaters

by

Yongjia Xin

A thesis submitted in fulfillment of the requirements for the degree of Doctor of Philosophy

August, 2014

School of Civil and Environmental Engineering

Faculty of Engineering

The University of New South Wales

ORIGINALITY STATEMENT

'I hereby declare that this submission is my own work and to the best of my knowledge it contains no materials previously published or written by another person, or substantial proportions of material which have been accepted for the award of any other degree or diploma at UNSW or any other educational institution, except where due acknowledgement is made in the thesis. Any contribution made to the research by others, with whom I have worked at UNSW or elsewhere, is explicitly acknowledged in the thesis. I also declare that the intellectual content of this thesis is the product of my own work, except to the extent that assistance from others in the project's design and conception or in style, presentation and linguistic expression is acknowledged.'

Signed …….....

Date …….....

COPYRIGHT STATEMENT

Signed …….....

Date …….....

AUTHENTICITY STATEMENT

Signed …….....

Date …….....

Abstract

While the use of submerged membrane bioreactor (MBR) technology has risen dramatically during last decade, the most significant challenge still remaining is the reduction in the severity of membrane fouling. In addition, this filtration technology performs poorly in removal of dissolved contaminants such as phosphorus with addition of adsorbing chemicals such as iron necessary to ensure satisfactory effluent quality. The addition of chemicals such as iron salts, which readily hydrolyse and precipitate as iron oxyhydroxides on addition to the wastewater stream, may however exacerbate the fouling problem, particularly in submerged MBRs where a sedimentation step is not used. In such situations, optimizing the dosage of iron salts is critical in ensuring the most cost effective performance of the MBR however, the relationship between iron dosage and membrane fouling is not completely understood. In particular, the presence of other wastewater constituents such as monovalent and divalent ions (such as sodium and calcium) may significantly influence the interaction of iron with soluble microbial products (SMP) present in the MBR supernatant.

In this thesis, the model polysaccharide alginate is used to investigate the interplay between SMP and iron and calcium under conditions typical of a submerged membrane bioreactor. The concentration of calcium present is shown to be a critical determinant of the severity of membrane fouling with low concentrations inducing alginate gelation and resultant severe membrane fouling while higher calcium concentrations result in gel breakage and alginate aggregation resulting in formation of porous cakes which facilitate rapid filtration. Our results also demonstrate that the

presence of sodium may lead to a worsening of fouling as these ions block binding sites and limit the ability of calcium to induce aggregation.

Comparison of the properties of the alginate assemblages formed in the presence of iron indicate that the Fe-alginate deposits induce even more severe fouling than Ca-alginate gels with lower concentrations of iron than calcium required to induce gelation. Increasing the concentration of iron leads eventually to a reduction in fouling propensity, most likely as a result of the adsorption of alginate to oxyhydroxide surfaces rather than alginate bridging as was the case for calcium. Importantly, the presence of calcium in a system to which iron salts are dosed is shown to lead to a significant reduction in fouling propensity. Investigations with SMP from an actual wastewater plant reveal similar interplay with iron and calcium as observed in the alginate system and highlight the possibility of fouling control through careful manipulation of iron and calcium concentrations in the supernatant.

Acknowledgements

First of all, I would like to express the deepest appreciation to my mentor and supervisor, Professor David Waite, who improved my research skills and prepared me for future challenges, whose guidance, encouragement and solid support have made the completion of this dissertation possible. I would also like to thank Dr. Mark Bligh for editing my manuscripts with many helpful discussions and useful suggestions.

Thanks to Dr Andrew Kinsela, Dr Yuan Wang and Dr Xiaomao Wang for their help in the earlier stages of my PhD. Thanks to Dr Qiaoying Wang for help on running experiments when she was an exchange scholar at UNSW. Thanks also to my friends Xiu Yuan, Lam Ho, Xiaoming Ma, Cecilia Azcurra, Daniel Boland, Anna Yeung and Yanpeng Mao for their great company. Particular thanks to Dr. Di He, Dr. Yi Liu and Dr. Tongxu Liu for the great times spent together over lunch breaks and weekends, which made my PhD journey more enjoyable.

Thanks to the School of Civil and Environmental Engineering and Water Research Centre for their support with instrumentation and professional assistance. Thanks also to Kelvin Ong and Dr. Gautam Chattopadhyay for their assistance in my laboratory work. Thanks to Pattie MacLaughlin for great administrative support.

Finally, I would like to thank my family for encouraging me to further my education. Especially thanks to my dear wife and great friend Xue Han for her love, understanding and encouragement throughout my PhD and the completion of this thesis.

The work of this thesis was financially supported by the Australian Research Council (ARC) for providing the Australian Postgraduate Award (APA), without which it would be impossible to do full time research. Also, additional support and funding from the ARC projects are also gratefully acknowledged.

Table of Contents

List of Figures

List of Tables

Symbols

A	effective filtration area of the flat-sheet membrane (m^2)
b	intercept of the linear regression of V and t/V (s/m)
C_1-C_4	model parameters in Eqs. (2-12) and (2-13)
$[Ca]_{bound}$	bound calcium concentration to alginate
$[Ca]_{free}$	free calcium concentration as measured by calcium ion-selective electrode
g	gravitational constant (m^2/s)
H_s	total solid height of the assemblage layer for quantification of the material properties (m)
H_T	physical height of the assemblage layer for quantification of the material properties (m)
J	permeate flux of the constant pressure flat-sheet dead-end filtration (m/s)
J_e	permeate flux of the constant pressure flat-sheet dead-end filtration just before stoppage (m/s)
J_{ss}	steady-state permeate flux for quantification of the material properties (m/s)

k	slope of the linear regression of V and t/V (s/m^2)
k_f	the ratio of the precipitation rate constant ($M^{-1}S^{-1}$)
k_L	rate constant between iron and alginate ($(g/L)^{-1}S^{-1}$)
k_{SSA}	rate constant between iron and SSA ($M^{-1}S^{-1}$)
K	local Darcy permeability (m^2)
K_{av}	average Darcy permeability (m^2)
L	alginate binding sites
P	trans-membrane pressure (Pa)
P_l	liquid pressure (Pa)
P_s	solid compressive pressure (Pa)
$P_{s,max}$	solid compressive pressure at the membrane deposit layer interface (Pa)
R	the average number of calcium ions bound to one G residue
R_c	Fe-alginate complex formation rate (MS^{-1})
R_m	membrane resistance (1/m)
R_p	iron precipitation rate (MS^{-1})

t time (s)

V the cumulative permeate volume (m)

W_g weight of the built-up layer (kg)

X the coordination number per iron ion

z the height within the layer measured away from the membrane at z=0 (m)

Greek symbols

α local specific resistance ($1/m^2$)

α_{av} average specific resistance ($1/m^2$)

ε_{av} average porosity

$\emptyset$ local solid fraction

$\emptyset_{av}$ average solid fraction

$\emptyset_g$ solid fraction at the gel point

$\emptyset_i$ solid fraction of the dispersion

μ liquid viscosity (Pa•s)

ρ liquid density (kg/m^3)

ρ_s	density of the solid (alginate) (kg/m^3)
ρ_w	density of the Milli-Q water (kg/m^3)

Chapter 1. Introduction

1.1. Membrane bioreactors (MBRs) and membrane fouling

The use of MBR technology has increased dramatically over the last ten years due in part to its advantages over conventional activated sludge (CAS) treatment. Its treatment efficiency is independent of sludge-settling characteristics and easy to operate but requires less space (reduced footprint) rendering it suitable for use in de-centralised areas and in wastewater reclamation. The increasing acceptance of MBR is also driven by the more stringent effluent quality requirements on receiving water bodies. Despite these advantages, significant challenges still remain especially with regard to reducing the severity of membrane fouling, improving the dewaterability of the waste activated sludge (WAS) and, in some instances, increasing the extent of removal of nutrients and other contaminants. Problems requiring attention vary depending on the nature of the plant in question and the intended use of the treated effluent. Among these problems, membrane fouling is of particular concern and considered inevitable in water and wastewater treatment using membrane filtration as a result of the ability of the membranes to retain the bulk of the particles present.

Membrane fouling is characterized as a reduction of permeate flux through the membrane as a result of increased flow resistance due to pore blocking, concentration polarization, and cake formation. The fouling is mainly governed by three kinds of parameters: membrane and module characteristics (membrane material, pore size, and membrane configuration), fluids parameters (viscosity, organic loading, size and

structure of aggregates) and MBR operating conditions (pressure, sludge retention time, aeration, and filtration mode) [1]. While routine operating procedures such as bubbling coupled with intermittent filtration are reasonably effective at removing large sludge particulates from the membrane surface during routine operation [2-4], the principal cause of severe membrane fouling is normally due to the formation of a thin but dense gel layer by the organic compounds present in the sludge supernatant [5, 6].

The dissolved organic matter is ubiquitous in natural and wastewaters [7] and considered the most recalcitrant foulants that significantly hampered the efficient application of membrane filtration technology [8, 9]. In water/wastewater reclamation, organic matter is normally in the form of cellular debris and algal organic matter (AOM), natural organic matter (NOM) in drinking water sources from runoff and leaching of vegetative debris from terrestrial sources within a watershed, and wastewater effluent (EfOM) consisting of background NOM from drinking water and synthetic organic matter produced by human activities plus the extracellular polymeric substances (EPS) from biological wastewater treatment [10-12]. In particular, of the organic compounds present in the supernatant, it is the EPS in either bound or soluble form that are considered to play a critical role in MBR fouling [13].

1.2. Important role of soluble microbial products (SMP) and polysaccharide in membrane fouling

The EPS has been differentiated into an extractable EPS (tightly bound EPS, TBEPS) that is bound tightly with solid surfaces, and a soluble EPS (loosely bound EPS, LBEPS) or soluble microbial product (SMP) that is able to move freely between

sludge flocs and surrounding liquor [14]. The TBEPS contains polysaccharide (PS) and some lipids, while the LBEPS (hereafter referred to as SMP) mainly contains polysaccharide, proteins, lipids, and some humic substances [15-17]. Permeate flux decrease when the soluble EPS (SMP) concentration rather than the total EPS concentration increases with the soluble fraction playing a more important role in fouling than the colloidal fraction [1, 3, 4].

Large quantities of SMP are prone to attach directly to the membrane surface resulting in formation of a gel layer and blocking membrane pores causing more organics to be captured, which leads to the significant increase in specific resistance of the cake layer [18, 19]. SMP gelation associated severe membrane fouling has been reported to be even worse in the presence of divalent metal cations such as calcium as a result of the ability of this divalent cation to bind to carboxylic acid functional groups of the polysaccharides present in SMP [20]. It is now generally agreed that the polysaccharides in SMP is a particularly significant contributor to fouling and could approach the fouling behaviour of SMP better than other constituents [17, 20], and therefore, polysaccharides are commonly used as surrogates to represent SMP in organic fouling of membrane filtration [21, 22]. Polysaccharides makes up 10-30% of the dissolved organic carbon (DOC) content in lakes [23], up to 50% of the DOC in marine waters [24] and typically constitutes around 35% of the DOC in MBR supernatants [25].

1.3. Alginate as a surrogate of polysaccharide in SMP

Alginate-like exopolysaccharides (ALE) have recently been extracted from laboratory [26] and pilot-scale reactors [27] with these materials containing a high percentage of poly-guluronic acid groups capable of forming rigid and non-deformable gels when linked by calcium cations. Indeed, alginate has been widely used as a surrogate of polysaccharide in SMP in a number of studies in membrane fouling [28-30]. Alginate is a naturally derived linear anionic copolymer extracted from various species of brown algae and certain species of bacteria such as in the protective cyst of *Azotobacter vilelandii* and in the biofilms produced by *Psuedomonas* and *Azotobacter* [31-33]. Chemically, alginate consists of α-L-guluronate (G block) and 1,4-linked β-D-mannuronate (M block) residues arranged in a non-regular pattern by varying proportions and sequential distributions of GG, MM, and MG blocks along the polymer chain depending on the source of the alginate [34, 35] with flexibility (elasticity) of the polymer series increasing in the order GG < MM < MG [36, 37]. Due to the subtle differences in biological function, alginates isolated from bacteria, comparing to the alginates extracted from algae, have a propensity to show more variable composition of polymer-blocks within species and be randomly acetylated [38].

In the presence of divalent cations such as calcium, alginate is recognized to form gel layers. This interaction between calcium and alginate is generally conceptualized in terms of the "egg-box model" proposed by Grant et al. [39] where cooperative binding involving two or more rigid and buckled guluronic chains with the

coordinated calcium ions "packed" into the sites created between the chains. Due to the gelling and water retaining properties, Ca-alginate has shown great application potentials in a number of industries such as cell encapsulation [40], wound dressing [41, 42] and other areas including food, cosmetics and agriculture [43]. Furthermore, as discussed at the beginning of this section, alginate has been used as a common model organic foulant to represent polysaccharides for better understanding of the SMP fouling propensity in membrane fouling research for desalination and wastewater treatment, both individually and in mixtures with proteins [44].

Despite of the limitations of lack of interactions between organic molecules, and absence of microorganisms (using alginate derived from algae) as well as other soluble and insoluble particles as a synthetic material, the alginate simplifies the complex wastewater system without introducing other interfering factors to gain some useful insights into the underlying mechanisms of severe fouling caused by polysaccharide in MBR treatment of wastewater. As discussed later in my thesis, the important conclusive results from modeling alginate system still stand when applying them to real SMP system from wastewater.

1.4. Methods to mitigate membrane fouling

In view of the potential savings in capital and operating costs, any process leading to a reduced severity of fouling, whether it is optimization of membrane characteristics and operating conditions, physical and chemical cleaning, or the addition of coagulants is worthy of investigation.

Various techniques have been used to reduce membrane fouling. Firstly, membrane fouling could be mitigated by improving the anti-fouling properties of the membrane module to obtain lower flux decline compared to that of unmodified membranes [45-47]. MBRs operate through a combination of filtration at fluxes less than critical flux (below which a decline of permeability with time does not occur, and above which fouling is observed), and intermittent operation of air scouring [48-50]. Additionally, periodic backwashing is effective in removing most of reversible fouling due to pore blocking, by partially dislodging loosely attached sludge cake from the membrane surface and transporting it back into the bioreactor with resultant improvement in membrane permeability and the development of stable operating conditions [51, 52].

Nevertheless, irreversible fouling eventually occurs necessitating relatively harsh chemical cleaning of the membranes with resultant treatment plant downtime and reduction in output [53].

1.5. Effect of coagulation in reducing membrane fouling

As implied above, irreversible membrane fouling is recognized to be a serious problem in submerged MBR operation [54] with the soluble and colloidal microbial products accounting principally for the problem in view of their propensity to form gels on the membrane surface and/or to penetrate membrane pores [55-57].

One approach to overcoming this problem involves the addition of coagulants which act by increasing particle size through aggregation. It has been reported that

particles near 0.2 um in diameter induce rapid fouling, while particles greater than 3 um in size have little effect on flux [58]. On coagulant addition, the population of small particles is reduced significantly with the resultant assemblage of larger flocs that deposit on the membrane are more readily removed by air scouring [59-62]. Therefore, in summary, the enhanced filterability of the mixed liquor on coagulant addition is achieved by the formation of larger particles through aggregation of soluble and colloidal fractions, thereby preventing particles entering the membrane matrix, reducing the adsorption of macromolecules to the membrane surface and enhancing particle transport away from the membrane surface [56, 57].

A flocculation process prior to the MBR filtration process has been shown to mitigate the formation of gel layer by flocculating the submicron particles to larger assemblages and adsorbing the soluble macromolecule substances [63, 64]. In addition, coagulant addition has also been recognized to assist greatly in reducing the extent of transmembrane pressure (TMP) build-up and the removal of phosphorus in wastewater treatment [65, 66] while aiding the dewatering of the highly gelatinous sludge that is typically produced in MBRs [57].

With regard to coagulant choice, both ferric chloride and aluminum sulfate (alum) have been widely used in water and wastewater treatment to reduce membrane fouling in MBRs [53], while polymeric coagulants such as polymeric aluminum chloride (PAC) and polymeric ferric sulfate (PFS) have also been applied [59]. Once dissolved in water, the oxyhydroxide precipitates formed from metal ion hydrolysis adsorb materials such as suspended particles, colloids and soluble organics and also act to neutralize negative charges on organic solutes. The more positive the charge of the coagulant supplied, the better is the coagulating performance of the added metal

salt. In addition to charge neutrality, another important mechanism of removal of supernatant organics involves bridging [59, 61, 67].

1.6. Role of calcium and sodium in floc stability

To optimize the coagulation process and to reduce membrane fouling to the largest extent, it is necessary to understand the characteristics of the bioflocs present and to understand how they interact with different coagulant metals. Activated sludge contains relatively large amounts of calcium, magnesium, aluminum, and iron. The contribution of Fe and Al to floc stability is of great importance because they have a higher charge than mono and divalent cations. However, to better understand flocculation, it is crucial to be clear about the effect of mono and divalent cations because they exist naturally and universally in wastewater. Indeed, the structural properties of wastewater activated sludge flocs is sensitive to small changes in ionic composition (eg. calcium concentration) and ionic strength [68].

Calcium and magnesium ions are the most abundant divalent cations in natural aquatic systems. Both of these cations may contribute to floc stability and may bind negatively charged biopolymers through bridging. Several studies have shown the importance of calcium in floc structure with a deterioration in settling observed after removing calcium from biological flocs [68-70]. Removal of small amounts of calcium from wastewater sludge has been shown to promote organic macromolecule desorption and floc disintegrations, and resulted in an increase in the negative surface charge and an increase in the number of small particles present [68]. In contrast, increasing calcium concentration decreased turbidity after settlement, indicating that

calcium binds to sludge particulates and plays an important role in flocculation in wastewater activated sludge [70].

With regard to the role of calcium in bioflocculation, research to date has been interpreted using various theories including DLVO (Derjaguin, Landau, Verwey, and Overbeek) theory, alginate theory, and divalent cation bridging (DCB) theory. The DLVO theory considers that the double layer surrounding the particle inhibits aggregation with the size of the double layer decreasing on addition of cations (such as sodium and calcium), leading to reduced repulsion between particles and promotion of aggregation. Several authors have invoked DLVO theory to explain the effect of salts on wastewater solids with sodium, potassium and calcium found to increase floc size and to reduce particle stability [71, 72].

The alginate theory was first proposed by Bruus et al, who suggested that a specific interaction occurred between calcium and alginate in comparison to that observed with magnesium and sodium [69]. At variance with DLVO theory, increased sodium concentration is proposed to induce ion-exchange and to displace calcium ions from within the activated sludge floc and thereby to deteriorate floc properties [69]. DCB theory suggests a non-specific binding of divalent cations rather than the specific interaction between calcium and alginate in alginate theory, because calcium and magnesium have been reported to produce similar improvement in floc formation [73, 74]. According to DCB theory, divalent cations bridge negatively charged functional groups within the EPS, and this bridging helps aggregation and promotes bioflocculation [73]. However, similar to alginate theory, high concentrations of monovalent cations, and especially sodium is considered detrimental to the flocculation process due to the displacement of divalent cations by

monovalent ions thereby rendering flocs weaker and more sensitive to physical stresses [75, 76].

Therefore, it would appear that the balance of mono and divalent cations is critical to the maintenance of good floc properties. Higgins and Novak proposed the use of the ratio of monovalent to divalent cations (M/D) as an indicator to determine whether the cation content is likely to cause sludge problems, and reported that an M/D ratio greater than 2 would deteriorate the floc properties due to the weak floc structure induced by the high concentration of monovalent cations [75]. The efficacy of the M/D ratio has also been supported by several other studies where problems with settling, effluent quality, and dewatering have resulted from changes in cation concentrations [77-79]. However, further investigation is still needed to clarity the controversial role of calcium and sodium in flocculation.

1.7. Knowledge gaps and objectives

Even though the use of iron as a coagulant to mitigate membrane fouling has proven effective (as discussed in section 1.4), controversial issues still remains with regard to the role of iron in controlling membrane fouling. For example, dosing of iron into the sewer as an aid for odour control upstream of the North Head MBR plant in Sydney results in satisfactory effluent quality for the intended on-site reuse but suffers from a greater degree of membrane fouling than desired. Meanwhile, the addition of ferric chloride to wastewater for the aid of phosphorus removal at Brooklyn MBR plant in the northern suburbs of Sydney also aggravates the membrane fouling.

In view of the issues raised above, the major aims of this thesis are to address the following:

- Does the addition of ferric chloride render the fouling in MBRs more or less severe?
- Does the gelling propensity of polysaccharides increase linearly with increase of iron or polysaccharide concentration? Once iron is added in excess of the polysaccharide binding capacity, does the resistance of the gel layer formed on the membrane plateau or keep increasing?
- Does the presence of calcium in wastewater influence the interaction of SMP with added iron? What happens if both calcium and iron are present in the system?

Before starting the research on the effect of iron, the fouling behaviour between calcium and SMP/polysaccharide should be investigated due to the universal and important role of calcium in aquatic systems. The concentration of calcium in wastewaters is typically in the range of 1.5 to 11 mM [80] with the actual content determined particularly by the hardness of the source drinking waters. Further, calcium is important for the floc formation in activated sludge (as discussed in last section) and plays a significant role in the extent and severity of gel formation and associated membrane fouling, while the exact effect of calcium on filtration behaviour remains controversial with a higher concentration of calcium shown to both increase [81-83] and decrease [84, 85] cake resistance during the filtration of alginate suspensions. Biphasic behaviour has also been reported during the membrane filtration of alginate where addition of calcium initially reduced filtration flux but then improved it upon further calcium addition higher than a critical concentration

[86, 87]. As such, it is necessary to be clear about the following key questions before moving on to the impacts of iron addition:

- How does the presence of calcium influence polysaccharide gelation and does this increase or decrease fouling? Does the gelling propensity of polysaccharides increase linearly with increase in calcium or polysaccharides concentration?
- Once the calcium binding capacity of the polysaccharide is reached, does the resistance of the gel layer formed on the membrane plateau or keep increasing in excess of the polysaccharide binding capacity?

Furthermore, same as the debatable role of calcium in alginate fouling, increasing sodium concentration with calcium present has also been reported to both mitigate [83] and aggravate membrane fouling [88]. Therefore, it is also important to investigate:

- How do monovalent cations such as sodium influence the binding behaviour of alginate for calcium?

The thesis is comprised of four major results chapters and has been organized to achieve the above aims in the following manner:

Chapter 3 reports on the role of calcium in alginate-induced membrane fouling by linking the characteristics of Ca-alginate in bulk solution to the subsequently formed gel/cake properties under different calcium and alginate concentrations. This chapter is a basic but important guide for the investigations that are described in the following chapters.

Chapter 4 presents the effect of the monovalent cation sodium on fouling behaviour by Ca-alginate. Together with Chapter 3, this chapter addresses many of the controversial issues associated with the reported combined effects of calcium and sodium on mitigation or aggravation of membrane fouling.

Chapter 5 investigates the role of iron in membrane fouling. In addition, the effect of the presence of calcium on Fe-alginate gel formation is addressed.

Chapter 6 extends the studies on model alginate in the preceding chapters to investigation of the impact of calcium and iron (both separately and together) on fouling behaviour caused by SMP from a real wastewater treatment plant. The results for the effects of calcium and iron on the activated sludge supernatant are quite similar to those obtained for the alginate model system.

All main chapters in this thesis are adapted from published and submitted scientific papers or from manuscripts in preparation, as detailed below:

Chapter 3: Yongjia Xin, Mark W. Bligh, Andrew S. Kinsela, Yuan Wang, T. David Waite, Calcium-mediated polysaccharide gel formation and breakage: impact on membrane foulant hydraulic properties, Journal of Membrane Science 475 (2015) 395-405.

Chapter 4: Yongjia Xin, Mark W. Bligh, Qiaoying Wang, T. David Waite, Effect of ionic strength on membrane fouling by alginate gels in the presence of calcium, submitted to Journal of Membrane Science.

Chapter 5: Yongjia Xin, Mark W. Bligh, Tongxu Liu, T. David Waite, Effect of iron (III) on membrane fouling by alginate in the absence and presence of calcium, Journal of Membrane Science 497 (2016) 289-299.

Chapter 6: Effect of calcium and iron (III) on membrane fouling by soluble microbial product (SMP), in preparation.

Chapter 2. General Experimental Methods and Modelling Approaches

2.1. General filtration setup and procedures

All filtration set-ups used in this work involved use of a small acrylic filtration cell (2 cm in height with an effective filtration area of 1.52×10^{-3} m^2) connected by a short Teflon tube to a 2 L reservoir containing a magnetic stirrer bar and pressurized with high purity nitrogen gas. A pressure controller (Bronkhorst P-602C) was used to maintain a precise and constant pressure in the range of 10 to 150 kPa (±0.1%). Durapore polyvinylidene fluoride (PVDF) 0.1 um pore size membrane (Millipore, Bedford, MA) was inserted in the base of the filtration cell to retain the forming cake, and accumulated filtrate mass was logged using an electronic balance connected to a personal computer. While the reservoir was stirred in order to prevent settling of particles when large aggregates are formed in some filtration runs, stirring of the filtration cell was avoided in order to minimize disturbance of the gel layer forming on the membrane. A schematic of filtration process has been shown in Figure 2-1.

Prior to a filtration run, a clean membrane was placed in the filtration cell, the reservoir filled with Milli-Q water, and the filtrate flux through the non-fouled membrane at the desired pressure measured in order to determine the membrane resistance (R_m). The reservoir was then emptied and filled with the solution of interest and re-pressurized to the same applied pressure as used in the R_m measurement. Filtration was then initiated and logging of the accumulated filtrate mass commenced.

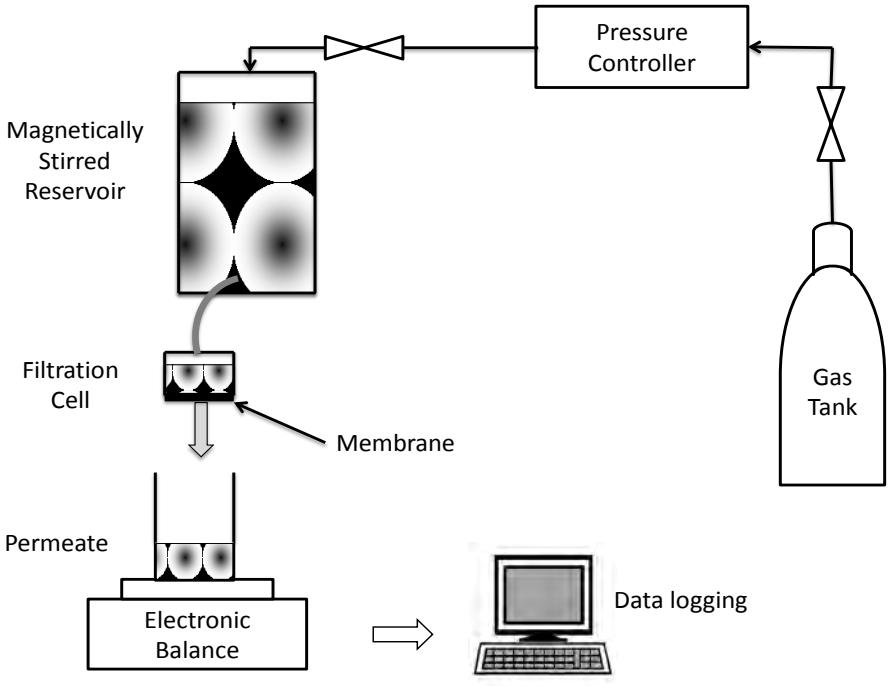

Figure 2-1. Schematic diagram of filtration process

2.2. Experimental filtration pressures

MBRs are typically operated at about 10-50 kPa. However, in order to determine properties of high resistance cakes using this operational pressure, extremely long filtration runs would have been required making the collection of a comprehensive data set impractical. Therefore, constant pressure filtration studies investigating the effects of calcium and alginate concentrations were conducted at 135 kPa in order to facilitate the development of a large data set. The applicability of these data to lower operating pressures was examined via a second set of constant pressure filtration studies conducted over a range of pressures at one alginate concentration and selected calcium concentrations. Modelling of the material properties that describe how the cake behaves under constant pressure filtration was then undertaken (see section 2.4)

to demonstrate that these key properties are independent of filtration pressure within the range considered here and that results developed at 135 kPa are applicable and can be extended to lower pressures typical of plant operation.

2.3. Modelling approach for the determination of material properties in alginate systems

Constant pressure dead-end filtration reaches a steady state condition when the deposited cake layer is fully consolidated and there exists a linear relationship between the cumulative permeate volume (V) and the filtration time (t) to volume ratio (t/V) according to

$$\frac{t}{V} = kV + b \tag{2-1}$$

where k and b are the slope and intercept respectively of the linear regression. The permeation flux (J) at any t, when Eq (1) is satisfied, is obtained from differentiation of Eq (1)

$$J = \frac{dV}{dt} = \frac{1}{t/V + kV} \tag{2-2}$$

The final flux (J_e) at the cessation of filtration, following the attainment of steady state filtration has been shown previously [29], and was shown on numerous filtration runs in this thesis, to be equal to the (constant) steady state flux (J_{ss}) that occurred when the remaining Ca-alginate solution was removed from above the gel layer and replaced with clean permeate and filtration recommenced [29]. Therefore, for all

subsequent filtration runs the value of J_e was substituted for J_{ss} in the derivations of cake properties and filtration performance.

At the end of the filtration run where J_e was recorded, the consolidated gel layer was peeled from the membrane and its weight (W_g) determined using a high precision (0.001g) electronic balance. By measuring the weight of the wet gel layer (W_g) and cumulative permeate volume (V), the total solid height H_s (which is the solid height if there were no porosity in the cake layer) and total physical height H_T (physical height of the whole cake layer from the top to the bottom) are related [29] as follows:

$$(H_T - H_s)\rho_w + H_s\rho_s = \frac{W_g}{A} \tag{2-3}$$

where A is the effective filtration area, ρ_s and ρ_w are the density of alginate and Milli-Q water respectively, and H_s and H_T are related to the initial solid fraction ($\emptyset_i$) and V according to

$$H_s = \phi_i(V + H_T) \tag{2-4}$$

The average solid fraction ($\emptyset_{av}$) of the gel layer can then be represented by the ratio of H_s and H_T

$$\phi_{av} = \frac{H_s}{H_T} \tag{2-5}$$

and the average porosity (ε_{av})

$$\varepsilon_{av} = 1 - \phi_{av} \tag{2-6}$$

The actual highest solid pressure ($P_{s,max}$) used can be obtained once R_m and J_e have been provided

$$P_{s,max} = P - uJ_eR_m \tag{2-7}$$

and the average permeability (K_{av}) deduced from Darcy's law

$$K_{av} = \frac{\mu H_T J_e}{P_{s,max}} \tag{2-8}$$

The average specific resistance (α_{av}) can then be determined from the relationship between K_{av} and $\emptyset_{av}$; i.e.

$$\alpha_{av} = \frac{1}{K_{av}\phi_{av}} \tag{2-9}$$

2.4. Modeling of material properties

Inherent material properties determine the filtration behaviour and the structure of the accumulated assemblage (particle) layer on the membrane. A numerical model [89], based on the Darcy permeability function for the local filterability of the accumulated assemblage

$$K = f(\phi) \tag{2-10}$$

and the compressibility of solid compressive pressure function

$$P_s = f(\phi) \tag{2-11}$$

where $\emptyset$ is the solid fraction, was fitted to the experimentally obtained values for cake porosity and resistance over a range of pressures at selected alginate and calcium concentrations. Although there is no restriction in selecting forms of $K(\emptyset)$ and $\emptyset(P_s)$, it has previously been shown [29] that a permeability function of the power law form

$$K(\phi) = C_1\phi^{C_2} \tag{2-12}$$

and the classical empirical compressive yield stress function [90, 91]

$$\phi(P_s) = \phi_g(1 + C_3P_s)^{C_4} \tag{2-13}$$

where C_1-C_4 are model parameters and $\emptyset_g$ is the solid fraction at the gel point (the point at which the dispersion becomes a connected network of particles, and was determined by extrapolation of the $\emptyset_{av}$ values and $P_{s,max}$ relation to $P_{s,max}$ = 0), provide good descriptions of the filtration behaviour.

At steady state discussed in last section, each trans-slice liquid pressure drop ($\delta P_l/\delta z$) within each discrete slice of the gel layer that drives liquid flow and the resulting solid pressure (P_s=P-P_l) gradient ($\delta P_S/\delta z$) are independent of time and can be described by Darcy's Equation

$$\frac{d_{p_l}}{d_z} = -\frac{d_{p_s}}{d_z} = \frac{\mu J_{ss}}{K} \tag{2-14}$$

where P_l is the local liquid pressure and P_s is the local solid pressure, μ is the liquid viscosity and z is the height within the layer measured away from the membrane surface at z=0. With given functions of $K(\emptyset)$ and $\emptyset(P_s)$, Eq. (2-14) can be easily integrated or numerically iterated from the top to the bottom of the built-up

layer (H_T) in order to obtain the highest solid pressure ($P_{s,max}$) (which is equal to the liquid pressure drop across the built-up layer) and the total solid height of the layer

$$H_s = \int_0^{H_T} \phi d_z \tag{2-15}$$

once one complete set of experimental data at five different nominal pressures were selected for data fitting, the unknown parameters (C_1-C_4) were thus obtained and optimised through numerical technique by minimizing the residual differences between the measured and modelled values of H_s and $P_{s,max}$ (sum of squares of modelled minus experimental data).

The average solid fraction ($Ø_{av}$), the average permeability (K_{av}) and the average specific resistance (α_{av}) can then be determined by the numerical integration of Eqs. (2-12) and (2-13) over P_s (0, $P_{s,max}$), which are performed at the constant flux J_{ss} (steady-state) for each generated synthetic discrete slice (a total number of 1000 cake slices), iterated from bottom of the cake (which is the slice adjacent to membrane) to each successive slice, and to the top of the cake. It was found in the following Chapter 3 and Chapter 5 that the calculated $Ø_{av}$, K_{av} and α_{av} match well with that obtained by experiments at various $P_{s,max}$, proving that the selected material properties functions are suitable for the alginate dispersion under consideration here.

Chapter 3. Effect of Calcium on Membrane Fouling by Alginate Gels

3.1. Introduction

The use of submerged membrane bioreactor (MBR) technology has increased dramatically over the last ten years due in part to its advantages over conventional activated sludge (AS) treatment including reduced footprint, superior effluent quality, and treatment efficiency independent of sludge-settling characteristics. However, significant challenges remain especially with regard to reducing the severity of membrane fouling. It is now recognized that organic compounds presenting in the sludge supernatant are the principal cause of severe fouling, particularly as operating procedures such as bubbling coupled with intermittent filtration are reasonably effective at removing sludge particulates from the membrane surface during routine operation [3, 4, 92]. Compounds present in the sludge supernatant include soluble and colloidal microbial products (SCMPs) such as proteins and polysaccharides with general consensus [3, 20] that the polysaccharide component is a particularly significant contributor to fouling. Wang and Waite [20] have shown that the presence of calcium cations is critical to SCMP gelation and associated occurrence of severe membrane fouling with these divalent metal ions inducing bridging between polysaccharide groups, particularly as a result of binding to carboxylic acid sites present in the polysaccharides.

Polysaccharides make up 10-30% of the dissolved organic carbon (DOC) content in lakes [23], up to 50% of the DOC in marine waters [24] and typically constitute around 35% of the DOC in MBR supernatants [25]. The exopolysaccharide content of wastewater sludge supernatant is recognized to be key to the formation of aerobic granules [93, 94] and alginate-like exopolysaccharides (ALE) have recently been extracted from laboratory [26] and pilot-scale [27] reactors. This ALE has been shown to contain a high percentage of poly-guluronic acid (G) blocks that are also capable of forming rigid and non-deformable gels when linked by calcium cations. Alginate is a naturally derived linear anionic copolymer and consists of α-L-guluronate (G block) and 1,4-linked β-D-mannuronate (M block) residues arranged in a non-regular pattern by varying proportions and sequential distributions of GG, MM, and MG blocks along the polymer chain depending on the source of the alginate [35, 95] and is recognized to form gel layers in the presence of divalent cations such as calcium. The interaction between calcium and alginate is generally conceptualized in terms of the "egg-box model" proposed by Grant et al. [39] where cooperative binding involving two or more rigid and buckled guluronic chains with the coordinated calcium ions "packed" into the sites created between the chains.

The calcium content of wastewaters is typically in the range of 1.5 to 11 mM [80] with the actual content determined particularly by the hardness of the source drinking waters. Additionally, lime ($Ca(OH)_2$) is used for pH adjustment in wastewater treatment with the required lime dosage depending primarily on the alkalinity of the wastewater [96]. As such, the polysaccharide content combined with the concentration of calcium present might be expected to play an important role with regard to the extent and severity of membrane fouling associated with gel formation.

While the importance of the polysaccharide and calcium content of wastewaters to gel formation and resultant membrane fouling are now well-recognized, limited insight into the effect of the relative polysaccharide and calcium content on the severity of membrane fouling is available. Important questions include "What is the relationship between suspension characteristics and filtration behaviour?", "Does the gelling propensity of polysaccharides increase linearly with increase in calcium or alginate concentration?" and "How does the resistance of the fouling layer vary as calcium is added in excess of the polysaccharide binding capacity?". This chapter aims to further the understanding of Ca-alginate interactions and implications of these interactions to filtration using alginate as a model of polysaccharides present in wastewaters. Ca-alginate solutions exhibiting a range of calcium concentrations have been characterized in terms of calcium binding behaviour and assemblage size with the resultant fouling layers formed on membranes investigated using dead-end filtration methods, with the specific purpose of linking the interactions occurring in bulk solution to filtration properties.

3.2. Materials and methods

3.2.1. Materials

Sodium alginate (Sigma-Aldrich Product No. 180947) that was mannuronate-rich (61% M, 39% G) with molecular weight (MW) ranging between 120,000 and 190,000 $g.mol^{-1}$ was used as received in all Ca-binding and filtration experiments. Sodium alginate solutions of 0.1, 0.4 and 1.0 g/L were prepared in high-purity water (Milli-Q, Millipore) with 50 mM NaCl background electrolyte and 2

mM morpholinepropanesulfonic acid (MOPS) and 1 mM $NaHCO_3$ as buffer (resulting in pH ~7) and were mechanically stirred until well dispersed. Ca-alginate solutions were prepared by adding the desired amount of $CaCl_2$ followed by overnight stirring. The pH of the solution was then adjusted by acid or base addition to 7.50 with the pH measured using an Orion 5 Star multifunctional meter (Thermo Electro Corporation, USA) prior to filtration.

3.2.2. Bulk solution

3.2.2.1. Calcium binding to alginate

The binding of calcium to alginate was examined by measuring the activity of free calcium ions (using an Orion ion selective electrode in conjunction with an Orion 5 Star multifunctional meter) in the Ca-alginate solutions after overnight equilibration. The calibration curves for the ion selective electrode were derived using $CaCl_2$ solutions of known concentrations. Free calcium measurements were also carried out using dialysis bags with the results from these studies confirming that interference of the probe by either the alginate or Ca-alginate complex was not occurring.

3.2.2.2. Viscosity

Viscosity measurements of samples prepared in the same manner as for the Ca-alginate binding experiments were undertaken using a DV-79 digital viscometer (Shanghai Bilon Instrument Co. Ltd).

3.2.2.3. Size

The sizes of aggregates in the Ca-alginate solutions were measured using dynamic light scattering (DLS) (Malvern Zetasizer Nano S). Sodium alginate solutions after overnight stirring were adjusted to pH 7.5 and filtered (0.45um Millex-HN syringe) prior to calcium addition in order to remove dust and large aggregates. The concentration of alginate in the solutions was unchanged by filtration as determined by total organic carbon (TOC) (Shimadzu TOC-500) measurements. Size was measured immediately after calcium addition with no significant change evident after sitting for 24 hours.

3.2.2.4. Scanning electron microscopy

To gain further insight into the structure of the cake deposited on the membrane, scanning electron micrographs (SEM) of the Ca-alginate cake layer formed in $0.1 g.L^{-1}$ alginate solution (at 6 and 12 mM calcium) were obtained using a cryo-snap preparation process similar to that described by Santiwong et al. [97]. These micrographs were obtained on a JEOL-JSM-6490 LA scanning electron microscope, operating at 15 kV. In brief, small strips (approximately 2 mm in width and 10 mm in length) of freshly filtered Ca-alginate cakes were placed on a holder and immersed in a liquid nitrogen bath for about 30s after which they were snapped with the broken untouched edge facing the lens. The SEM images of the filter cake cross-section were then quickly analyzed (within a few minutes of freezing) on a normal stage, under high vacuum.

3.2.2.5. General filtration methods and the determination/modelling of material properties

Constant pressure dead-end filtration was applied for the prediction of filtration behaviour and material properties. Detailed filtration setup and methods, and the determination/modelling of cake properties in alginate systems have been provided in Chapter 2 General Experimental Methods and Modelling Approaches.

3.3. Results

3.3.1. Bulk solution

3.3.1.1. Calcium binding to alginate

A plot of bound calcium (deduced from the difference between total added calcium concentration and measured free calcium concentration, normalized to the alginate concentration added and presented as the number of calcium ions per G residue (R), where $\mathrm{G} = \frac{\text{weight of alginate}}{\text{MW of Na}\sim\mathrm{C_6H_8O_6}} \times \text{percentage of G blocks (39\%)}$ versus total added calcium concentration (Figure 3-1) reveals that the behaviour of the Ca-alginate system is complex and transitions through a number of phases (and stages within these phases) as calcium concentration changes. At any alginate concentration, two clearly defined phases can be identified (Figure 3-1): i) typical binding behaviour between 0 and 6 mM of total added calcium, where the degree of calcium binding generally declines as more calcium is added such that a plateau region is being approached suggesting binding site saturation; and ii) a second phase of binding for calcium concentrations >6 mM where the rate of calcium binding (i.e., the fraction of

added calcium that was bound) increased and remained constant with continued addition of calcium, resulting in a linear dependence of R on total added calcium concentration.

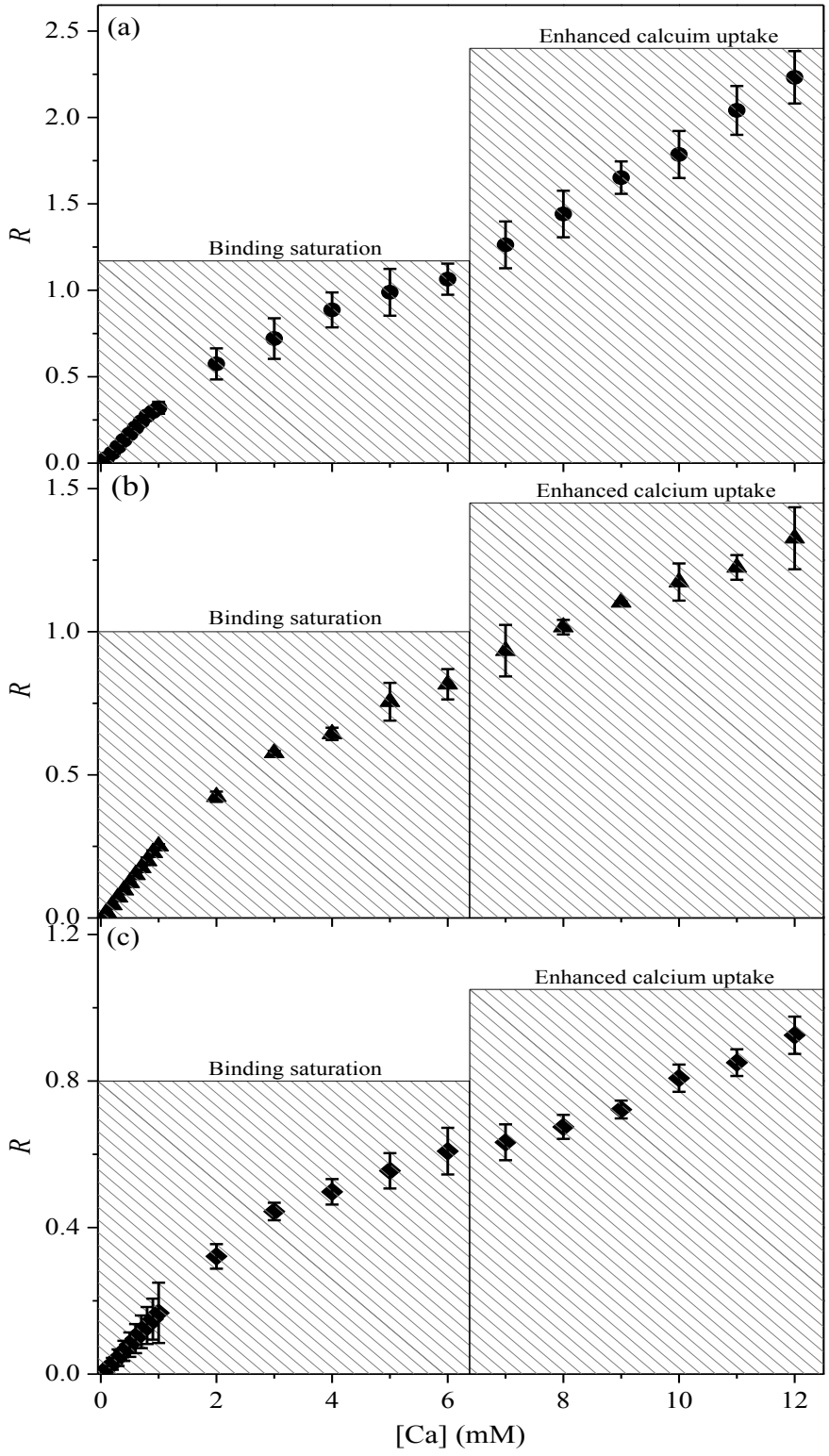

Figure 3-1. Uptake of calcium in a) 0.4 $g.L^{-1}$, b) 1 $g.L^{-1}$, or c) 2 $g.L^{-1}$ alginate solutions as a function of total calcium concentration. R is the molar ratio of bound calcium to G residues. The shaded areas represent the two phases of calcium uptake. Standard errors bars are from triplicates.

The convex shape of the data up to 6 mM calcium when presented as a Scatchard plot (Figure 3-2a) indicates the occurrence of positive cooperative binding during the first phase of binding as has been described previously [98]. This convex region of the Scatchard plot (0 to 6 mM calcium) also displays three stages which correlate well with those reported by Fang et al. [99]. These stages are considered to represent the following processes: Stage I - formation of Ca-alginate monocomplexes by interaction between Ca^{2+} and a single guluronate unit, Stage II - propagation and formation of "egg-box" dimers via pairing of monomer-complexes, and Stage III - lateral association of dimers to form multimers [99]. In the region of the second phase of binding, where the removal of free calcium is apparently enhanced, the ratio of $R/[Ca]_{free}$ becomes independent of total added calcium, indicating that calcium is being bound as a constant proportion of added calcium, as had been indicated previously by the linearity of the second phase in the binding plot.

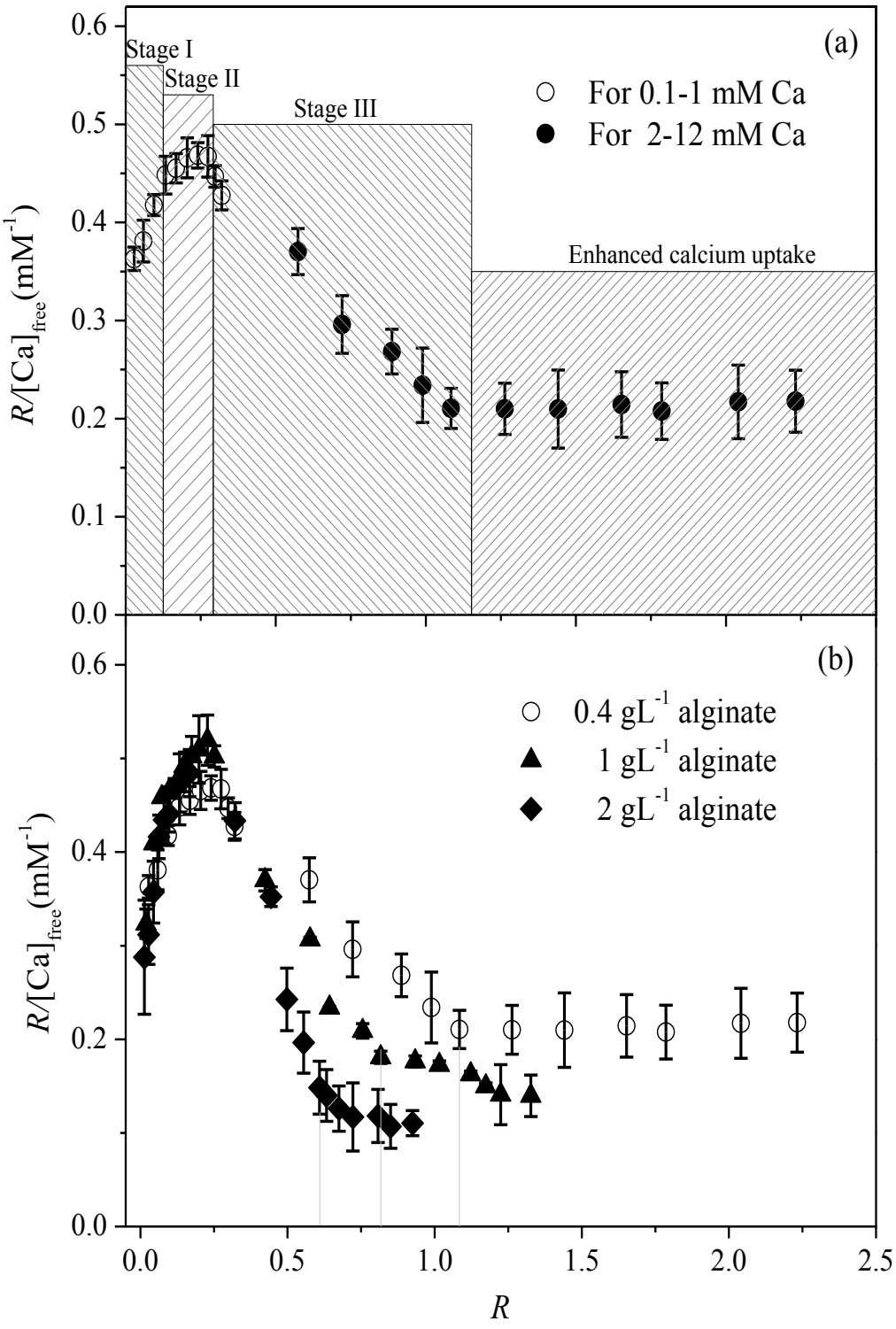

Figure 3-2. Scatchard plots derived from Figure 3-1 for various alginate concentrations. a) Plot for 0.4 $g.L^{-1}$ showing the 3 stages of initial typical binding phase that correlate with those proposed by Fang et al [23]. b) Comparative plots for all alginate concentrations, with vertical grey lines showing the total calcium concentration of 6 mM in each titration. Standard errors bars are from triplicates.

The binding behaviour at higher alginate concentrations of 1 and 2 $g.L^{-1}$ was similar to that at 0.4 $g.L^{-1}$ (Figure 3-2b). The general shapes of Scatchard plots are similar with a large degree of overlap between the curves during cooperative binding resulting in the formation of dimers (Stages I and II). The co-occurrence of the peaks at $R \sim 0.25$ concurs with the theoretical value for dimers [39]. Interestingly, during Stages I and II, the values of $R/[Ca]_{free}$ were quite similar among the different alginate concentrations for a given value of R (Figure 3-2b). During Stage III, the slope of the Scatchard plot for 0.4 $g.L^{-1}$ alginate is lower than that at the higher alginate concentrations, however, transitions to the plateau region of the second phase all occur at close to 6 mM and therefore at lower values of R as alginate concentration increases.

3.3.1.2. Viscosity

As expected, viscosity was higher at higher alginate concentrations [100, 101] and, for all alginate concentrations, maximum viscosity occurred at a calcium concentration of 1 mM or less (Figure 3-3) due presumably to gel formation [102]. This work is particularly interested in the effects of further additions of calcium where viscosity was shown to continually decrease for calcium concentrations > 1 mM with sharper decreases commencing from around 6 mM.

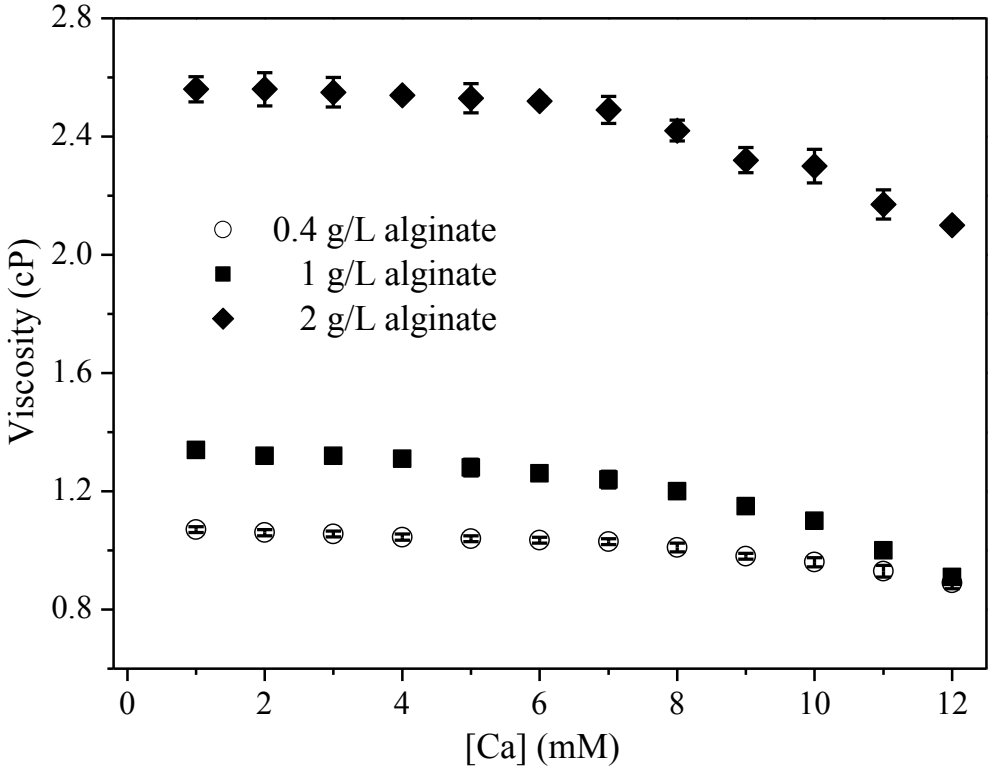

Figure 3-3. Viscosity of Ca-alginate solutions as a function of calcium concentration for alginate concentrations of 0.4, 1 and 2 $g.L^{-1}$. Standard errors bars are from duplicates.

3.3.1.3. Size

For alginate concentrations of 0.1 and 0.4 $g.L^{-1}$, the initial additions of calcium resulted in decreases in the measured size (Figure 3-4), most likely due to the formation of more compact egg-box structures [103]. Further addition of calcium resulted in increased size with the rate of size increase per unit of added calcium increasing for calcium concentrations > ~6 mM. Greater size increase occurred at higher alginate concentrations. An alginate concentration of 1 $g.L^{-1}$ exhibited self-aggregation and so is not included in the results presented here [104].

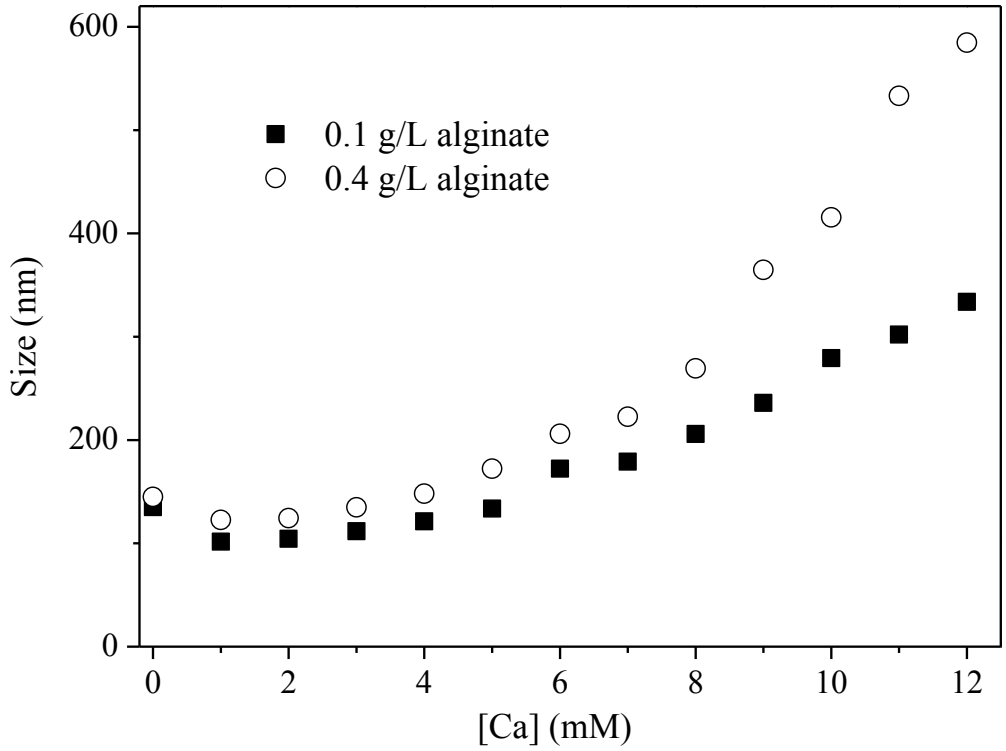

Figure 3-4. Size of Ca-alginate assemblages as a function of calcium concentration for alginate concentrations of 0.1 and 0.4 $g.L^{-1}$. Error bars are eliminated for clarity.

3.3.2. Cake properties

3.3.2.1. Porosity and cake resistance

Porosity, and therefore water content, of the accumulated cake generally decreases as calcium concentration increases, with the rate of decrease per unit of added calcium increasing for calcium concentrations > 6 mM (Figure 3-5). These effects of calcium concentration on cake porosity somewhat mirror those observed for viscosity of the bulk solution pointing to potential links between the properties of the bulk solution and the resultant cake properties.

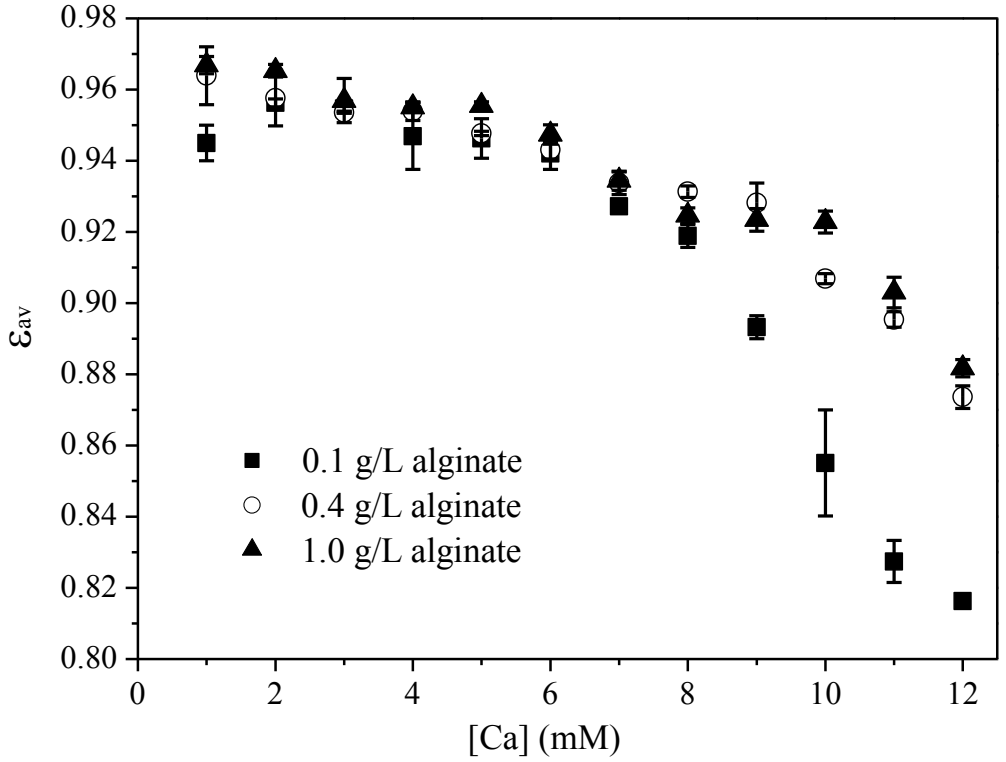

Figure 3-5. Porosity (ε_{av}) of Ca-alginate cake-layer formed at 135 kPa at different calcium concentrations for alginate concentrations of 0.1, 0.4 and 1 $g.L^{-1}$. Standard errors bars are from duplicates.

The pattern for the dependency of cake resistance on calcium concentration is similar to that of porosity, with the most notable difference being the far more dramatic decrease in resistance for calcium concentrations > 6 mM (Figure 3-6). However, the cake resistance of 0.1 $g.L^{-1}$ alginate increases as calcium concentration increases up to 6 mM. This is due to the limited retention of alginate by the membrane before the gel was formed with this an issue when both calcium and alginate concentrations are low [83]. Overall, both resistance and porosity follow remarkably similar trends over a 10-fold range of alginate concentration.

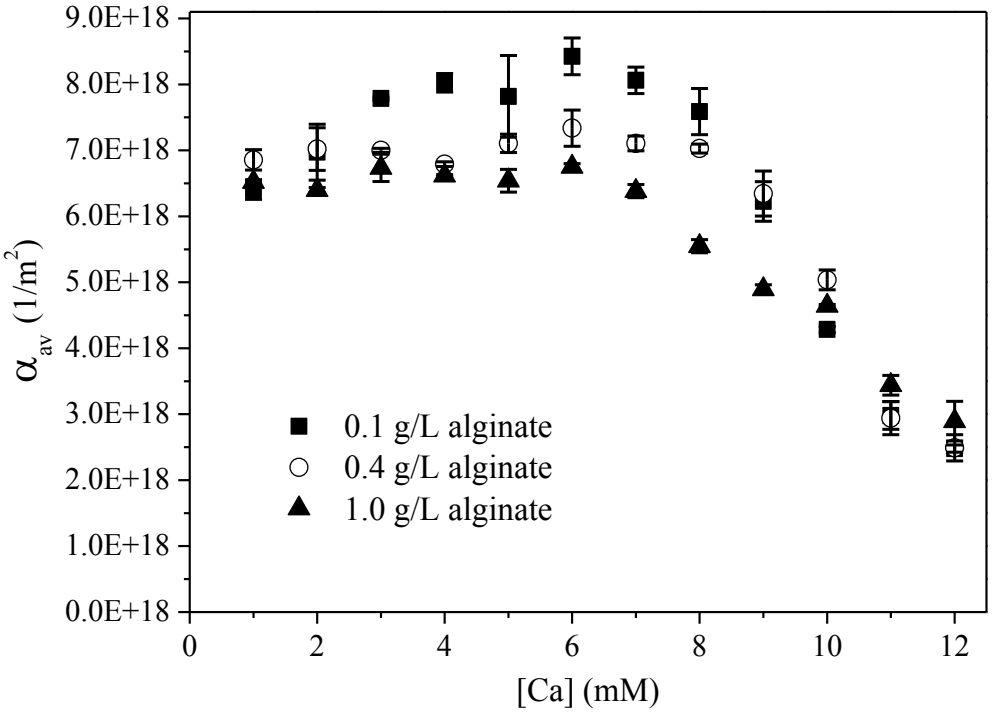

Figure 3-6. Resistance (α_{av}) of Ca-alginate cake layer formed at 135 kPa at different calcium concentrations for alginate concentrations of 0.1, 0.4 and 1 g.L^{-1}. Standard errors bars are from duplicates.

3.3.2.2. Alginate assemblage properties at different pressures

When the filtration pressure, expressed as the maximum solid pressure ($P_{s,max}$), was varied between 10 and 140 kPa for selected concentrations of calcium, the experimentally derived value for the average solid fraction, $\emptyset_{av}$, increases with pressure, with this increase becoming almost negligible at high calcium (and therefore high $\emptyset_{av}$) (Figure 3-7a). At the same time, the other experimentally derived cake property, the average Darcy permeability, K_{av} (Figure 3-7b), is observed to decrease as filtration pressure increases, with most of this decrease occurring between 10 and 50 kPa (which are pressures that are typical of MBR operation). Most notable

here is the difference in the variation of K_{av} with calcium concentration between low and high pressures. At low pressure, the values for $K_{av,}$ vary about four fold over the calcium concentration range, whereas at high pressure the variation is much lower such that the values are quite similar. The calculated values for α_{av} (Eq. 2-9) increase with increasing pressure (Figure 3-7c), with the pattern of variation with calcium concentration at high pressure, as observed in the previous experiments (Figure 3-6), being maintained at low pressure.

The values for the cake properties ($\emptyset_{av}$, K_{av}, α_{av}) derived from the modeled cake profile very closely match the experimentally derived values over the entire range of filtration pressures (Figure 3-7). This result provides strong evidence that the cake formation process for a given feed is essentially the same across the range of pressures of interest, and suggests that the results of porosity and cake resistance obtained at 135 kPa (Figure 3-5 and 3-6) can be extended to lower pressures more typical of MBR operation. The fitting parameters $C_1 - C_4$, and $\emptyset_g$ (Eqs 2-12 and 2-13) show distinct patterns of variation over the modeled calcium concentration range (Table 1, Table A1) with dramatic changes in the parameter values occurring at calcium concentrations of 6-7 mM (Table 1, Figure A1) indicating change in the cake formation process with increase in calcium concentration with significant implications to the filterability and compressibility behaviour of the cake layer. Beyond a calcium concentration of 6 mM, the compressibility of the cake layer increases, with a greater solid fraction $\emptyset$ associated with a given solid pressure P_s, and the filterability increases, with greater hydraulic conductivity K for a given $\emptyset$.

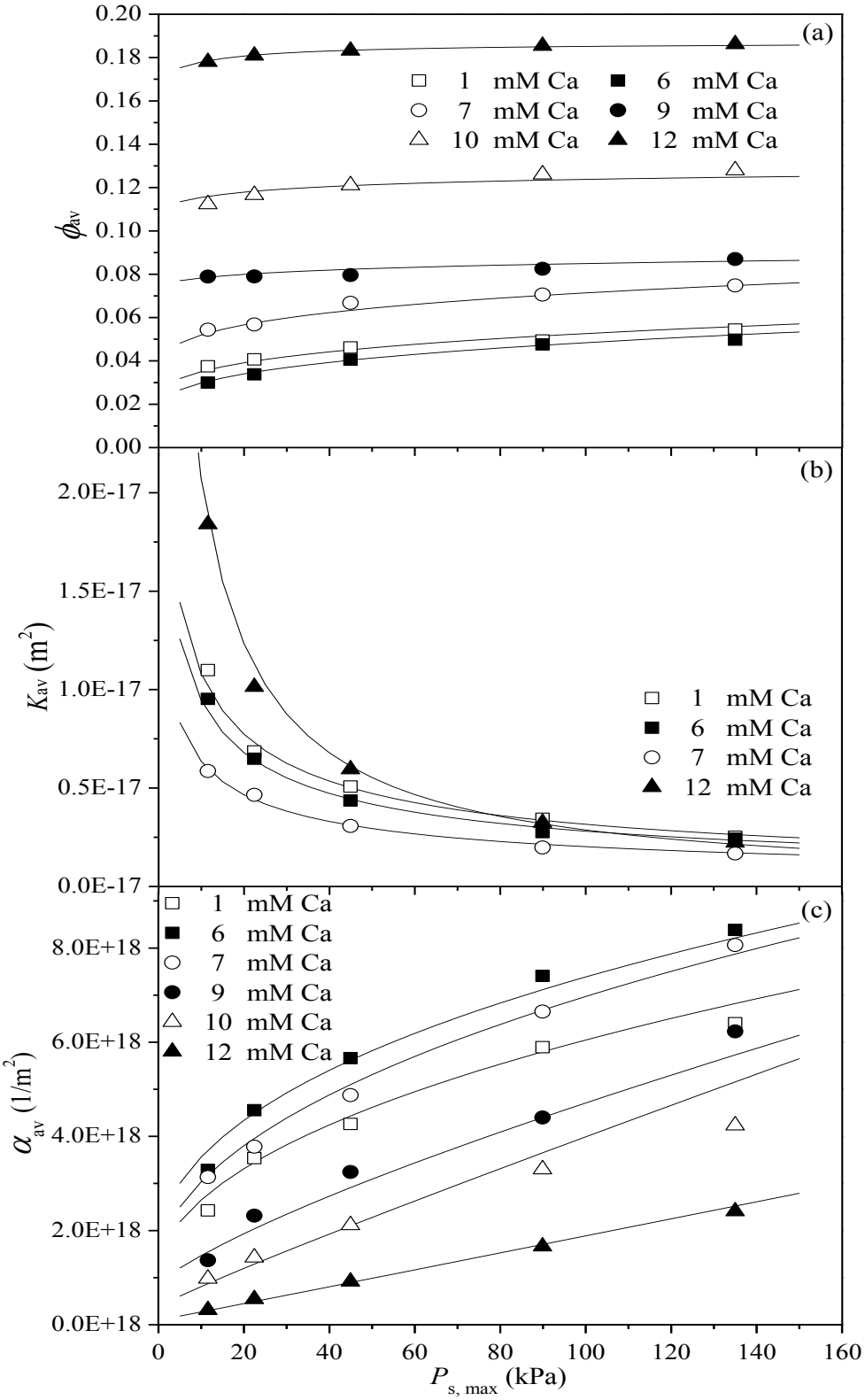

Figure 3-7. Comparison of measured and modeled (a) solid fraction (ϕ_{av}), (b) permeability (K_{av}) and, (c) resistance (α_{av}) of cake layer formed in 0.1 g.L^{-1} alginate solution at various constant pressures for selected calcium concentrations (1, 6, 7, 9, 10, 12 mM).

Table 3-1. Filterability and compressibility functions (as defined in Eq (2-12) and (2-13)) for Ca-alginate cake layers at different calcium concentrations. The parameters $C_1 - C_4$ were optimized at each calcium concentration to minimize the residual differences between the measured and modelled values of cake height (H_s) and maximum solid pressure ($P_{s,max}$). The solid fraction at the gel point ϕ_g was estimated by extrapolation of the solid fraction curve to $P_{s,max}$ of 0 kPa. Average absolute deviations for fitting parameters C_1 to C_4 are provided in Table A1.

[Ca] (mM)	Filterability	Compressibility	$\emptyset g$
1	$K_1 = 1.221 \times 10^{-21} \emptyset^{-2.727}$	$\emptyset_1 = \emptyset_{g1} \times (1 + 0.00086 \times P_s)^{0.256}$	0.025
6	$K_6 = 3.152 \times 10^{-21} \emptyset^{-2.291}$	$\emptyset_6 = \emptyset_{g6} \times (1 + 0.00086 \times P_s)^{0.299}$	0.020
7	$K_7 = 4.251 \times 10^{-22} \emptyset^{-3.269}$	$\emptyset_7 = \emptyset_{g7} \times (1 + 0.00086 \times P_s)^{0.197}$	0.040
9	$K_9 = 6.036 \times 10^{-31} \emptyset^{-12.031}$	$\emptyset_9 = \emptyset_{g9} \times (1 + 0.00016 \times P_s)^{0.115}$	0.075
10	$K_{10} = 3.129 \times 10^{-31} \emptyset^{-14.472}$	$\emptyset_{10} = \emptyset_{g10} \times (1 + 0.00016 \times P_s)^{0.109}$	0.110
12	$K_{12} = 7.006 \times 10^{-32}$ $^{-19.327}$	$_{12} =$ $_{g12} \times (1 + 0.00016 \times P_s)^{0.109}$	0.170

3.3.2.3. Filtration time

The time taken to filter 300 mL of permeate clearly decreases for calcium concentration > 6 mM, with much greater improvements occurring at low pressures (Figure 3-8). So great was the improvement at 12 mM calcium, that the filtration time at 12 kPa was only 1.6 times greater than that at 135 kPa, whereas at 6 mM calcium the time required to filter 300 mL was almost 5 times greater. The short filtration times for 1 mM calcium were due to the slow formation of the cake layer and the resulting initial passage of alginate through the membrane.

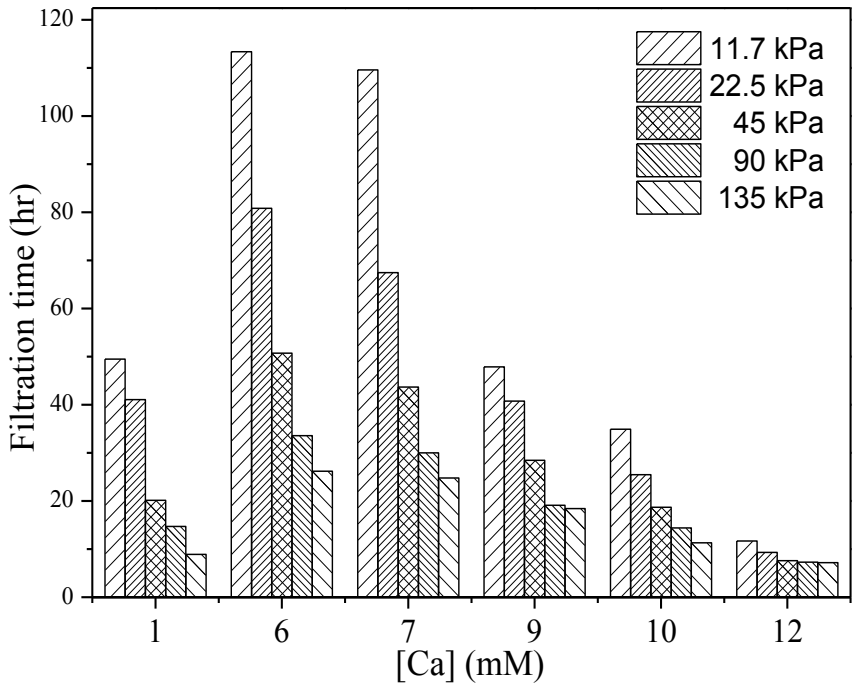

Figure 3-8. Filtration time required to obtain 300 mL of permeate at various applied pressures and different calcium concentrations in 0.1 $g.L^{-1}$ alginate solution.

3.3.2.4. Scanning electron microscopy

Cross sections of filter cakes produced with 0.1 $g.L^{-1}$ alginate in the presence of 6 mM and 12 mM Ca, both at 22.5 kPa, are shown in the SEM images presented in Figure 3-9. The images are representative of multiple points of analysis across each cake and clearly show the dramatic difference in assemblage structure and pore size between the two treatments. The Ca-alginate assemblage formed at lower calcium concentration (Figure 3-9a) displays a distinct "honeycomb" structure, with large, self-contained pores consistent with the measurement of high porosity and low hydraulic conductivity under these conditions. In comparison, the cake formed at high calcium concentration (Figure 3-9b), which was shown to have significantly higher hydraulic conductivity than the low calcium case, exhibits smaller pores with reduced cross-linking.

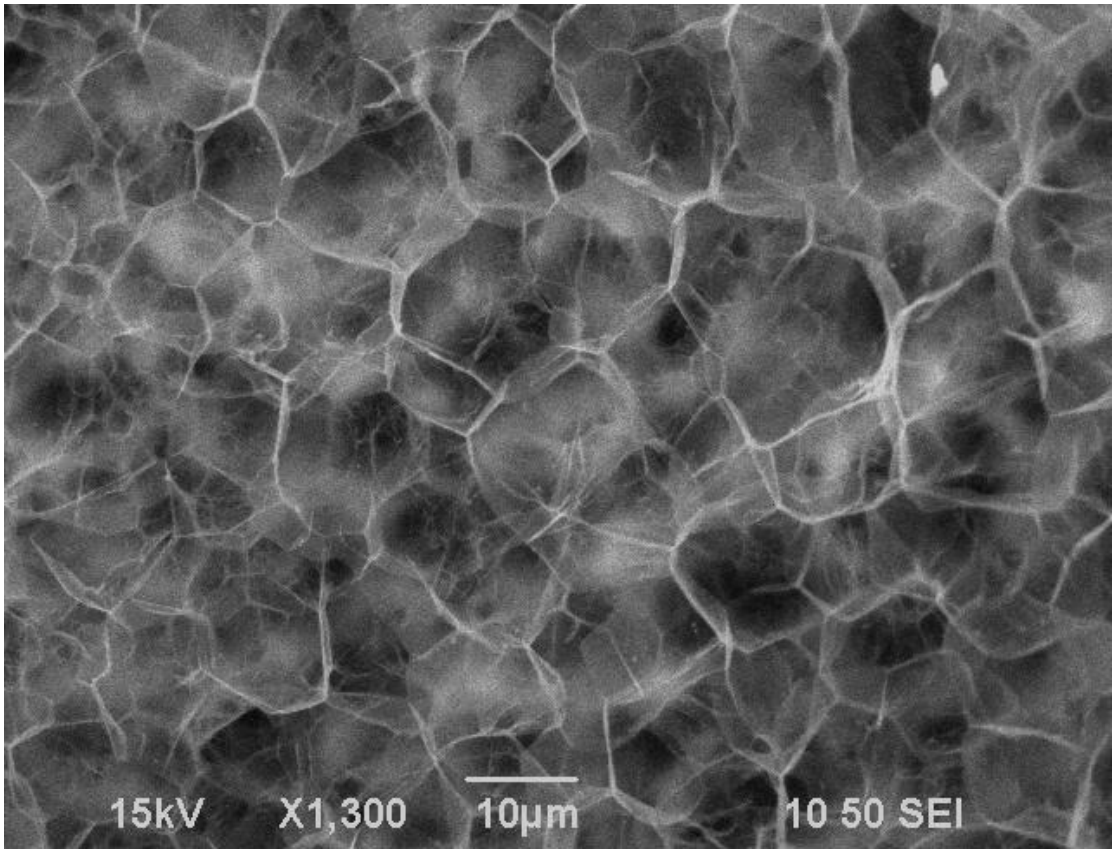

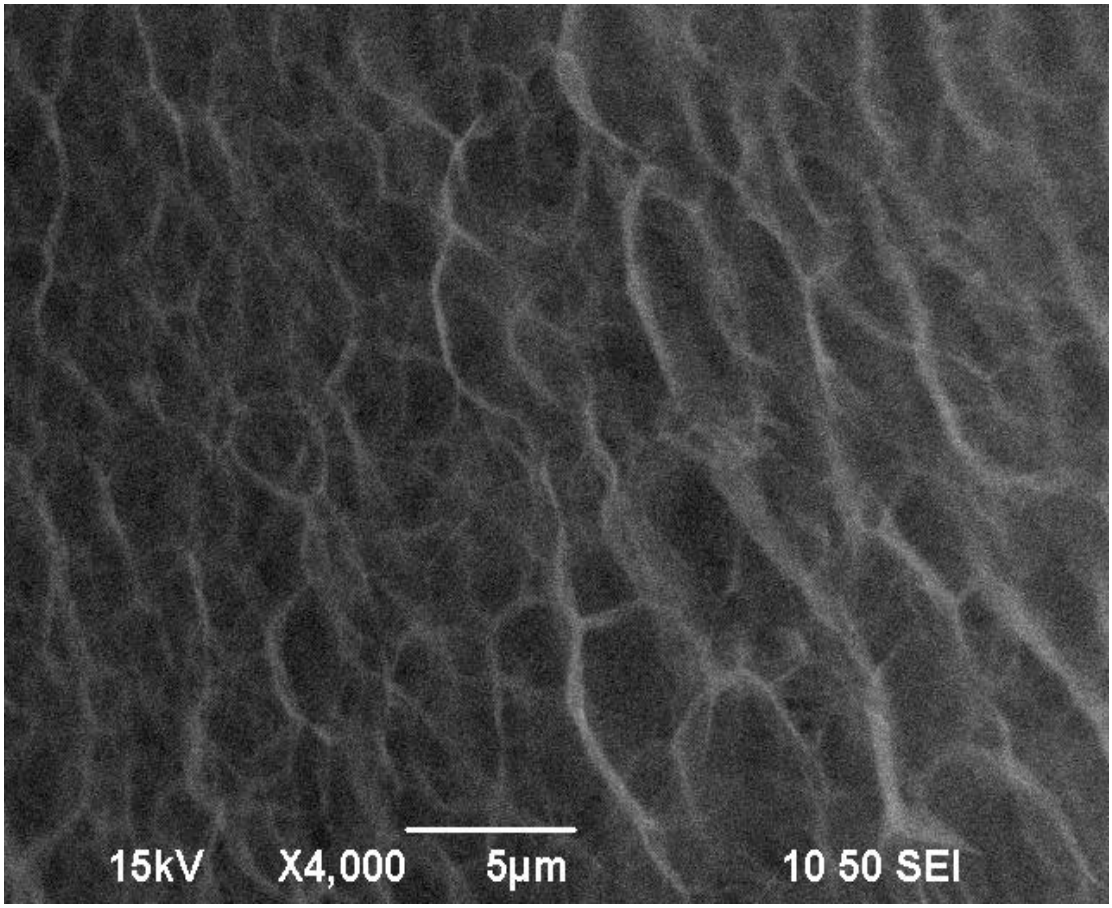

Figure 3-9. Scanning electron microscopy images taken from inside the alginate gel layer formed from 0.1 $g.L^{-1}$ alginate solution under 22.5 kPa at (a) 6 mM and (b) 12 mM calcium.

3.4. Discussion

3.4.1. Biphasic binding and fouling behaviour in the presence of calcium

The relative concentrations of calcium and alginate are expected to play an important role in the formation of alginate gel networks with a higher proportion of calcium shown to both increase [81-83] and decrease [84, 85] cake resistance during the filtration of alginate suspensions. Biphasic behaviour has also been reported during the membrane filtration of alginate where addition of calcium initially reduced

filtration flux but then improved it upon further addition [86, 87]. Mo et al. reported the existence of a critical calcium concentration of 3 mM, below which increasing calcium concentration led to more severe fouling and above which fouling was increasingly mitigated [87]. Here, I have observed similar biphasic filtration behaviour, with a critical concentration of around 6 mM, but have also revealed concomitant, and likely linked, biphasic behaviour in the binding of calcium by alginate in bulk solution. There is a strong correlation evident between the calcium concentration at which a switch in binding behaviour occurred and the calcium concentration at which a switch in filtration behaviour occurred.

The apparent link between the behaviour of the Ca-alginate system in bulk solution and the properties of the resultant cake is not unexpected since the assemblages formed in solution are concentrated on the membrane surface and therefore likely to impact cake properties. Particle size has previously been proposed as responsible for biphasic filtration behaviour [87], however, while particle size was shown to increase with calcium addition (Figure 3-4), size analysis did not reveal a distinctive change indicative of a critical calcium concentration.

Two distinct phases of calcium binding in the bulk solution have been delineated by the critical calcium concentration of approximately 6 mM (Figure 3-1). At low calcium concentration ($\leq$ 6 mM), overall calcium binding is typical of that expected for a ligand containing a finite number of binding sites that are progressively filled and asymptotically approach saturation. For the initial part of this phase (Stages I and II), however, the Scatchard plots (Figure 3-2) reveals the existence of positive cooperative binding, previously proposed to be due to the high stability of the "egg-box model" dimer conformation [39] where calcium occupies the spaces between two

G blocks and each calcium is complexed by the carboxyl groups of four G units. The dimer formation stage is characterized by the positive slopes of the Scatchard plots which overlap for all alginate concentrations and peak at the ratio of cross-linked Ca-alginate to total alginate (R=0.25) expected for complete dimer formation.

Further binding of calcium (Stage III) leads to the aggregation of dimers producing junction zones with the resultant gel containing narrow or impassable channels for the passage of water [103, 105]. Charge neutralization and intermolecular bridging in the presence of calcium may accelerate the cross-linking of alginate gel layers and produce significant hydraulic resistance to permeate flow [7, 82]. The smaller slope of the lower concentration alginate plot during Stage III (Figure 3-2b) suggests that a greater proportion of the binding sites remain accessible during this stage where gel formation is occurring. This behaviour is likely linked to the higher value of R at which the transition to the second binding phase occurs for the lower alginate concentrations. This phenomenon and its significance will be discussed further in later sections.

By increasing the calcium concentration beyond the region typical of that required for gel formation, as indicated by the convex shape of the Scatchard plot, a second phase of binding was observed, which might be considered an extension of the multi-step calcium binding behaviour observed by Fang et al. [99]. This plateau region of the Scatchard plot corresponds to the linear region of the binding plot and is characterized by a distinct increase in the fraction of added calcium that is removed and an apparent large increase in the binding capacity. A key feature of this study is the coincidence of the switch to the second phase of calcium binding with the marked

improvement in filtration properties of the resultant cake, which will be discussed in detail in following sections.

3.4.2. Possible mechanisms for enhanced calcium uptake

The observation of enhanced calcium uptake was unexpected based on previous investigations of calcium binding by alginate. Possible mechanisms for the increase in removal of dissolved calcium at calcium concentrations greater than 6 mM, following the typical saturation of binding sites, include 1) enhanced binding of calcium to alginate, and 2) precipitation of $CaCO_3$. These possibilities are considered in detail below.

3.4.2.1. Enhanced binding

Calcium binding by alginate appears to approach saturation in the low calcium region, which is typical binding behaviour despite the early existence of positive cooperativity. Calcium has a much higher affinity for guluronic acid (G) blocks compared to mannuronic acid (M) blocks and, when alginate is unconstrained, binding of calcium by M and alternating guluronic acid-mannurinic acid (MG) blocks is energetically unfavourable [106]. The marked increase in the binding capacity at the start of the second phase of binding may indicate that a new mode of binding had become energetically highly favorable. Such an occurrence would indicate some major change in the state of the Ca-alginate binding system. Under conditions of high calcium concentration, leading to the saturation of G block binding sites and resultant changes in conformation of the Ca-alginate complex, binding by MG blocks, for example, via formation of secondary junctions, may become energetically favorable [107]. Alternatively, or perhaps in addition, collapse of the gel structure at high

calcium concentrations may result in exposure of binding sites previously inaccessible to solution phase calcium due to the formation of an impermeable gel structure during Stage III of the first phase of binding. These newly accessible binding sites are likely to be a mixture of G, MG, and M blocks that, due to the now more constrained conformation, provide enhanced energetic favorability for binding as evidenced by the moderately steep slopes of the binding plots during this phase (Figure 3-1).

3.4.2.2. Calcite precipitation

The distinct switch in calcium uptake behaviour and the linear slope of the binding plots during the second phase (Figure 3-1) are behaviour that might be expected if $CaCO_3$(s) had commenced precipitation at this level of calcium addition. However, speciation analysis (Visual MINTEQ) of the bulk solution in equilibrium with atmospheric CO_2 indicated that at pH 7.5, a calcium concentration of 43 mM is required to reach the solubility limit for $CaCO_3$ and therefore, at the observed critical concentration of 6 mM, the system is undersaturated with respect to $CaCO_3$. Nevertheless, this analysis does not take into account the possible role that alginate may play in $CaCO_3$ precipitation.

The impact of alginate on $CaCO_3$ precipitation has been investigated by a number of workers. The presence of alginate may lower the energy barrier and provide sites for the nucleation of $CaCO_3$ [107, 108]. Sites of calcium adsorption on the surfaces of cyanobacterial cells are thought to act as sites of calcite nucleation [109] and localized concentrations of calcium due to adsorption by EPS may cause local supersaturation of calcite [110]. Due to its lower surface energy, aragonite has been

proposed as the likely phase resulting from EPS induced nucleation but, because of the lack of long range order and small size, this phenomenon may be difficult to detect [111]. A mechanism has been proposed whereby EPS binding sites are reorganized creating a template enabling $CaCO_3$ nucleation [112, 113]. Such reorganization could result from the relatively ordered complexation of calcium and formation of junction zones. However, in all studies described above, the systems under investigation were closer to $CaCO_3$(s) saturation than is the case here.

From the slope of the linear sections of binding plots, it can be seen that not all of the added calcium is being taken up during the enhanced calcium uptake phase; rather, it is a constant proportion of the added calcium with this observation confirmed by the constant value of the Scatchard plot ordinate (R/[Ca]$_{free}$) in this region. This differs from what might be expected from $CaCO_3$ precipitation where, given sufficient carbonate, all added calcium would be expected to be removed by precipitation and free calcium would remain constant once the solubility limit has been exceeded and nucleation occurred. That this is not the case argues against significant calcium carbonate precipitation, at least at the concentrations used in this study.

Of the two possible mechanisms discussed above, the balance of evidence would suggest that an enhanced binding mechanism is responsible for the switch in physical property behaviour. While the data superficially suggests that $CaCO_3$ precipitation has occurred, the significant under-saturation of the system and the continued increase in free Ca^{2+} with calcium addition renders this possibility unlikely. Further lending support to this hypothesis are the SEM images, which do not reveal $CaCO_3$ precipitation, at least within the micron size range.

3.4.3. Mechanisms for improved cake filterability

The controls on cake filterability are varied and complex [114], however, the coincidence of the changes in calcium binding behaviour in the bulk solution and resistance of the cake layer indicates that the two are closely related and provides strong evidence that calcium concentration is controlling both bulk solution properties and gel/cake layer formation. As such, the mechanism of improved filterability of the cake layer should be considered within the context of the properties of the filterable components of the bulk solution that accumulate at the membrane surface.

3.4.3.1. Viscosity

The viscosity of the bulk solution is high at low calcium concentrations as shown in Figure 3-3 with the possibility that the local viscosity of the gel formed on membrane surface may have been even higher [115]. However, further calcium concentration increase beyond 6 mM leads to a dramatic decrease in viscosity with this decrease presumably associated with the calcium-induced breakdown of the gel structure (Figure 3-10) and subsequent aggregation of alginate gel particles at high calcium concentrations [102, 116]. Low viscosity results in a lower transmembrane pressure and consequently a lower cake resistance [86, 115].

3.4.3.2. Aggregate size

The specific cake resistance is inversely proportional to the particle diameter according to the Carman-Kozeny equation and, as such, the combination of lower viscosity and larger floc size could lead to significant filterability improvement [28,

86]. At low calcium concentration, the size of the Ca-alginate assemblage is small as shown in Figure 3-4. However, as further calcium is added, a dramatic increase in size was observed with this increase in size likely to be occurring because of i) the reduction in repulsive charge between alginate groups resulting from calcium binding and/or ii) calcium bridging of alginate groups and/or (at very high calcium concentration only) iii) calcium carbonate precipitation [117]. An "enhanced aggregation" process similar to that proposed for alginate coated hematite particles may also be operative where suspended alginate polymers are bridged and bound to each other on particle surfaces via calcium complexation to form larger alginate clusters which may significantly accelerate the rate of aggregate formation and growth in overall aggregate size [118].

Large alginate aggregates have been proposed to have little capability to participate in gel formation since the alginate binding sites are likely saturated and incapable of binding other alginate molecules [87]. The size of the Ca-alginate assemblage would also be expected to play a role in whether the deposit formed on the membrane surface is gel-like or more characteristic of a more porous cake layer with larger particles generally forming more open cake structures than the more impermeable assemblages formed from smaller particles [84].

3.4.3.3. Syneresis

A key indication of transfer from gelation to the more permeable cake deposit is the significant volume reduction of the Ca-alginate gel (Figure 3-5) with average porosity decreasing almost linearly with increasing calcium concentration beyond the critical calcium concentration of ~6 mM. A progressive reduction in the water content

(or syneresis) on increasing calcium concentration would be expected as the assemblage becomes more densely cross-linked and more compact [119, 120]. A similar reduction in gel volume on increasing calcium concentration has been reported by Martinsen et al. [35] with Draget et al. observing a dramatic increase in syneresis on exposure of alginate gels to increasing concentrations of calcium [36].

This decrease in gel layer water content has been suggested as being due to the involvement of MG binding at higher calcium concentrations as the dimensions of the networks formed from interaction of poly(MG) chains are recognized to be substantially less than that of assemblages formed from interaction of poly(G) chains [121, 122]. Therefore, the involvement of MG alternating sequences in the presence of increasing calcium concentrations, possibly via the formation of secondary (MG/MG) junctions, should enhance the syneresis process and, as a consequence, lead to collapse of the gel network [107, 123]. Collapse of the gel network may well expose functional groups previously "hidden" within the relatively inaccessible gel to Ca2+ ions. An even more rapid collapse of the gel network due to the lowering of repulsive negative charge within the assemblage may ensue with resultant dewatering and volume reduction [106]. Despite the denser nature of the collapsed alginate assemblage on the membrane, the fouling layer exhibits higher hydraulic conductivity than the gelatinous assemblage that predominates at lower calcium concentrations.

Very similar behaviour to that described here has previously been reported in studies of the effect of Ca2+ ions on the hydraulic behaviour of montmorillonite assemblages formed on membranes [97]. The hydraulic conductivity of the filter cakes was dramatically affected by suspension calcium concentration with significantly higher hydraulic conductivity observed at the higher calcium

concentrations compared to that observed at lower concentrations. Cake moisture profiles of the montmorillonite system showed that high calcium concentration resulted in denser or less voluminous filter cakes that retained less water (and exhibited lower resistance) than was the case at the low calcium concentration. These changes were observed by a transformation from a highly "cross-linked" voluminous honeycomb type structure of low permeability at low calcium concentrations, to that of a high permeability, nematically ordered and more compact structure at high calcium concentrations. In the case of Ca-alginate, our SEM results suggest the formation of a vastly different structural assemblage at high calcium concentration. An increase in the calcium concentration from 6 to 12 mM resulted in a marked void size reduction (Figure 3-9), along with a consolidation of the filter cake assemblage (Figure 3-5). The more compact structure observed at 12 mM Ca (Figure 3-9b) displays some nematic ordering in parallel with the membrane surface (and imposed pressure), likely due to the associated dewatering and compression of the assemblage. The resultant increase in hydraulic conductivity at higher Ca concentrations is likely due to a reduction in forces acting to retard water movement through the assemblage together with a greater interconnectivity between pores [124].

The proposed sequence of events occurring in the alginate system on increase in calcium concentration are summarized below and depicted in Figure 3-10.

- At very low calcium concentrations (< 1 mM), calcium binds strongly in suspension to G block sites forming dimer chains of GG blocks with our results indicating that one calcium ion can binds approximately four G blocks. These unrestricted chains accumulate on the membrane surface forming a gel-like water impermeable fouling layer.

- At slightly higher calcium concentrations (2 to 6 mM), multimers form and cross-linking supports gel formation. Calcium ions are unable to access sites within the gel leading to an increase in free calcium ion concentration in solution (reaching calcium binding saturation) with minimal associated change in gel layer properties on the membrane. Higher alginate concentrations tend to form larger gel structures leading to a greater fraction of inaccessible sites.
- Further increase in calcium concentration (> 6 mM) results in calcium binding to M and MG sites leading to increased charge shielding and cross-linking and a breakdown in gel structure. The newly accessible binding sites permit further Ca2+ binding leading to collapse of the gel network. These gel aggregates form higher solid content yet more porous assemblages on the membrane surface resulting in improved filterability.

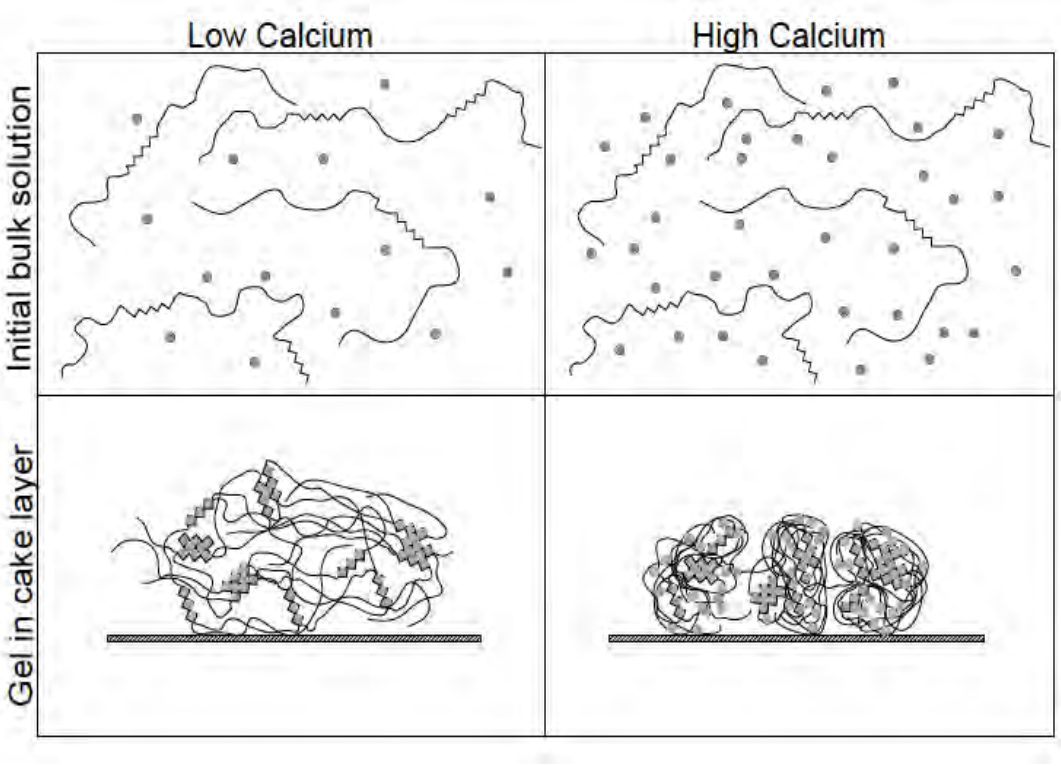

Figure 3-10. Schematic of proposed mechanism of gel-network collapse at high calcium concentration resulting in increased access to internal Ca-binding sites as well as the improvement of filtration performance.

3.5. Conclusions

This chapter has shown here that the changes in calcium binding behaviour of alginate in bulk solution and resistance of the cake layer formed on flat sheet membranes are closely related with calcium concentration controlling both the alginate characteristics in bulk solution and the properties of the gel/cake layer formed. In brief, at low calcium concentrations, Ca^{2+} ions interact strongly with G block functional groups to form high water content, highly impermeable gels on the membrane surface. A further increase in calcium concentration results in the breakdown of the gel structure with aggregation of alginate units in suspension and the formation of a highly porous assemblage on the membrane surface. Similar

dramatic sensitivity of the behaviour of fouling layers formed on membranes in membrane bioreactors is to be expected where alginate-like polysaccharides are known to undergo gel formation at low calcium concentrations but aggregate at higher calcium concentrations with resultant formation of substantially more porous (and less troublesome) cake layers.

The materials properties of the alginate layers formed on flat sheet membranes have been determined for a range of calcium concentrations and applied pressures. These materials properties provide a description of both fouling layer hydraulic conductivity and compressibility as a function of applied pressure and, as such, could be used to determine the expected filterability of an alginate solution for any calcium concentration and trans-membrane pressure. As such, the information obtained here could well be applied (in a manner similar to that described previously (Kovalsky et al., 2009 [89]; Yang et al., 2011 [125])) to predict the filtration behaviour of an alginate-rich solution for a range of calcium concentrations under constant flux (and thus time varying TMP) conditions.

Chapter 4. Effects of Ionic Strength on Membrane Fouling by Alginate Gels in the Presence of Calcium

4.1. Introduction

The increasing use of membrane bioreactors (MBRs) for the treatment of wastewaters is driven by the shortage of potable water around the world and the increasingly stringent effluent quality requirements. MBRs are also relatively easy to operate and require less space thereby rendering them suitable for decentralised use where reuse of the treated wastewater may be desired. Despite these attractive attributes, the separation process is inevitably plagued by membrane fouling as a result of its ability to reject particles, colloids and, depending on the membrane pore size, certain solutes. While coarse bubbling in the membrane zone is reasonably effective at removal of large sludge particulates from the membrane surface, particular problems are experienced with the gelatinous assemblages that are formed on retention of extracellular polymeric substances (EPS) present in the MBR supernatant [2-6]. Use of a separate coagulation/flocculation/sedimentation process prior to membrane filtration, in which coagulant chemicals are added to adsorb solutes and the resulting particulate assemblages given time to grow in size and settle out of suspension, can assist in minimizing the severity of fouling but comes at the expense of significantly reduced throughputs, increased plant size and substantial increases in chemicals and waste disposal costs [63, 64]. As a result, submerged

MBR systems where the membranes are placed directly in the wastewater are preferred with coagulating chemicals added to the reactor to assist in solute removal. Successful operation of such a system however requires a clear understanding of the relationship between coagulant behaviour and filtration performance with many factors likely to influence this relationship including the type and dose of coagulant used and the composition of the aqueous stream including dissolved salts concentration and pH.

The EPS mentioned earlier not only induces severe fouling in its own right but influences the aggregation of bacteria [126, 127]. Indeed, 3-5 times more exocellular polymer has been found in the settled sludge than in the clear liquor after settling velocity and sludge volume index (SVI) tests, suggesting that the EPS readily associates with microorganisms during the settling process [126]. The aggregation/gelation behaviour of the EPS will be strongly influenced by the ionic composition of the medium with divalent cations such as calcium and magnesium recognised to play a key role in polysaccharide behaviour through ion binding and bridging mechanisms [70, 71, 75, 127-130]. Indeed, DLVO theory suggests that calcium concentrations of 0.36 to 1 mM should be sufficient to induce EPS flocculation [73, 75] though this theory does not account for Ca-induced gelation of polysaccharides which is recognized to induce severe fouling in membrane filtration at intermediate concentrations but to result in more porous assemblages at high calcium concentrations [131].

While the flocculation behaviour of EPS is particularly strongly influenced by divalent cations, the presence of monovalent cations is also recognised to influence polysaccharide aggregation behaviour. Thus, an ionic strength on the order of 5 to 50

mM has been reported to result in optimum floc stability [71], but an appropriate ratio of monovalent to divalent cations (M/D) should be maintained as well because monovalent cations compete with divalent cations for binding sites of EPS. Not only will the ionic strength affect the properties of bulk solution, but also the gel layer formation on the membrane surface. Ionic strength has significant impact on membrane fouling due to the membrane-foulant and foulant-foulant interactions by altering the surface properties of membrane and foulants. Generally, a high ionic strength would enhance the accumulation of foulants on membrane surface [132]. For example, increasing the ionic strength by the KCl or NaCl addition increases the filtration resistance due to the formation of a denser gel as a result of decreased electro-static repulsion between the macromolecules [115].

Therefore, based on above discussions, both concentrations of EPS and balance of cations are vital for the flocculation and filtration processes. Since polysaccharide (PS) in EPS plays a particular important role responsible for aggregation and severe membrane fouling, I have again selected alginate as a surrogate of PS in this study. As noted in previous chapters, alginate is one of the principle polysaccharides produced by the commonly occurring Pseudomonas and Azotobacter species [133] and consists of α-L-guluronate (G unit) and 1,4-linked β-D-mannuronate (M unit) residues [35, 105]. Since last chapter has investigated the effect of calcium concentration in solution-phase binding and cake filtration behaviour in the Ca-alginate system and has observed that the alginate concentration does not have a significant influence on solution binding and cake properties [134], this chapter will focus on the effects of different ionic strengths generated by the addition of NaCl on i) the calcium binding behaviour of alginate in solution, ii) the characteristics of the resultant aggregates, and iii) the characteristics of the assemblages formed during

dead-end constant pressure filtration. The results obtained demonstrate the contrasting effects of sodium and calcium in alginate fouling and provide insight into the interplay between mono- and di-valent cations on solution phase binding and surface gelation/aggregation processes.

4.2. Materials and methods

4.2.1. Materials

Sodium alginate (Sigma-Aldrich Product No. 180947) that was mannuronate-rich (61% M, 39% G) with molecular weight (MW) ranging between 120000 and 190000 $gmol^{-1}$ was used as received in all ion-binding and filtration experiments. Sodium alginate solutions of 0.4 $g.L^{-1}$ were prepared in high-purity water (Milli-Q, Millipore) with 2 mM morpholinepropanesulfonic acid (MOPS) and 1 mM $NaHCO_3$ as buffer (resulting in pH ~7), and various concentrations of NaCl depending on the required ionic strength. These solutions were mechanically stirred until well dispersed then the required amount of $CaCl_2$ was added to the dispersion followed by overnight stirring. The pH was then adjusted by acid/base addition to 7.50 with the pH measured using an Orion 5 Star multifunctional meter (Thermo Electro Corporation, USA) prior to filtration.

4.2.2. Bulk solution

4.2.2.1. Calcium binding to alginate

The binding of calcium to alginate was examined by measuring the activity of free calcium ions (using an Orion ion selective electrode in conjunction with an Orion 5

Star multifunctional meter) in the Ca-alginate solutions after overnight equilibration. The calibration curves for the ion selective electrode were made using $CaCl_2$ solution of known concentrations at the relevant ionic strengths. Free calcium measurements were also carried out using dialysis bags to confirm that interference of the probe by either the alginate or Ca-alginate complex was not occurring.

4.2.2.2. Size and zeta-potential

Size and zeta-potential of the Ca-alginate aggregates were measured by laser Doppler micro-electrophoresis and dynamic light scattering (DLS) respectively using a Malvern Zetasizer Nano ZS. Sodium alginate solutions after overnight stirring were adjusted to pH 7.5 and filtered (0.45um Millex-HN syringe) prior to calcium addition in order to remove dust and large aggregates. The concentration of alginate in the solutions was unchanged by filtration as determined by total organic carbon (TOC) (Shimadzu TOC-500) measurements. Size and zeta-potential were measured immediately after calcium addition with no significant change evident after sitting for 24 hours.

4.2.2.3. Viscosity

The viscosity of samples prepared in the same manner as for the Ca-alginate size measurements was determined using a DV-79 digital viscometer (Shanghai Bilon Instrument Co. Ltd).

4.2.2.4. General filtration methods and the determination/modelling of material properties

Constant pressure dead-end filtration was applied for the prediction of filtration behaviour and material properties. Detailed filtration setup and methods, and the determination/modelling of cake properties in alginate systems have been provided in Chapter 2 General Experimental Methods and Modelling Approaches.

4.3. Results

4.3.1. Characteristics of bulk solution

4.3.1.1. Calcium binding to alginate

From binding plots for calcium addition to 0.4 $g.L^{-1}$ alginate (Figure 4-1), two phases of binding can be identified. During the first phase the concentration of bound calcium (*R* is the average number of calcium ions bound per G unit) begins to plateau as calcium is added, suggesting typical binding behaviour with binding sites becoming progressively saturated. Values of *R* at saturation range between 0.75 and 1.2 and increase with decrease in ionic strength. The second phase is characterized by an increased rate of calcium uptake (per unit added calcium) that is maintained to the end of the titration resulting in a linear binding plot (Figure 4-1) [134]. The transition between the first and second phases occurred between 4 to 6 mM of added calcium for 10, 20 and 50 mM NaCl, with lower ionic strength leading to transition at a lower calcium concentration. For 200 mM NaCl, only the first phase is readily apparent.

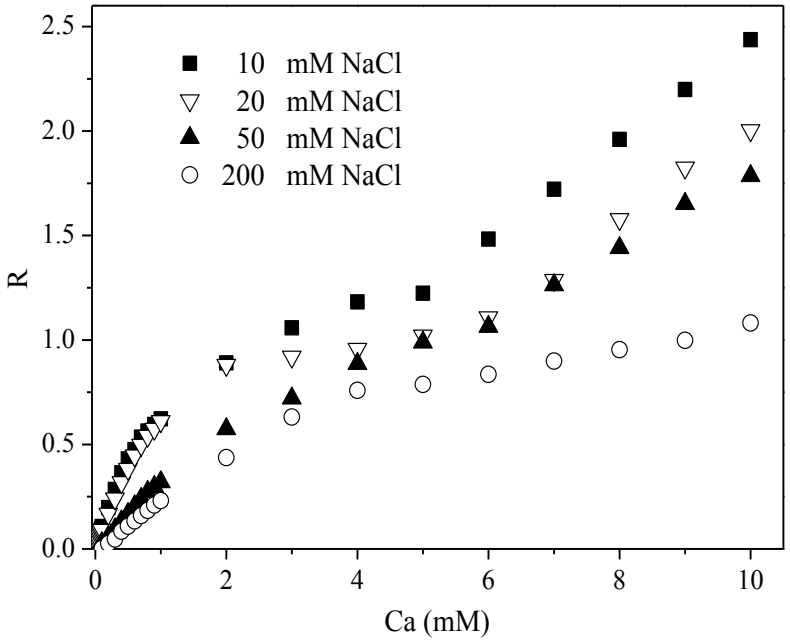

Figure 4-1. Uptake of calcium as a function of total calcium concentration at NaCl concentrations of 10, 20, 50 and 200 mM. R is the molar ratio of bound calcium to G residues calculated from measurements of free calcium by ion-selective electrode following 24 hours equilibration and the known guluronate content of the alginate. Error bars are eliminated for clarity.

Binding plots in the Scatchard form of Figure 4-2 (a) and (b) reveal more details of binding behaviour. As reported earlier [134], the initial positive cooperative binding corresponds to the saturation phase, while the subsequent plateau region is related to the second linear section of enhanced calcium uptake. However, the value of $R/[Ca]_{free}$ in the Scatchard plot is always lower in the presence of greater NaCl concentrations, and the initial cooperative binding is more distinct at higher NaCl concentrations of 50 and 200 mM compared to that at 10 and 20 mM NaCl. In addition, the transition to the second phase where the ratio of $R/[Ca]_{free}$ becomes independent of added calcium in the Scatchard plot, also occurs at higher total calcium concentration in higher ionic strength solutions as in the binding plot (the

solid symbols represent studies with calcium concentrations from 0.01 to 1 mM while the open symbols represent studies where the calcium concentrations are 2 to 10 mM).

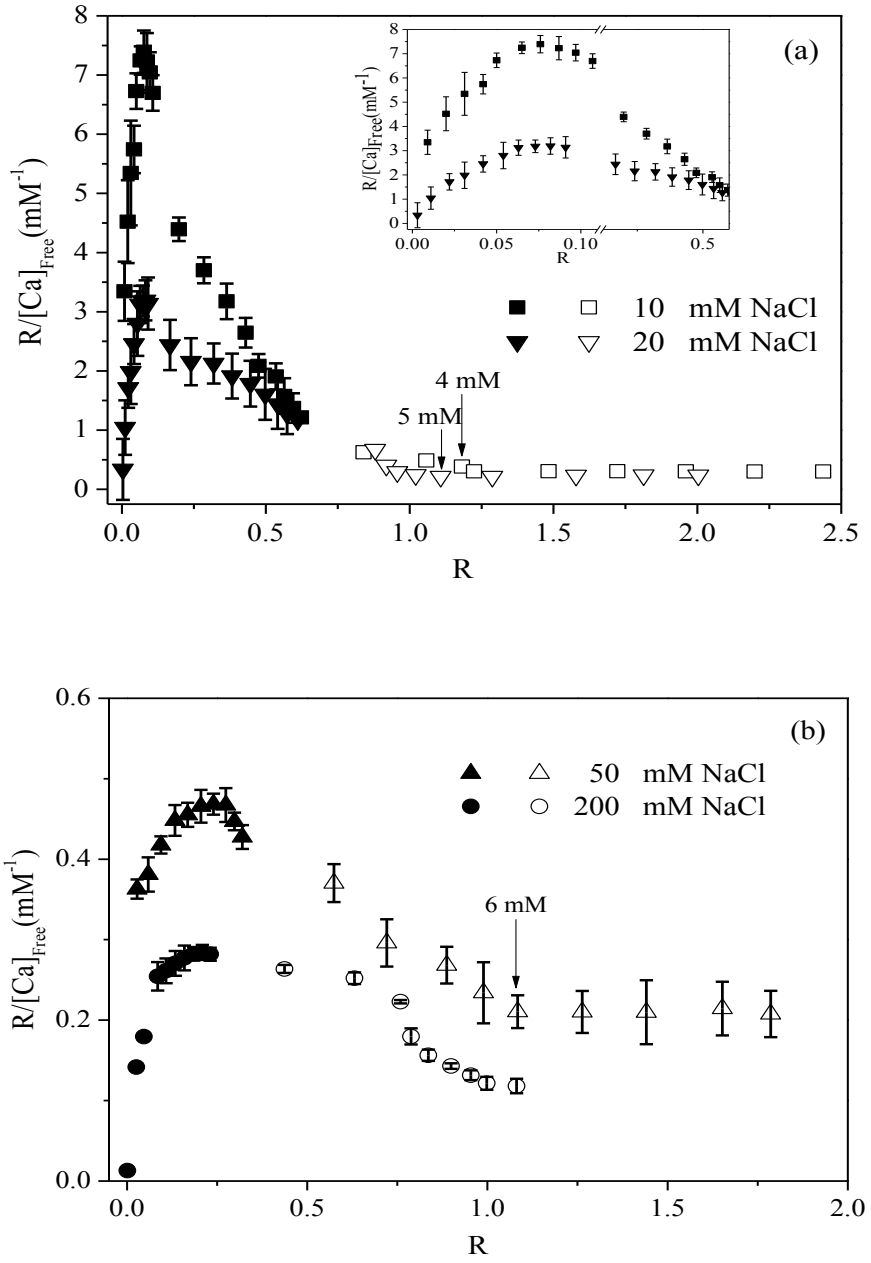

Figure 4-2. Scatchard plot derived from Figure 4-1 at NaCl concentrations of (a) 10, 20 mM (insert shows the cooperative binding at low R values) and (b) 50, 200 mM (the solid symbols represent solutions with calcium concentrations ranging from 0.01 to 1 mM while the open symbols represent solutions with calcium concentrations ranging from 2 to 10 mM calcium). Standard errors bars are from duplicate measurements.

4.3.1.2. Size

If only considering the effect of Na^+ ions without calcium addition, the alginate size decreases as ionic strength increases (Figure 4-3 (insert)). Similar behaviour has been reported by Frank and Belfort (2003) who found that the hydrodynamic radii of anionic polysaccharide decreased on increasing KCl concentration [21]. It has been proposed that the introduction of electrolytes results in electrostatic shielding of alginate functional groups causing the folding and retraction of the polyelectrolyte [118]. The charge of the alginate molecules is also reduced due to NaCl addition, presumably leading to greater self-entanglement of the polymer chains, which reduces the size of the molecules in solution [21].

Upon calcium addition, the size change initially displays similar behaviour to that observed in 50 mM NaCl solutions in Chapter 3 [134]; that is, a reduction in size at low calcium concentrations due possibly to both greater self-entanglement as a result of electrostatic shielding and to the formation of more compact egg-box structures. At higher calcium concentrations however, an increase in assemblage size is observed due most likely to the association of "egg-box" dimmers or multimers and, at high calcium concentrations, a more significant increase in size as calcium induces aggregation of particles.

The effect of NaCl concentration on the calcium-induced changes in size is dramatic with a high (200 mM) concentration of NaCl essentially inhibiting these effects of calcium addition (Figure 4-3).

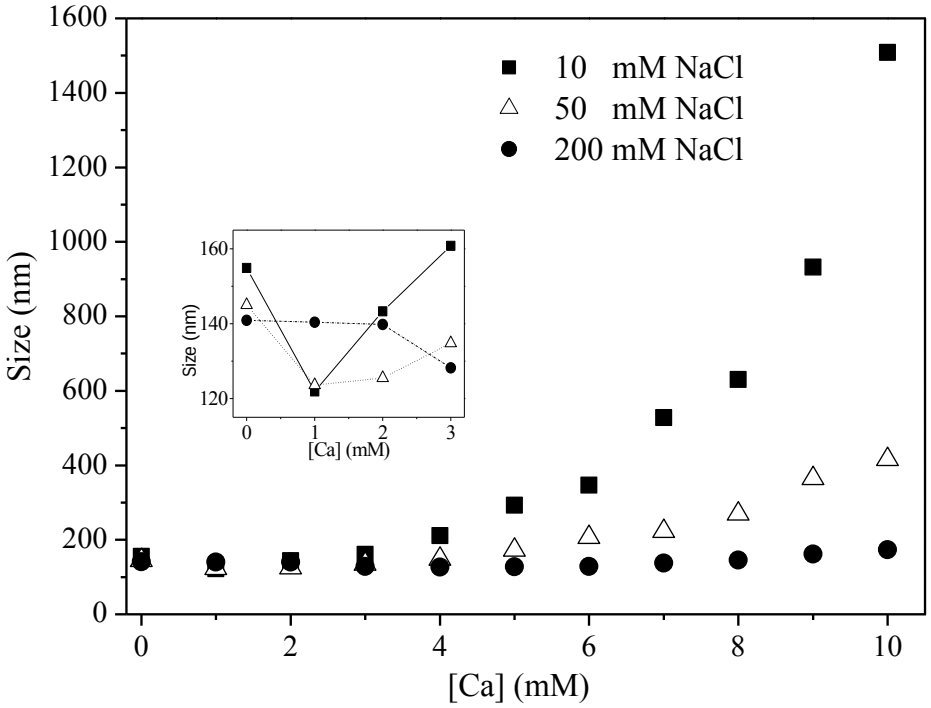

Figure 4-3. Size of Ca-alginate assemblages as a function of total calcium concentration at NaCl concentrations of 10, 50 and 200 mM. Size measured using dynamic light scattering. Error bars are eliminated for clarity.

4.3.1.3. Zeta potential

In the absence of calcium, increased NaCl concentrations results in a significant decrease in the absolute value of the zeta potential from around -60 mV in 10 mM NaCl, to -37 mV in 50 mM NaCl and -20 mV in 200 mM NaCl (Figure 4-4), indicating the role of Na^+ ions in charge neutralization of alginate molecules. As expected, the zeta potential increases (becomes less negative) on increasing calcium concentration, with the most dramatic effect in solutions of lowest NaCl concentration (10 mM) although it remained below -25 mV even with 10 mM calcium addition. In comparison, the change in zeta potential in 200 mM NaCl was almost negligible. The significant influence of NaCl on zeta-potential is consistent with the effect of NaCl on change in particle size.

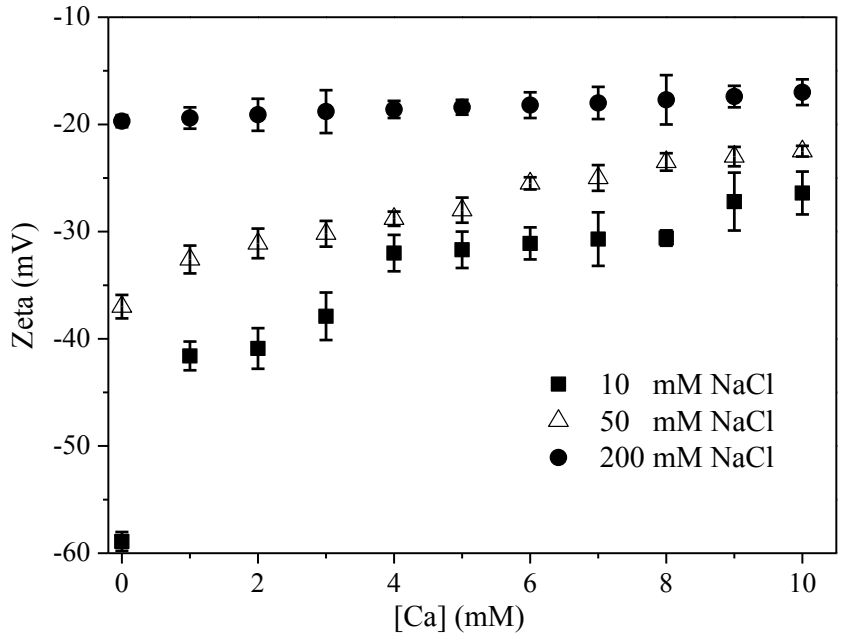

Figure 4-4. Zeta-potential of Ca-alginate assemblages as a function of total calcium concentration at NaCl concentrations of 10, 50 and 200 mM. Standard errors bars are from duplicate measurements.

4.3.1.4. Viscosity

At relatively low ionic strengths of 10 and 50 mM NaCl, the viscosity decreases on addition of calcium [134] with the effect being larger for lower NaCl concentrations (Figure 4-5). However, the viscosity variation is small and remains almost constant in 200 mM NaCl, which is in agreement with the reported viscosity change for high ionic strength solution [102].

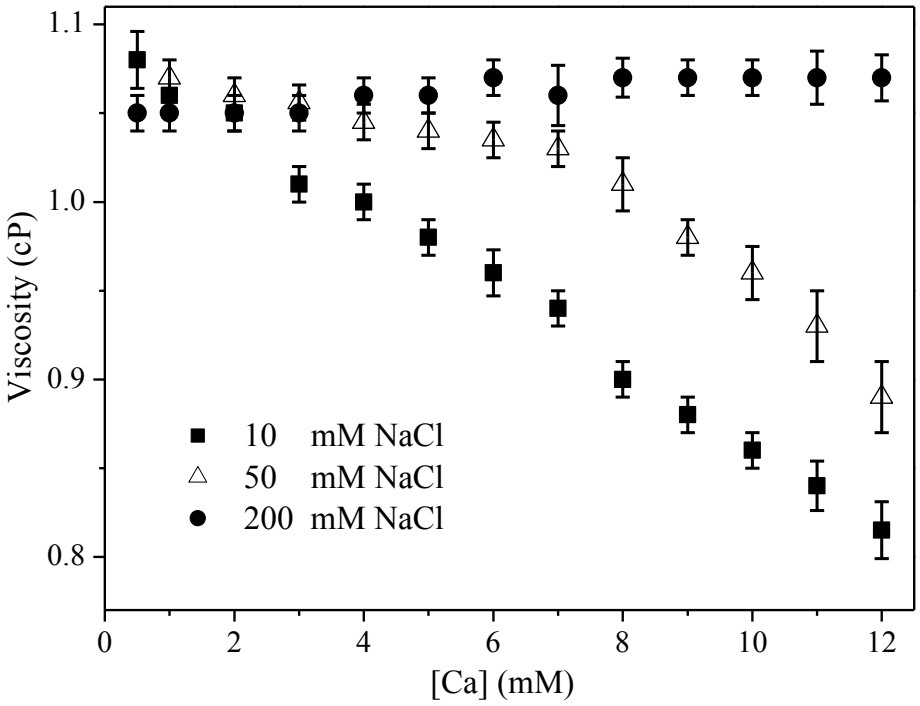

Figure 4-5. Viscosity of Ca-alginate assemblages as a function of total calcium concentration at NaCl concentrations of 10, 50 and 200 mM. Standard errors bars are from duplicate measurements.

4.3.2. Cake properties

4.3.2.1. Porosity

The effect of calcium on cake porosity (Figure 4-6) displays a similar pattern to that on viscosity and could be related [102]. At lower NaCl concentrations of 10, 20 and 50 mM, porosity decreases on increasing calcium addition with the rate of decrease increasing as NaCl concentration decreases. However, for 200 mM NaCl, the porosity is high and almost unchanged although it is substantially lower at 1 mM calcium than the other NaCl concentrations.

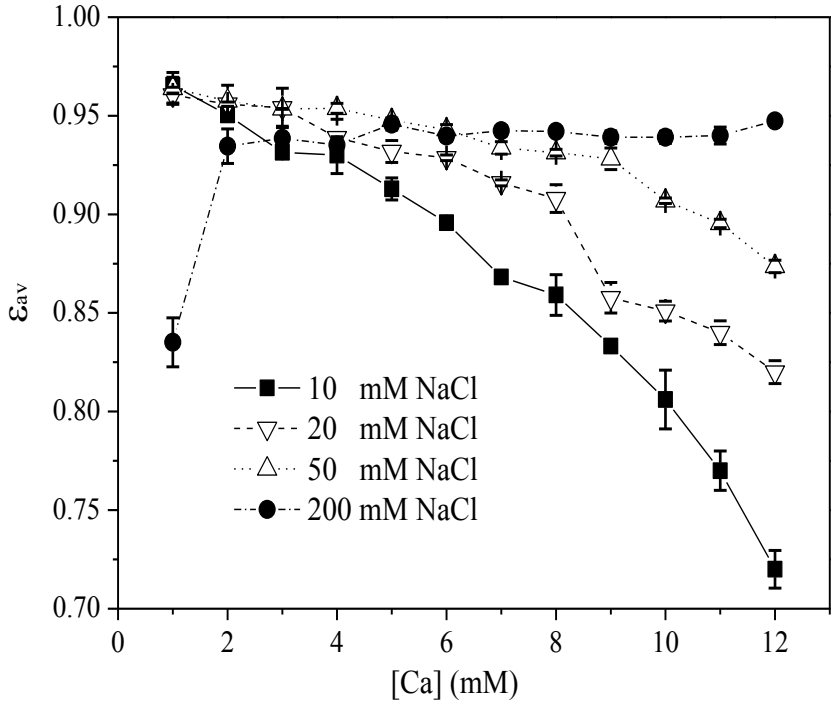

Figure 4-6. Porosity (ε_{av}) of Ca-alginate cake-layer formed at 135 kPa during dead-end filtration at different calcium concentrations for NaCl concentrations of 10, 20, 50 and 200 mM. Standard errors bars are from duplicate measurements.

4.3.2.2. Cake resistance

The pattern for the dependency of cake resistance on calcium concentration is similar to that of porosity (Figure 4-7). At NaCl concentrations of 10, 20, and 50 mM, cake resistance is high at low calcium concentration, but further calcium addition resulted in a sharp decrease with the onset of decrease occurring at higher levels of calcium addition as NaCl concentration increased. The decrease of cake resistance commenced at 4, 5, and 6 mM calcium respectively for 10, 20, and 50 mM NaCl, which correspond to the occurrence of enhanced calcium uptake in the binding plot. However, in the presence of 200 mM NaCl, the effect of calcium addition on cake resistance is almost completely opposite to that at lower NaCl concentrations, where

resistance increased as increasing calcium concentration to 3 mM but then remained very high and almost constant (compared to the sharp decrease observed at high calcium concentrations at lower NaCl concentrations).

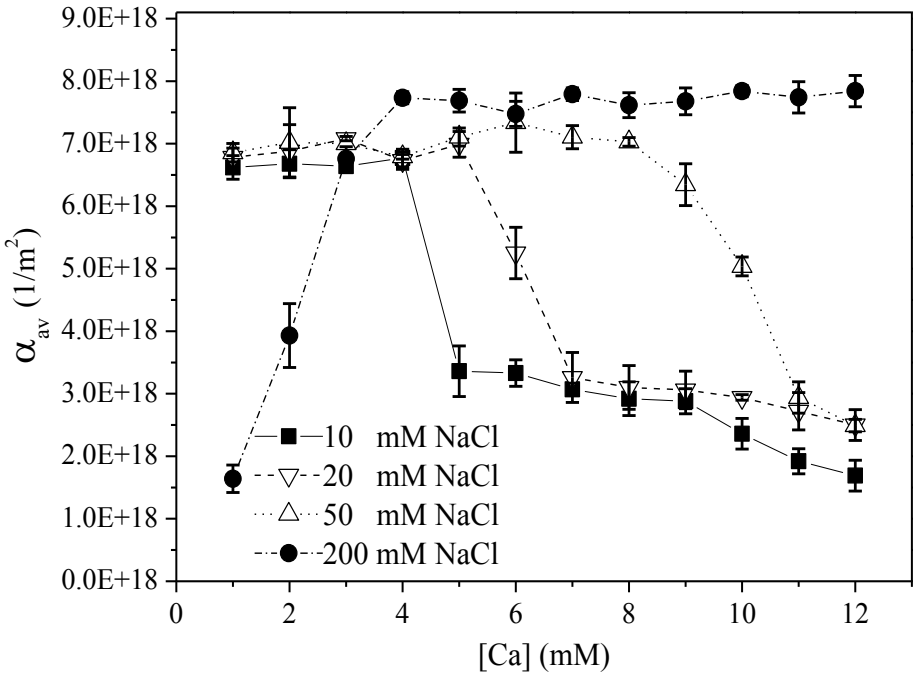

Figure 4-7. Resistance (α_{av}) of Ca-alginate cake-layer formed at 135 kPa during dead-end filtration at different calcium concentrations for NaCl concentrations of 10, 20, 50 and 200 mM. Standard errors bars are from duplicate measurements.

4.4. Discussion

4.4.1. Binding behaviour of Ca-alginate in the presence of NaCl

The binding of calcium to alginate has previously been divided into two distinct phases [134]. The initial binding stage of calcium to alginate reveals typical positive cooperative binding in the Scatchard plots (asymptotically approaching saturation in the binding plots) with this behaviour first suggested by Grant et al. [39] as evidence

for the 'egg-box' model of Ca-alginate association resulting from the high stability of the dimer conformation. The second phase evident in the Scatchard plots (i.e., the "linear relationship" following the plateau region) suggests that calcium is bound at a constant proportion of added calcium. It has previously been proposed that this second phase was caused by the exposure of binding sites that were previously rendered inaccessible by the impermeable gel formed in the first phase and involved calcium binding with MG blocks at increasing calcium concentrations with this increased binding inducing collapse of the gel network [134].

4.4.1.1. Influence of NaCl on cooperative binding

The first phase in the binding plots (Figure 4-1) exhibit an initial near-linear rise with subsequent formation of a plateau region in a manner consistent with results reported for Ca-PAA (polyacrylic acid), Mn-PAA and Mn-alginate [135]. However, the convex shape of the Scatchard plots in the first phase is more distinct in 50 and 200 mM NaCl, but less so in 10 and 20 mM NaCl, indicating a lowered extent of cooperative Ca-alginate binding as ionic strength decreased. Two types of interactions have been reported depending on the solvent conditions: i) anti-cooperative character in water and ii) cooperative character in the presence of NaCl as a result of typical polyelectrolyte effects [136]. As such, it seems that the higher the ionic strength, the more cooperative is the binding of calcium ions to polysaccharides [137, 138].

Although the ionic strength could reduce anti-cooperative effects, the sharp increase in the initial part of the Scatchard plots for 10 and 20 mM NaCl (Figure 4-2(a) and insert) indicates that positive cooperativity still exists in low ionic strength

solutions. It should be noted however that these effects could be readily neglected if calcium additions were to commence at higher calcium concentration (e.g., 0.1 mM).

4.4.1.2. Influence of NaCl on the transition to second stage of enhanced calcium uptake

Since cooperative binding was complete at low calcium concentrations in the presence of lower NaCl concentrations, the subsequent transitions to the second phase of enhanced calcium uptake occurred at lower total calcium concentration for low NaCl concentrations (4, 5 and 6 mM calcium for 10, 20 and 50 mM NaCl respectively), whereas the transition is barely apparent at 10 mM calcium in 200 mM NaCl solution. However, all the transitions appear to occur consistently at $R \approx 1.1$ independent of ionic strength despite the different total calcium concentrations.

These findings differ from those of our previous study at a uniform ionic strength (of 50 mM NaCl) where a lower proportion of binding sites were accessible at higher alginate concentrations during the first binding phase (stage III) resulting in a lower transition value of R to the second binding phase [134]. It may be surmised that more contact sites exist between polymer chains in concentrated solutions than in dilute solutions and, as a result, a smaller fraction of cross-links is required to form the gel [100] during the first binding phase. Regards to the lower transition value of R at higher alginate concentration, it is probably due to that the critical R value might be achieved at the aggregate surface largely and vary within an aggregate with greater values at the surface and lower values internally. Since the transition to second phase is due to the presence of new exposed MG binding sites [134], the rapidity of gel formation at higher alginate concentration [100, 101, 139] likely renders a larger

proportion of internal sites and so with relatively lower ratio of surface area. In addition, higher alginate concentration promotes self-aggregation [104] with this process typically also resulting in the formation of larger aggregates [134] of relatively low surface area compared to the small assemblages formed at lower alginate concentration.

Excluding the alginate concentration influence in this study, *R* is constantly around 1.1 at different ionic strength, indicating it is the degree of bound calcium rather than total present in solution that is driving the onset of the second binding phase which has significant implications for aggregation and filtration behaviour. The different total calcium concentrations at transition are probably due to the blocking effects of sodium to calcium binding sites at higher NaCl concentration, and so the functional groups of alginate (including MG blocks) are not easily exposed for calcium binding.

4.4.2. Blocking effect of NaCl to Ca-alginate binding and filtration

The sodium blocking effect not only affects the total calcium required to reach the transition *R* value, but also leads to lower average bound calcium at both binding stages in the presence of higher NaCl concentrations (Figure 4-1 and 4-2). It has been investigated previously that alginate films produced in the absence of Na^+ containing significantly larger amounts of cross-linking cations (Ca^{2+}) than is the case with added Na^+ [140]. Similarly, the affinity of pectin chains for calcium ions showed a progressive decrease when the ionic strength was increased by NaCl addition [136]. In activated sludge systems, the addition of monovalent cations (Na^+, K^+) have also been shown to result in a release of Ca^{2+} from the polymer structure [69, 75]. All of

these indicate that, although alginate has a higher affinity for calcium than sodium ions due to the presence of guluronic acid blocks [102, 141], a majority of sites are covered by Na^+ in high NaCl concentration solutions resulting in less available binding sites for calcium and a much smaller degree of binding.

The sodium blocking also affects the Ca-alginate fouling behaviour. The intermolecular adhesion force (determined by AFM) is pronounced in the presence of calcium with the strength of the adhesion forces attributed to the strong bonds formed between negatively charged guluronate sites by sequestration of calcium ions. As a result, the complexes of Ca-alginate extend further into solution forming gel-like layers with high cake resistance [142]. Although sodium ions do not participate in the cross-linking of alginates in the same manner [140], the competition with calcium for carboxyl groups via an ion-exchange equilibrium would be expected to influence the extent of cross-linking throughout the entire alginate matrix and thus the alginate gelling behaviour [83, 121, 142]. The presence of sufficient sodium ions could overshadow the presence of calcium and significantly inhibit the complexation of alginate molecules with calcium thereby resulting in decreased bond strength between alginate molecules (indicated by decreasing adhesion forces). As a result, the conformation of polyelectrolytes might be expected to transform from extended structures (gels) to coiled structures behaving as individual alginate molecules typical of that observed in the absence of calcium [142, 143]. Therefore, at calcium concentrations lower than 3 mM, the cake resistance in 200 mM NaCl solution was much lower than those in lower ionic strength solutions (Figure 4-7) due to the incomplete gelation from lack of calcium cross-linking when Na^+ competed strongly for binding sties. This also leads to the lower porosity of cakes formed in 200 mM

NaCl at low calcium concentration (especially for 1 mM calcium) (Figure 4-6) because of the penetration of alginate before the gel is fully formed.

4.4.3. Aggregation mechanism

For the same calcium concentration, the size of Ca-alginate assemblages is much larger in 10 mM NaCl than is the case in 200 mM NaCl due presumably to a lower extent of bridging by calcium. This means that the extent of aggregation on the addition of calcium was far greater at lower ionic strength. At high ionic strength where there was strong competition of sodium for binding sites, higher total calcium concentrations were required to bring about aggregation.

This result is the opposite of that expected from DLVO theory where aggregation is controlled by electrostatic forces, and salt-mediated compression of the double layer decreases repulsion between particles [144]. According to DLVO, increasing NaCl concentration decreases the thickness of the double layer and the repulsive forces between alginate chains thereby allowing short-range attractive forces to promote aggregation. This is obviously not the case in Ca-alginate system. From a zeta-potential perspective, significant size increase in 10 mM NaCl solution occurred at low calcium concentration before zeta-potential reduced to an unstable value (i.e. -30 to 30mV), while in 200 mM NaCl solution, aggregation was barely detected even though the zeta-potential consistently ranges between -20 to -17 mV. This indicates that aggregation did not accompany a lower absolute value of zeta-potential; an observation which does not comply with DLVO theory either.

Pavoni et al. showed that surface charge reduction was not considered a necessary precursor in biological flocculation, because microelectrophoretic mobility readings

clearly depicted a relatively constant bacterial surface charge regardless of the flocculability of the culture [145]. Therefore, Ca-alginate aggregation may be better interpreted by divalent cation-bridging (DCB) theory which is largely independent of surface charge reduction. According to DCB, divalent cations act as a bridge between cations and negatively charged functional groups through creation of a more tightly bound floc matrix within the biopolymer network with this process resulting in an increase in floc size and promotion of flocculation [73]. When sodium ions are present at high concentrations, the floc structure is weakened due to the ion-exchange process in which divalent cations are replaced by the sodium ions. Such a process has previously been involved to explain the effect of sodium ions on settling properties of activated sludge [73, 75].

In a similar manner, Chen et al. showed that, for a given calcium concentration (4.7 mM), the aggregation of alginate-coated hematite particles was diffusion controlled for sodium concentrations above a critical value (about 40 mM NaCl at pH 5.2), while aggregation was greatly enhanced at lower NaCl concentrations [146]. This result suggests that when Na-blocking is decreased sufficiently to allow calcium bridging, aggregation is greatly enhanced by any further calcium bridging. The results described here are in line with those of Chen et al. [146] showing that either decreasing NaCl concentration (for constant calcium concentration) or increasing total calcium concentration (for a particular sodium concentration) could result in aggregation once the sodium blocking effect is overcome and sufficient calcium is present to bridge alginate units.

4.4.4. Effect of NaCl on Ca-alginate cake properties

4.4.4.1. Biphasic filtration behaviour

The presence of calcium in feed waters has often been thought to promote intermolecular interactions and to be responsible for high cake resistance due to the formation of gels on the membrane [7, 147, 148] though others have shown the exact opposite effect of the presence of calcium resulting in a lowering of the fouling layer resistance because of the formation of agglomerates [115, 149]. Recently, the biphasic effect of calcium on the filterability of alginate solutions has been reported where progressive addition of calcium initially reduced filtrate flux but then improved it during the filtration of alginate [86, 87]. Our own studies have further confirmed and elaborated these effects [134].

This study further demonstrates that for any particular NaCl concentration, the biphasic filtration behaviour of Ca-alginate is essentially unchanged. At low calcium concentrations, calcium interacts strongly with G block functional groups to form highly impermeable gels with high cake resistance on the membrane surface with further increase in calcium concentration resulting in eventual breakdown in gel structure and formation of highly porous assemblages associated with the occurrence of aggregation in bulk [134]. However, the critical calcium concentration at which a sharp reduction in cake resistance occurred was lower for the solutions of lower ionic strength, namely, 4, 5 and 6 mM total calcium for 10, 20 and 50 mM NaCl respectively. Nevertheless, these critical concentrations still match well with the transition concentration of enhanced calcium uptake regime identified in the Scatchard plots, which further supports the strong link between the Ca-alginate

binding behaviour in solution and the cake properties formed from bulk aggregates regardless of ionic strength. This strong link is also supported by the decreased viscosity (Figure 4-5) and increased size (Figure 4-3) which were shown to improve the filtration behaviour previously [134]. In addition, the progressive reduction in porosity (increased syneresis) of Ca-alginate gels with increasing calcium concentration is another significant indicator of reduced cake resistance [134].

4.4.4.2. Syneresis

The change in porosity follows a similar trend to that observed for cake resistance; i.e., smaller values at lower ionic strength, though the transition points are not that pronounced. Cations are responsible for maintaining the gel structure, but the extent to which the alginate matrix exhibits de-watering will depend on the ratio of Na^+ to Ca^{2+} [35, 121]. At lower ionic strength, most carboxylate sites are occupied by calcium ions due to less sodium blocking, and so a more densely cross-linked but less swelled structure is to be expected. This also favors the involvement of MG binding and the collapse of gel network at higher calcium concentrations as discussed earlier, leading to reduced cake resistance. However, the presence of high sodium concentrations prevents the volume reduction of the gel by displacement of divalent cations with sodium ions [121]. As the loss of cross-links by ion displacement on guluronic residues occurs, major swelling of the gel layer takes place with an associated decrease in the solid volume fraction [35, 121, 142, 150, 151], Therefore, the porosity at 200 mM NaCl remains high even at high calcium concentrations but, as indicated in the Scatchard plot, the hypothesised phase of enhanced binding with MG blocks and resultant aggregation does not occur with resultant ongoing high cake resistance maintained.

4.4.4.3. Overall effect of sodium and calcium on filtration behaviour

As discussed above, the resistance of the cakes formed in 200 mM NaCl has the opposite fouling behaviour to that of cakes formed in lower NaCl concentration solutions, with cake resistance increasing to a peak and then remaining high. The effect of sodium on fouling behaviour has also been controversial while the calcium effect on alginate fouling has been less debated. A decreased severity of fouling with increasing ionic strength with calcium present has been reported for alginate solutions [83], whereas more severe fouling has been observed in some instances upon increasing the ionic strength of the alginate solutions [88]. In activated sludge systems, the addition of sodium has been observed to result in a significant deterioration in sludge volume index (SVI), capillary suction time (CST), specific resistance to filtration (SRF) and cake solid concentration when compared to data associated with divalent cation addition [73]. The results presented in this chapter provide an in depth explanation for the particular role of sodium and calcium in alginate fouling.

Based on our research, the effect of calcium or sodium does not simply improve or degrade the filtration behaviour of alginate solutions. The stoichiometry between calcium and sodium concentrations is expected to play an important role in the formation of an alginate gel or more permeable cake deposit. Under any sodium concentration, the effect of calcium should be biphasic as discussed, but the NaCl concentration will influence the transition calcium concentration significantly. At lower NaCl concentrations, low calcium concentrations could cause gelation because of the lower extent of sodium blocking, but the amount required to trigger reduced

cake resistance is also very low. In this situation, it is likely that the presence of calcium will improve filtration performance as a result of the biphasic behaviour observed under such conditions.

However, in 200 mM NaCl, under the same total calcium concentration (1, 2 mM) where the cake resistance is high in lower ionic strength, loss of Ca-alginate bridging due to strong sodium blocking results in insufficient bound calcium to trigger gelation; as such, it may appear that sodium addition reduces fouling. On further increase in total calcium concentration, effective charge neutralization caused by complexation of calcium cations to alginate carboxylic groups has a more significant effect (compared to charge screening induced by sodium) on electrostatic interactions which plays an important role in fouling behaviour [82]. Under such conditions, a gel layer with significant hydraulic resistance is formed, with the resistance actually even higher than those cakes formed at lower NaCl concentration. In this case, the increased sodium concentration promotes alginate gel formation by compressing the electric double layers around the alginate molecules, resulting in a reduction in electrostatic repulsion between alginate molecules in bulk solution and on the membrane surface, and thus a denser fouling layer with a higher resistance [84]. As such, under these conditions, it appears that an increase in sodium concentration results in a deterioration in filtration performance.

4.5. Conclusion

In this particular component of study, I have investigated the effect of the monavalent cation sodium on alginate aggregation and filtration behaviour over a range of calcium concentrations, and further demonstrated the strong relationship

between bulk solution and cake properties. At any NaCl concentration, the changes in calcium-alginate binding behaviour in solution relate well to the properties of the cake layer formed on flat sheet membranes with the critical transition calcium concentration to a second phase of enhanced calcium uptake in solution corresponding to the calcium concentration that causes significantly reduced cake resistance and gel breakdown on the membrane surface. However, this critical transition calcium concentration depends largely on the monavalent sodium concentration, and increases as NaCl concentration increases.

In comparison to the observation that the Ca-alginate interaction results in decreased cake resistance (at least at high calcium concentrations), the sodium blocking effect at high NaCl concentrations could also cause reduced fouling due to incomplete gelation. Alternatively, severe fouling could result at low calcium and low NaCl concentrations due to the ease of calcium-alginate bridging, or at high calcium and high NaCl concentrations once the blocking of binding sites by NaCl has been overcome. As such, it is clear that the precise impact of mono- and divalent cations on membrane fouling by polysaccharides is complex with the insights obtained here hopefully of some use in understanding both the impacts of solution composition on membrane fouling and possible changes that could be made to influence solution composition such that the severity of membrane fouling is reduced. The possibility exists that severe membrane fouling could be prevented by chemical addition but, as is clear from this study, selection of the appropriate chemical dosage by balancing the monovalent and divalent cation concentrations is far from trivial.

Chapter 5. Effect of Iron(III) on Membrane Fouling by Alginate in the Absence and Presence of Calcium

5.1. Introduction

Although the use of membrane bioreactors (MBR) has increased dramatically in recent years as a result of both the effectiveness of the treatment and the decreasing cost of membranes, significant issues remain with regard to managing membrane fouling. While coarse bubbling in the membrane zone is reasonably effective at removal of large sludge particulates from the membrane surface, particular problems are experienced with the gelatinous assemblages that are formed on retention of soluble microbial products (SMP) present in the MBR supernatant [2-4]. The well-recognized, limited removal of soluble contaminants such as phosphorus is another disadvantage of MBR technology. Commonly, chemicals such as ferric and ferrous chloride are added to assist in phosphorus removal (and are also widely used for odor control) with the most appropriate chemical dependent upon both precise treatment configuration and local chemical costs [152]. However, iron addition often increases the severity of membrane fouling.

The polysaccharide component of SMP is generally considered to be the major source of membrane fouling [3, 20] due to the formation of gelatinous assemblages as a result of the strong association between carboxylic acid functional groups present in the SMP and divalent or multi-valent metal ions [20]. Alginate has been commonly

used as a model polysaccharide in membrane fouling studies [28, 29] and is used to investigate the effect of iron addition on membrane fouling in the studies described here. The algae-derived polysaccharide, alginic acid, is a linear anionic copolymer and consists of α-L-guluronate (G) and 1,4-linked β-D-mannuronate (M) residues arranged in a non-regular pattern of varying proportions [35, 95]. Furthermore, inconsistent sequential distributions of GG, MM, and MG blocks exist along the polymer chain depending on the source of the alginate, with the flexibility (elasticity) of the polymer series increasing in the order GG < MM < MG [36, 37]. The alginate carboxyl groups play a key role in the gelation of this polysaccharide with the presence of divalent or multi-valent cations critical to the nature and extent of the gels formed [153]. Ca-alginate gels have been widely studied with a strong focus on the nature of calcium binding by the G blocks and the resultant 'egg-box' structure that is formed [39]. Interest in the formation and nature of Ca-alginate gels has been high because of their widespread use in cell encapsulation [40], wound dressing [41, 42] and other areas including food, cosmetics and agriculture [43].

Fe-alginate gels are of emerging interest as a result of their existing and potential application in the field of drug delivery systems, particularly given their biocompatibility [154-157]. Furthermore, the formation and properties of these gels may provide important insights into fouling behaviour in MBR wastewater treatment given their likely similarity to the Fe-polysaccharide assemblages that will be present in such systems. Fe-alginate ionic cross-links are established between negatively charged alginate carboxyl groups and positively charged iron through electrostatic interactions. Recent studies of the gelation mechanism of alginate solutions in the presence of ferrous (Fe(II)) iron using confocal Raman spectroscopy and viscoelastic measurements indicate relatively low binding ability of iron cations to alginate

urinate chains, with the formation of random aggregates observed to occur, in contrast to the rod-like structure exhibited by high-affinity Ca-alginate gels [158]. While these insights are useful, they provide little information on the interaction of alginate with ferric (Fe(III)) iron, especially in the mid-pH range where the solubility of ferric iron (Fe(III)) is extremely limited.

While I have recently made progress in understanding the relationship between suspension properties of Ca-alginate assemblages and the corresponding membrane fouling behaviour for different alginate and calcium concentrations [159], limited insight into the relationship between relative polysaccharide and iron content and membrane fouling is available. For example, how do the gel layer properties of Fe-alginate assemblages differ from those of Ca-alginate assemblages? Does Fe-alginate show similar biphasic fouling behaviour to that recently observed for Ca-alginate [159]? Furthermore, how does the presence of calcium influence the Fe-alginate interaction and the associated fouling behaviour? Considering the almost ubiquitous use of iron as coagulant, the amount of information available with regard to its contribution to, or mitigation of, fouling behaviour in the treatment of wastewaters is surprisingly small. This chapter addresses the issues raised above by examining the characteristics of the fouling layer formed from solutions containing various alginate and iron concentrations in the absence and presence of calcium, using constant pressure dead-end filtration methods, material properties characterization and electron micrograph imaging.

5.2. Materials and methods

5.2.1. Materials

Depending on the required iron concentration, stock solutions of 0.3, 10, 50 and 100 mM Fe(III) were prepared by dissolving an appropriate amount of $FeCl_3.6H_2O$(Sigma) in 2, 10 and 50 mM HCl with stock solutions retained for no longer than one week. Sodium alginate (Sigma-Aldrich Product No. 180947) that was mannuronate-rich (61% M, 39% G) with molecular weight (MW) ranging between 120,000 and 190,000 $g.mol^{-1}$ was used as received in all filtration experiments. Sodium alginate solutions of 0.1 and 0.4 $g.L^{-1}$ were prepared in high-purity water (Milli-Q, Millipore) containing 50 mM NaCl background electrolyte and 2 mM morpholinepropanesulfonic acid (MOPS) and 1 mM $NaHCO_3$ as buffer (resulting in pH ~7) with mechanical stirring until well dispersed. If investigating the effect of calcium, Ca-alginate solutions were prepared by adding the desired amount of $CaCl_2$ to alginate solution followed by overnight stirring. Fe(III) stock solution was subsequently pipetted into the solution of interest to achieve the required iron concentration, followed by fast mixing. The pH was adjusted by acid/base addition to 7.50 with the pH measured using an Orion 5 Star multifunctional meter (Thermo Electro Corporation, USA) prior to filtration.

5.2.2. Analytical methods

5.2.2.1. Zeta-potential and size

Sodium (or, in some cases, calcium) alginate solutions were stirred overnight, the pH adjusted to 7.50 after iron addition then the zeta-potential and size of Fe-alginate aggregates measured by laser Doppler micro-electrophoresis and dynamic light scattering (DLS) respectively using a Malvern Zetasizer Nano ZS. A Malvern 2000 Mastersizer was used when alginate sizes were too large (> 0.5 μm) for DLS measurement.

5.2.2.2. Viscosity

The viscosity of samples (prepared in the same manner as for the Fe-alginate size measurements) was determined using a DV-79 digital viscometer (Shanghai Bilon Instrument Co. Ltd).

5.2.2.3. Determination of extent of adsorbed alginate

Thirty minutes after the addition of ferric iron to the alginate solution, an aliquot of the supernatant was removed by syringe and filtered through a 0.45 μm Millex-HN filter. The total organic carbon (TOC) content of the filtrate was determined using a Shimadzu TOC-5000 analyzer and the concentration of alginate in the supernatant determined from the TOC content by reference to a calibration curve relating alginate concentration to TOC content. The concentration of alginate adsorbed to any iron oxyhydroxides formed (in the 30 minutes following ferric iron addition) and which did not pass through the 0.45 μm filters was determined by subtracting the supernatant alginate concentration from the total concentration of alginate used.

While particles of size less than 0.45 μm may pass through the filter and the organic content of these particles be determined in the TOC analysis, the extent to which this occurs is expected to be minimal in view of the relatively large size of assemblages formed under the conditions used in these studies.

5.2.2.4. Kinetics of Fe(III) complexation by alginate

The competitive ligand method was used to determine the rate of complexation of ferric iron by alginate [160]. Sulfosalicylic (SSA) was used as the competing ligand as it binds Fe(III) with a known rate constant of $k_{SSA} = 3.5\times10^4$ $M^{-1}S^{-1}$ [160] and forms a coloured complex, the rate of formation of which, at different alginate concentrations, can be used to determine the rate constant for formation of the Fe-alginate complex. An appropriate amount of alginate was mixed with 100 mM SSA stock solution in 10 mM MOPS buffer solution (with 50 mM NaCl) to create a 2 mM SSA solution with alginate concentrations of 0.2, 0.5, 0.75, 1 and 2 $g.L^{-1}$. After adjusting solution pH to 7.5 by acid/base addition, a 10 mL aliquot was transferred to a 10 cm pathlength reduced volume cuvette in a Cary 50 Bio UV-Visible spectrophotometer and the instrument zeroed. The solution in the cuvette was then spiked with 0.3 mM Fe(III) stock to generate a final concentration of 1.5 μM Fe and mixed by shaking. The concentration of the Fe(III)SSA complex formed over time was then determined spectrophotometrically. Further details of the competitive ligand method are provided in the Appendix.

5.2.2.5. Calcium binding to alginate

The binding of calcium to alginate during iron addition was examined by measuring the activity of free calcium ions (using an Orion ion selective electrode in

conjunction with an Orion 5 Star multifunctional meter) in the Fe-Ca-alginate solutions. The calibration curves for the ion selective electrode were developed using $CaCl_2$ solutions of known concentration. The possible effect of alginate (or other solution components) on free calcium measurements was examined by placing dialysis bags around the probe with similar results in the absence and presence of the dialysis bag confirming that interference of the probe from either the alginate or other entities in solution was minimal.

5.2.2.6. Scanning electron microscopy (SEM)

To gain further insight into the structure of the cake deposited on the membrane, scanning electron micrographs of the Fe-alginate or Fe-Ca-alginate cake layer formed in 0.1 $g.L^{-1}$ alginate solution were obtained using a cryo-snap preparation process similar to that described by Santiwong et al. [97]. These micrographs were obtained using a JEOL-JSM-6490 LA scanning electron microscope, operating at 15 kV. In brief, small strips (approximately 2 mm in width and 10 mm in length) of freshly filtered alginate cakes were placed on a holder and immersed in a liquid nitrogen bath for about 30s after which they were snapped with the broken untouched edge facing the lens. The SEM images of the filter cake cross-section were then quickly analyzed (within a few minutes of freezing) on a normal stage, under high vacuum.

A piece of gel was also cut from the membrane for surface morphology analysis by SEM (Hitachi S3400). Before imaging analysis, the specimen was placed in a Labec GWD115 drying cupboard at a set temperature of ~ 35 ^{o}C to dry and outgas overnight prior to being inserted in the EM chamber.

5.2.2.7. General filtration methods and the determination/modelling of material properties

Constant pressure dead-end filtration was applied for the prediction of filtration behaviour and material properties. Detailed filtration setup and methods, and the determination/modelling of cake properties in alginate systems have been provided in Chapter 2 General Experimental Methods and Modelling Approaches.

5.3. Results

5.3.1. Properties of alginate in bulk solution

5.3.1.1. Zeta-potential and viscosity

As can be seen from Figure 5-1, the zeta-potential of particles formed in a 0.4 $g.L^{-1}$ alginate solution in the absence of calcium was nearly independent of the level of iron addition with the little variation observed considered to be within the measurement error range. The presence of 2 mM calcium increased the zeta-potential by approximately 7 mV (Figure 5-1) but, in a manner similar to the case without calcium, further iron addition had little effect on the zeta-potential. Reliable zeta potential measurements could not be obtained in the 0.1 g/L alginate-Fe suspensions as a result of the presence of large iron oxyhydroxide assemblages.

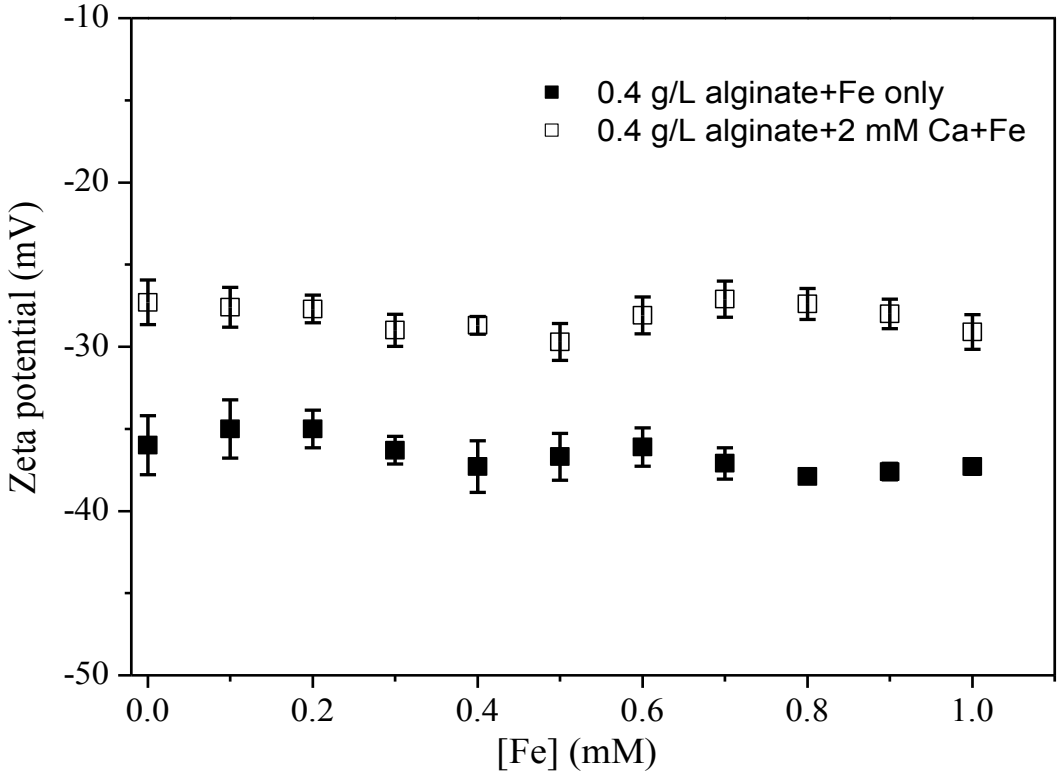

Figure 5-1. Zeta potential of 0.4 $g.L^{-1}$ alginate solution as a function of iron concentration in the absence and presence of 2 mM Ca. Errors bars represent standard deviations from experimental duplicates.

The viscosity of a 0.4 $g.L^{-1}$ alginate solution showed minimal deviation upon the addition of up to 1 mM of iron, both in the absence and presence of calcium (Figure 5-2). However, at the same level of iron addition, the presence of 2 mM calcium resulted in a small but observable decrease in viscosity (Figure 5-2).

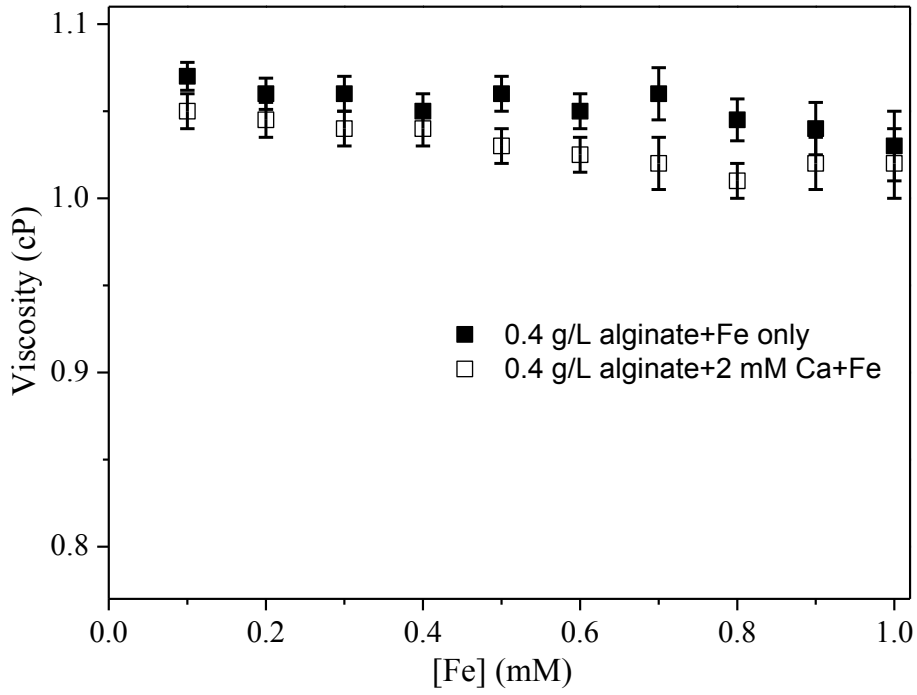

Figure 5-2. Viscosity of 0.4 $g.L^{-1}$ alginate solution as a function of iron concentration in the absence and presence of 2 mM Ca. Errors bars represent standard deviations from experimental duplicates.

5.3.1.2. Alginate adsorption

The fraction of alginate in a 0.1 $g.L^{-1}$ alginate solution associated with settlable particles increased with the addition of iron, both in the absence and presence of calcium (Figure 5-3). The presence of calcium increased the fraction of particulate alginate such that 100% removal was achieved with addition of 0.6 mM Fe compared to 0.8 mM Fe in the absence of calcium (Figure 5-3). Adsorption in 0.4 $g.L^{-1}$ alginate solutions could not be measured in the absence of calcium, as the solution remained clear with no observable precipitation occurring up to iron concentrations of 1 mM.

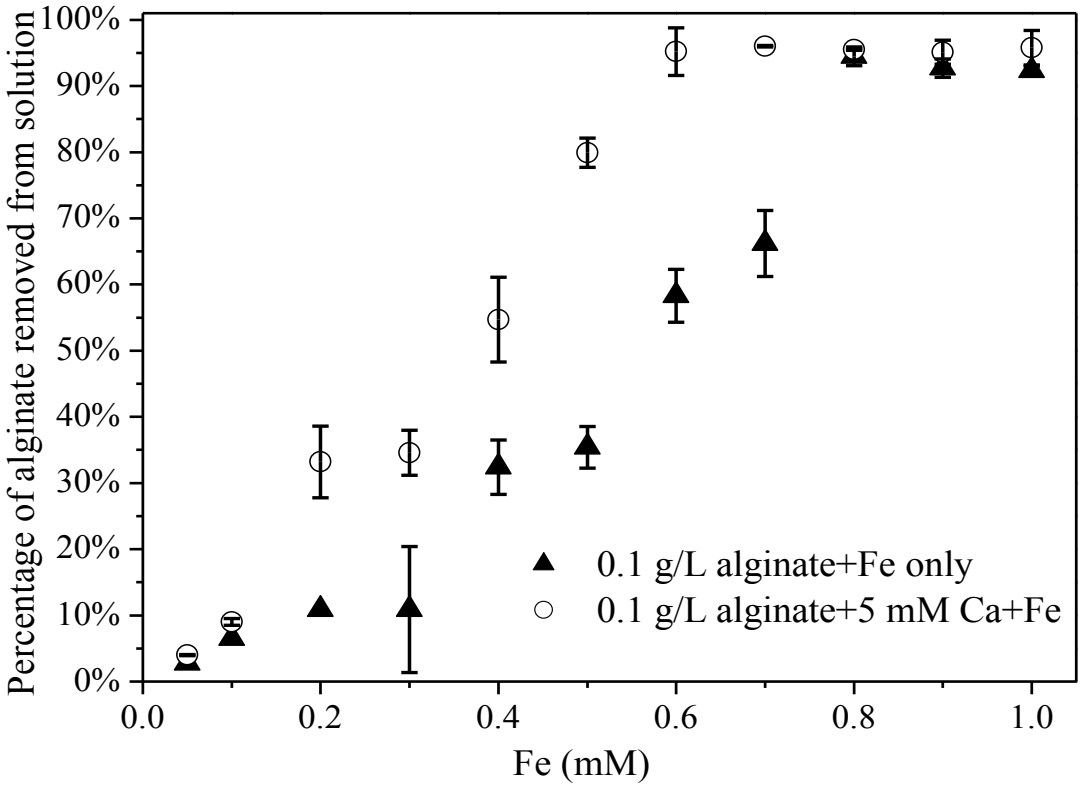

Figure 5-3. Percentage of complexed/adsorbed alginate at different iron concentrations with and without 5 mM Ca present in 0.1 $g.L^{-1}$ alginate solution. Errors bars represent standard deviations from experimental duplicates.

5.3.1.3. Rate of iron precipitation compared to Fe-alginate complex formation

The rate of iron precipitation (R_p), previously determined at pH 7.5 by Pham et al. [161], was compared with the rate of Fe-alginate complex formation (R_c) determined from the competitive ligand studies (see Appendix). As shown in Table A1, the ratio of R_p/R_c is well above 10 under all circumstances and increases substantially with increasing iron concentration, indicating the low probability of formation of iron-alginate complexes, especially at the high iron concentrations used in this study.

5.3.1.4. Size

Addition of Fe(III) to a 0.1 $g.L^{-1}$ alginate solution (in the absence of calcium) resulted in almost no particle size growth at iron concentrations of 0.4 mM or less (Figure 5-4). Beyond 0.4 mM Fe, a continual increase in particle size up to ~100 μm was observed. However, in the presence of 5 mM calcium (where the size of the Ca-alginate complex in the absence of Fe is ~ 134 nm [159]), even the addition of 0.05 mM Fe resulted in the formation of large particles (>100 μm) (Figure 5-4). Large measurement variability and polydispersity, as indicated by the large errors between replicates, indicates a chaotic precipitation process and associated particle formation. The presence of 2 mM calcium resulted in the same phenomenon being observed with large visible particles forming immediately upon iron additions (data not shown). While the results shown in Figure 5-4 for the 0.1 $g.L^{-1}$ alginate + Ca + Fe case suggest there was a decrease in assemblage size at high Fe doses, I caution against over-interpretation in view of the high polydispersity and thus imprecision of size measurement by light scattering under such conditions.

Particle size was not measured in 0.4 $g.L^{-1}$ alginate solution, as the addition of iron (in the absence of calcium) resulted in a clear solution without the formation of visible particles or aggregates, as was similarly observed in the 0.1 $g.L^{-1}$ alginate solution at low Fe concentrations. Despite the higher alginate concentration, the presence of 2 mM calcium in 0.4 $g.L^{-1}$ alginate solution had the same effect as observed in 0.1 $g.L^{-1}$ alginate (in the presence of both calcium and iron) with the formation of large visible precipitates, even at low iron concentrations, indicating the

significant role of calcium in iron precipitation and subsequent aggregation (data not shown).

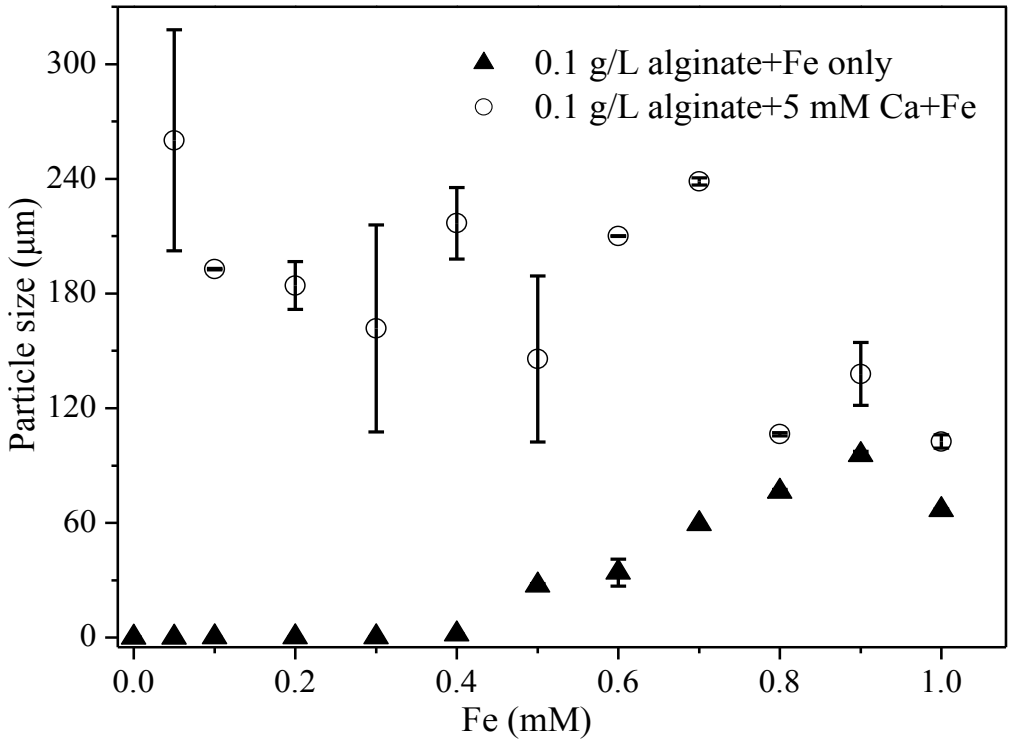

Figure 5-4. Size of particles formed in 0.1 $g.L^{-1}$ alginate solution as a function of iron concentration in the absence and presence of 5 mM Ca (point "0" is the original alginate size without Fe addition). Errors bars represent standard deviations from experimental duplicates.

5.3.2. Gel/Cake properties

5.3.2.1. Porosity and cake resistance

The addition of iron to both 0.1 and 0.4 $g.L^{-1}$ alginate solutions in the absence of calcium resulted in decreased porosity only in solutions containing the lower alginate concentration (i.e. 0.1 $g.L^{-1}$) and at high levels of iron addition (Figure 5-5). However, in the presence of either 2 or 5 mM calcium, porosity declined substantially upon

addition of iron, with a slightly greater initial decrease at the higher calcium concentration (Figure 5-5).

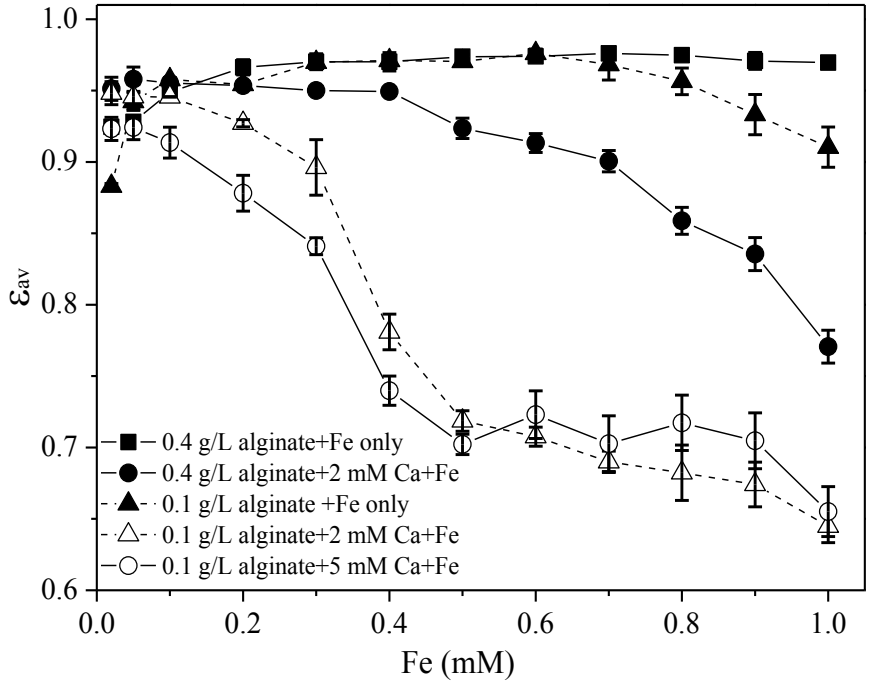

Figure 5-5. Porosity (ε_{av}) of Fe-alginate cake-layer formed at 135 kPa during dead-end filtration at different iron concentrations for alginate concentrations of 0.1 and 0.4 $g.L^{-1}$ in the absence and presence of calcium. Errors bars represent standard deviations from experimental duplicates.

In the absence of calcium, cake resistance initially increased for both 0.1 and 0.4 $g.L^{-1}$ alginate solutions on the addition of iron before plateauing then decreasing with further iron addition (Figure 5-6a). Cake resistance declined dramatically for iron additions greater than 0.6 mM in the 0.1 $g.L^{-1}$ alginate solution, while only showing a slight decrease from that observed for 0.3 mM iron in 0.4 $g.L^{-1}$ alginate solution. However, the presence of 2 mM calcium resulted in a large improvement in cake filterability compared to that observed in the absence of calcium with substantially

lowered cake resistance for iron additions greater than 0.1 mM (Figure 5-6a). The presence of calcium resulted in an even more dramatic decrease in cake resistance on iron addition at the lower alginate concentration (0.1 $g.L^{-1}$) with up to two orders of magnitude reduction in cake resistance compared to that observed in the absence of calcium. As shown in Figure 5-6b, while the effect of presence of calcium was dramatic, the actual calcium concentration present (i.e. 2 or 5 mM) was not critical. In addition, the morphology changed significantly, from a smooth impermeable gel surface in the absence of calcium to large particle deposits with visible permeation pathways between the particles in the presence of calcium (Figure A3).

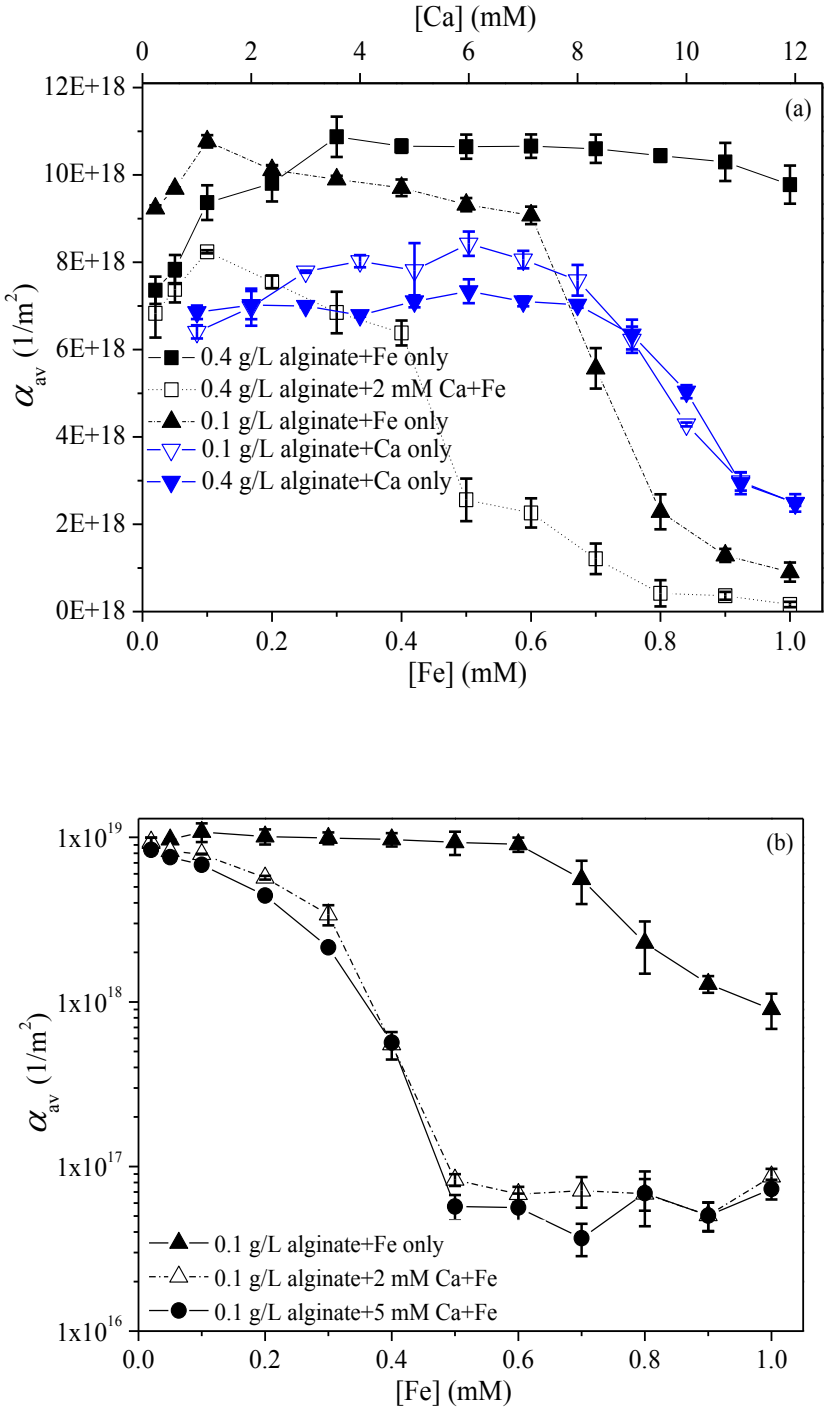

Figure 5-6. Resistance (α_{av}) of Fe-alginate cake-layer formed at 135 kPa during dead-end filtration at different iron concentrations for alginate concentrations of 0.1 and 0.4 g.L^{-1} in the absence and presence of calcium. Errors bars represent standard deviations from experimental duplicates. (b) Resistance (α_{av}) of Fe-alginate cake-layer formed at 135 kPa during dead-end filtration at different iron concentrations for alginate concentrations of 0.1 g.L^{-1} in the absence and presence of calcium. Errors bars represent standard deviations from experimental duplicates.

5.3.2.2. Alginate assemblage properties at different pressures

Cake layer properties were also experimentally determined for a range of filtration pressures for three conditions: 1) Fe only, 2) Ca only, and 3) Fe + Ca, with results shown in Figure 5-7 and filterability and compressibility functions describing these results provided in Table 5-1. As expected, with increasing pressure, K_{av} decreased and ϕ_{av} increased, and the resultant calculated value for α_{av} increased (Figure 5-7). The most notable observation here is still the substantial effect of calcium, which markedly improved the filterability of Fe-alginate. The values for the cake properties (K_{av}, ϕ_{av}, α_{av}) derived from the modeled cake profile very closely match the experimentally derived values over the entire range of filtration pressures. This result provides strong evidence that the cake formation process for a given feed is essentially the same across the range of pressures of interest, and suggests that the results obtained at 135 kPa could be applied and extended to lower pressures more typical of MBR operation.

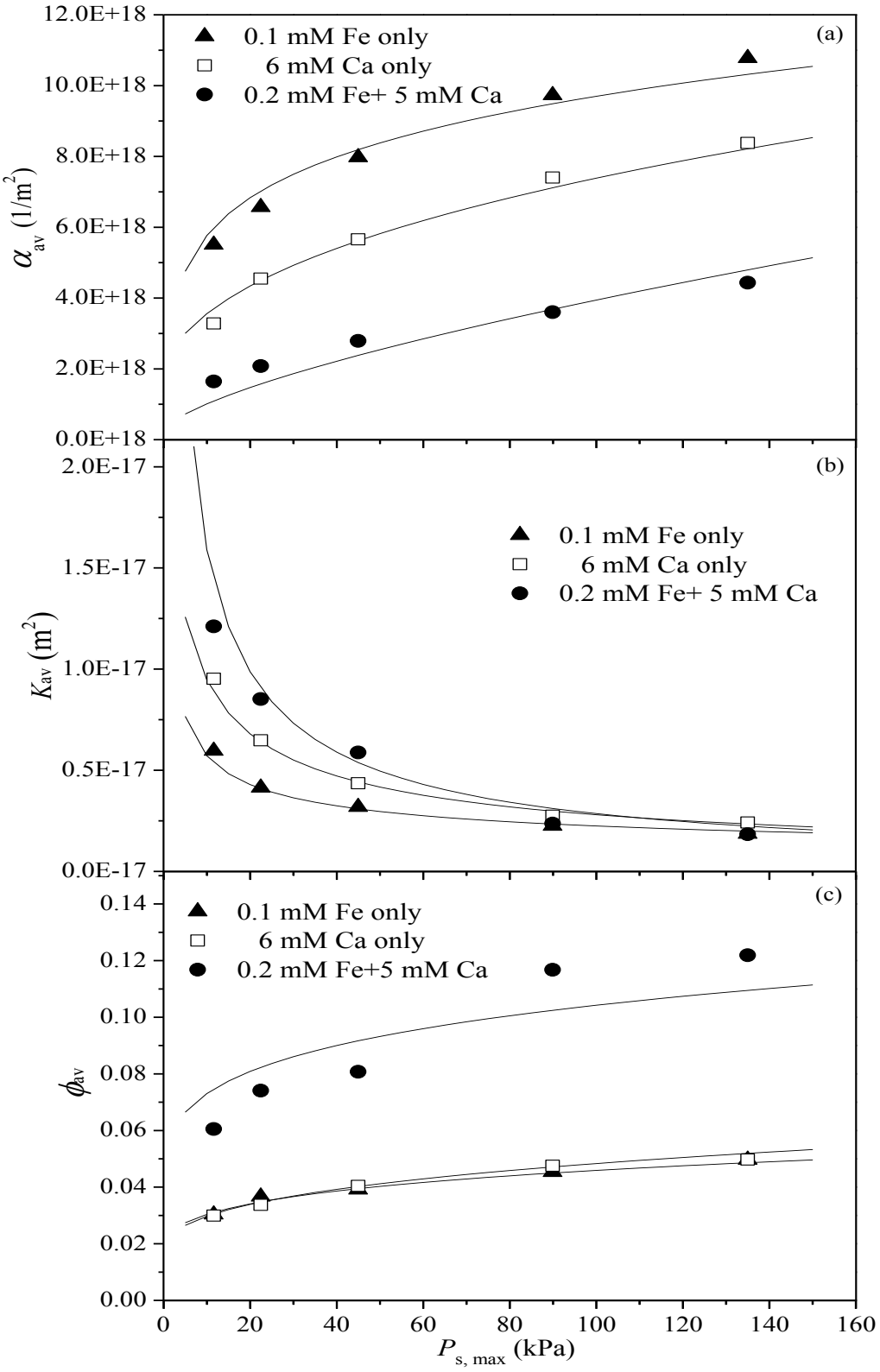

Figure 5-7. Comparison of measured and modeled of (a) resistance (α_{av}), (b) permeability (K_{av}), and (c) a solid fraction (ϕ_{av}) during dead-end filtration of 0.1 g.L^{-1} alginate solution at various constant pressures (12 to 135 kPa) for selected systems: 0.1 mM Fe, 6 mM Ca, and 0.2 mM Fe+5 mM Ca.

Table 5-1. Filterability and compressibility functions (as defined in Eq (2-12) and (2-13)) for alginate cake layers at different Fe/Ca concentrations. The parameters $C_1 - C_4$ were optimized by minimizing the residual differences between the measured and modelled values of cake height (H_s) and maximum solid pressure ($P_{s,max}$). The solid fraction at the gel point ϕ_g was estimated by extrapolation of the solid fraction curve to $P_{s,max}$ of 0 kPa.

	Filterability	Compressibility	*Øg*
0.2 mM Fe	$K_{Fe} = 2.40 \times 10^{-22} \emptyset_{Fe}{}^{-2.58}$	$\emptyset_{Fe} = \emptyset_{g,Fe} \times (1 + 0.0088 \times P_s)^{0.196}$	0.030
6mM Ca	$K_{Ca} = 3.65 \times 10^{-21} \emptyset_{Ca}{}^{-2.29}$	$\emptyset_{Ca} = \emptyset_{g,Ca} \times (1 + 0.0010 \times P_s)^{0.299}$	0.020
0.2 mM Fe+ 5mM Ca	$K_{Fe+Ca} = 1.34 \times 10^{-21} \emptyset_{Fe+Ca}{}^{-3.66}$	$\emptyset_{Fe+Ca} = \emptyset_{g,Fe+Ca} \times (1 + 0.0012 \times P_s)^{0.283}$	0.050

5.3.2.3. Scanning electron microscopy (SEM)

Cross sections of filter cakes produced with 0.1 $g.L^{-1}$ alginate in the presence of 0.1 mM and 0.5 mM iron (in the absence of calcium), and in the presence of both calcium (5 mM) and iron (0.2 mM), are shown in the SEM images presented in Figure 5-8. The images selected are representative of multiple points of analysis across each cake and clearly show the dramatic effect that calcium addition has upon the Fe-alginate assemblage structure and pore size. The overall structure of Fe-alginate assemblages formed in the absence of calcium (Figure 5-8a and 5-8c) is quite similar, with larger pores close to the membrane surface, possibly due to the unique gelation behaviour of the Fe-alginate system. However, in the presence of calcium, there is a dramatic increase in the density of the Fe-Ca-alginate assemblage (Figure 5-8e) and a significant decrease in the pore size (as is apparent by comparing micrographs in Figure 5-8b, 5-8d and 5-8f) with the transition from smaller to the larger pores towards to the top of the cake (furthest away from the membrane). It is worth noting that, at high iron concentrations (> 0.6 mM), SEM imaging was not performed (either in the absence or presence of calcium) because the deposit on the membrane surface was composed of highly non-uniform "sticky" large aggregates rather than a well-distributed uniform gel.

The SEM observations are consistent with measurements of porosity (Figure 5-5) where a high porosity was observed for the case of iron only (0.1 and 0.5 mM) but dramatically decreased in the presence of calcium. Despite the fact that higher porosity was observed in the absence of calcium, the hydraulic conductivity remained very low along with elevated cake resistance (Figure 5-6).

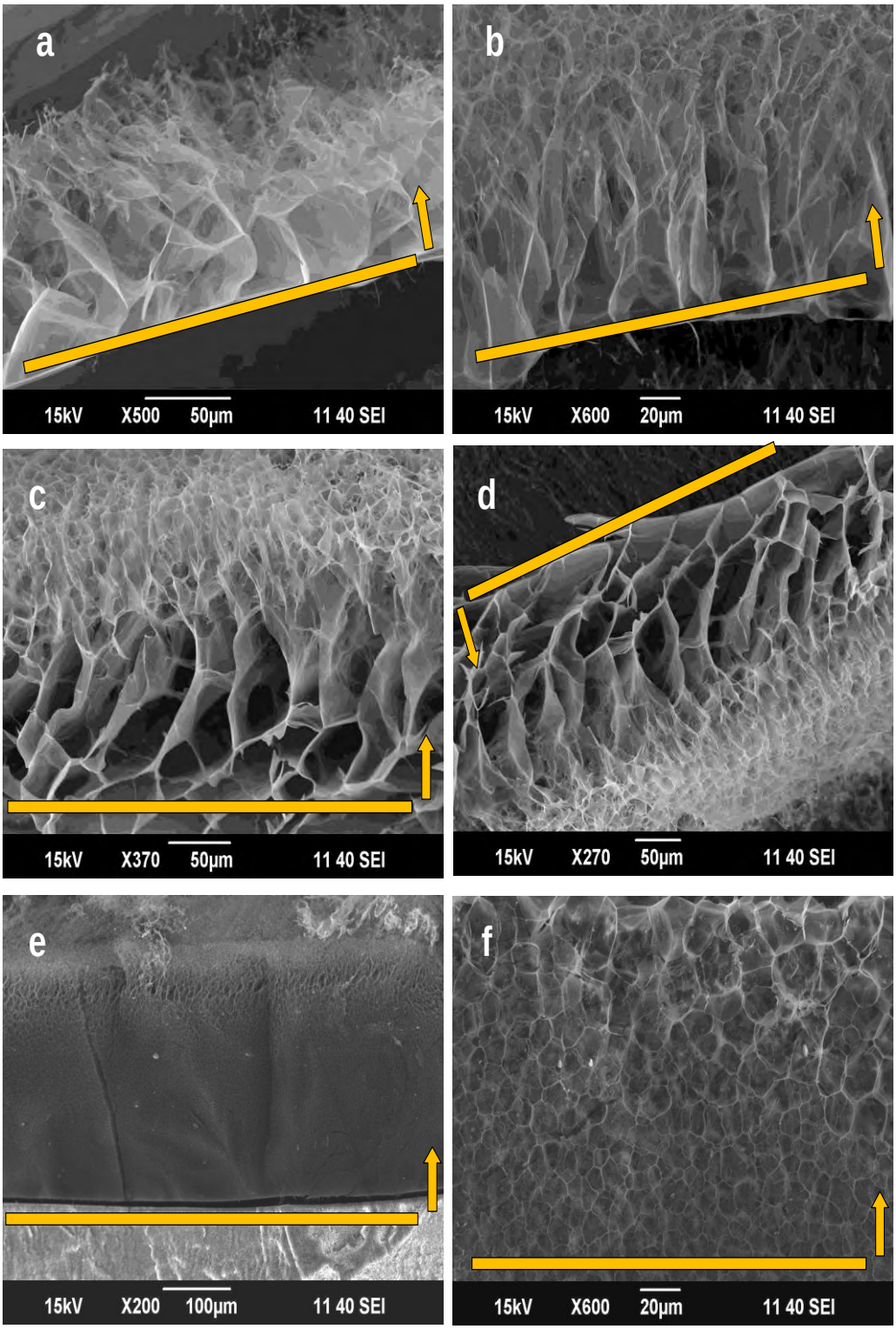

Figure 5-8. Scanning electron microscopy images of alginate gel layer cross-sections formed from; 0.1 $g.L^{-1}$ alginate solution under 22.5 kPa at 0.1 mM iron (a and b), 0.5 mM iron (c and d), and 5 mM calcium + 0.2 mM iron (e and f). Solid bars indicate approximate location of membrane, with arrows representing the direction away from the membrane to the surface of the filter cake.

5.4. Discussion

5.4.1. Binding and aggregation between Fe and alginate

Determination of the binding mechanism between iron and alginate is made difficult due, in part, to the tendency of ferric iron to precipitate at circumneutral pH [162]. The Fe(III)-alginate system is further complicated by the presence of the alginate which may prevent iron hydrolysis by forming soluble Fe-alginate complexes [160, 161] though this complexation process may be countered by precipitation of amorphous ferric oxides (AFO) which can induce the net dissociation of any Fe-organic complexes that may have initially formed [163]. Simplistically, two competing reactions may be envisaged to occur when Fe(III) is added to alginate solution,

$$Fe' + L_x = FeL_x \quad (5\text{-}1)$$

$$Fe' + Fe' = AFO \quad (5\text{-}2)$$

where Fe' represents dissolved inorganic Fe(III), L represents alginate binding sites and the suffix x is the coordination number.

The above reactions form the basis of two conceptual models commonly used to describe Fe-alginate interactions [164]. The site binding model assumes that Fe(III) is coordinated by binding sites on the alginate molecule resulting in spatially separated Fe(III) centers along the polymeric alginate backbone [165-167]. Alternatively, in the colloidal model, Fe(III) is presumed to form iron oxide precipitates (FeOOH) which

are covered by alginate and, provided sufficient alginate is present, stabilized as nanoparticles against further aggregation [168, 169].

Based on the rate of iron precipitation (R_p) compared to the rate of Fe-alginate complex formation (R_c) determined by the competitive ligand method (Table A2), it is apparent that the Fe-alginate system, at least under the conditions used here, is predominately characterized by the behaviour of colloidal iron oxides rather than by formation of Fe-alginate complexes. This indicates that, at least at the circumneutral pH of 7.5 (where FeOOH precipitation is particularly rapid [161]) and the high iron concentrations used in this study, complex formation is unable to outcompete precipitation. It is also expected that the polysaccharide will prevent particle-particle interaction thereby limiting the formation of large FeOOH aggregates by creating a protective layer around FeOOH particles, especially at higher alginate concentrations. As shown by Sipos and coworkers, the cationic polysaccharide chitosan can inhibit the growth of iron oxyhydroxides (to no more than 10 nm) at metal to ligand ratios of 1:1 [164]. A number of other studies have reported similar 'stabilization' of colloidal iron oxides by various polysaccharides [169-171].

Further evidence in support of the colloidal model is the independence of zeta-potential upon iron addition to alginate solutions (Figure 5-1), which indicates that alginate coverage is highly effective at screening the iron oxide charge, even at higher iron concentrations. If iron is bound directly to alginate, ferric iron addition should neutralize the negative charge of the alginate with increase in zeta potential in line with previous observations on Ca-alginate [159]. In addition, and in accordance with the findings of Sipos et al. [164] in studies on Fe-chitosan systems, the viscosity of alginate solutions was also independent of Fe(III) addition (Figure 5-2), suggesting

minimal alginate cross-linking as Fe(III) loading increased. If anything, the viscosity decreased slightly with increasing iron addition. Such an effect would be expected if the increasing availability of sorbing surfaces resulted in the removal of alginate from solution, as shown in Figure 5-3.

Therefore, the conclusion drawn from zeta-potential and viscosity data is consistent with the competitive ligand results, in that, under all conditions examined here, the rate of precipitation (R_p) exceeds the rate of Fe-alginate complex formation (R_c), supporting the hypothesis that iron oxide formation outcompetes Fe-alginate complex formation. Particle size (Figure 5-4) does not increase significantly (for 0.1 $g.L^{-1}$ alginate solutions) until the concentration of iron exceeds 0.4 mM. As such, it appears that there is sufficient alginate present to stabilize iron oxyhydroxide particles up to 0.4 mM iron. At the higher alginate concentration (0.4 $g.L^{-1}$), the solution remains clear and there is no observable change in size, even at the highest iron concentration of 1 mM. This indicates that sufficient alginate is present to stabilize relatively high concentrations of iron oxides.

5.4.2. Aggregation in the presence of calcium

While alginate is able to maintain low concentrations of iron in solution, either as dissolved Fe-alginate complexes or, more likely (as discussed above), as stabilized colloidal iron oxides with an alginate coating on the surface, the presence of 5 mM calcium results in the formation of large assemblages of around 200 μm in size (Figure 5-4), even at concentrations of iron as low as 0.05 mM. In comparison, recent results of Xin et al. (2014) show that assemblages of only 135 nm in size are obtained in 0.1 $g.L^{-1}$ alginate solutions containing only 5 mM calcium and no added iron [159].

These results suggest that once alginate binding sites are occupied by calcium, alginate molecules are unable to either complex added iron or to stabilize freshly formed iron oxides by adsorbing to the iron oxide surfaces. Although all alginate binding sites are unlikely to be occupied at calcium concentration up to 5 mM as shown by Xin et al. [159], this concentration of calcium is sufficient to induce significant cross-linking with formation of assemblages in which "internal" sites are inaccessible to either water or added constituents such as iron. In this event, iron oxides will rapidly form and proceed to aggregate.

It is likely that as the alginate polymers (and Ca-alginate gel) progressively coat the FeOOH particles, new binding sites are exposed and undergo bridging with other alginate polymers (or alginate coated FeOOH) via calcium complexation, resulting in significant aggregation and precipitation of FeOOH-alginate assemblages, a process similar to the "enhanced aggregation" described by Chen et al. in alginate-Ca-hematite systems [117, 118]. This is evident from the results presented in Figure A4 where the addition of iron resulted in a small but observable reduction in free Ca^{2+} concentration. This result may also be viewed as further evidence of inaccessibility of binding sites within Ca-alginate gels. Alternatively, this result may simply reflect the rapid kinetics of iron oxide formation if alginate binding sites are already occupied by cations [172, 173] and unable to compete (with OH^-) for added Fe(III) ions to form soluble complexes thereby resulting in formation of large aggregates.

5.4.3. Filtration behaviour of Fe-alginate and Fe-alginate-Ca assemblages

5.4.3.1. Fe-alginate gel and comparison with Ca-alginate gel

As shown in our earlier study, the properties of the bulk solution are closely linked to the hydraulic properties of the fouling layer deposited on the flat sheet membranes [159]. In a similar manner to that observed with the size of the aggregates, the synergistic effect of calcium and iron was also evident in the α_{av} versus [Fe] plot (Figure 5-6). Since the specific resistance of the assemblage is, according to the Carman-Kozeny equation, inversely proportional to the particle diameter [28], the formation of much larger aggregates in bulk solution in the presence of calcium should result in the formation of a more open cake structure. This would facilitate water flow between the pores of these assemblages, compared to the impermeable gel that is formed from the smaller particles that predominate in the absence of calcium. Therefore, in the Fe-Ca-alginate assemblages, the specific resistance decreases dramatically once alginate is unable to prevent further iron oxide precipitation and significant aggregation occurs. Figure 5-6b shows that an increase in iron concentration from 0 to 0.5 mM results in a greater than two orders of magnitude decrease in cake resistance with calcium present. Note that the precise concentration of calcium present does not appear to be critical with similar Fe-dependent behaviour in the presence of both 2 and 5 mM calcium with this result possibly indicative of the importance of the presence of pre-formed Ca-alginate gel prior to iron addition to the formation of large aggregates and thus improved filtration behaviour.

The influence of assemblage size on cake formation was also evident from the optical microscope images shown in Figure A5 with these images providing further evidence of the link between the nature of the assemblages in suspension and the properties of the assemblage formed on the membrane surface. In the absence of calcium, the gel formed from 0.1 mM Fe addition is quite uniform (Figure A5-a). The color of the Fe-alginate gel becomes more orange-brown (characteristic of Fe(III) precipitation) as the iron concentration is increased to 0.5 mM (Figure A5-b). However, with calcium present, the cake becomes non-uniformly distributed, with 'patches' of orange-brown interspersed within the wider matrix (Figure A5-c).

In addition to the effect of assemblage size, addition of calcium leads to a significant reduction in porosity (Figure 5-5) with ε_{av} decreasing from a consistent value of 0.95 for Fe concentrations ranging from 0.02 mM to 1 mM in the absence of added Ca to a value of around 0.70 in suspensions containing Fe concentrations greater than 0.5 mM Fe and a Ca concentration of 2 mM (Figure 5-5). Further, the compressibility of the cake layer formed in the presence of both Fe and Ca was significantly higher than that of the gelatinous assemblages typical of Fe-alginate-only and Ca-alginate-only cakes, with the solid fraction ϕ at least two times higher at any given solid pressure $P_{s,max}$ (Figure 5-7c). The more compact, less gel-like Ca-Fe-alginate fouling layers exhibit higher hydraulic conductivities, particularly at the lower operating pressures typical of MBR operation (Figure 5-7b). This implies that syneresis and the collapse of the gel network is integral to the improved hydraulic conductivity of the fouling layer.

The SEM images (Figure 5-8) further highlight the porosity reduction and syneresis that occurs in the presence of both Fe and Ca with these results complimenting the results of previous investigations into the effects of calcium concentration on alginate fouling [159]. Our previous studies showed that systems with high calcium concentrations (> 6 mM) resulted in denser (less voluminous) filter cakes that retained less water (and exhibited lower specific resistance) than gels formed at low calcium concentrations. These observations corresponded with the transformation from a highly "cross-linked" voluminous honeycomb type structure of low permeability at low calcium concentrations (< 6 mM) to a nematically ordered, compact structure of high permeability at high calcium concentrations (> 6 mM). In the iron and calcium cases presented here, SEM images show the formation of a structure that is quite similar to the high calcium case described by Xin et al. [159] with a reduced void size (Figure 5-8f) and consolidated cake assemblage (Figure 5-5) facilitating increased hydraulic conductivity. In addition to a greater interconnectivity between pores contributing to the improved hydraulic performance, a reduction in the electrostatic forces that act to retard water movement through the assemblage is also a possible contributing factor [124].

5.4.3.2. Filterability of Fe-Ca-alginate assemblages

The specific resistance of the Fe-alginate assemblages (in 0.1 $g.L^{-1}$ alginate) is generally higher than that of the Ca-alginate gels (Figure 5-6a and Figure 5-7a) at low Fe concentrations (< 0.6 mM Fe) though the formation of large aggregates at Fe concentrations > 0.6 mM results in a significant reduction in specific resistance. This is likely due to the greater binding strength of alginate for iron compared to calcium, as the conditional stability constant of Fe-alginate is 5.04×10^4 M^{-1} at pH 3.5 [174],

while the stability constant for Ca-alginate is $1.07 \pm 0.26 \times 10^4$ M^{-1} [99]. It follows then that the Fe-alginate forms a stronger, more electrostatically stable gel. In accord with this, the gelation of alginate occurs at much lower iron concentrations (less than 0.1mM) compared to calcium (> 1mM). Ferric ions have the capacity to combine with not only G blocks but also MG and/or M blocks present in alginate, enabling the formation of Fe-alginate hydrogels [175] and thus offer additional coordination sites compared with calcium. The ability of substantially lower concentrations of iron to induce gelation may also indicate a different mechanism of gelation compared to calcium that induces gelation by simply cross-linking alginate groups (Figure 5-9). It is likely that iron induces gelation by not only cross-linking but also through the formation of randomly-oriented independent FeOOH-alginate aggregates (Figure 5-9).

The difference in gelling mechanism may also be reflected by the dependence of fouling behaviour on the alginate concentration. In the previously investigated Ca-alginate gels, calcium concentration controls the gel structure formation with gel properties found to be independent of alginate concentration (Figure 5-6a) [159]. However, in the Fe-alginate system, higher alginate concentrations (0.4 $g.L^{-1}$) are able to stabilize additional FeOOH nanoparticulates (even at 1 mM Fe(III)) and, in doing so, inhibit the formation of larger aggregates, leading to an assemblage with higher specific cake resistance (Figure 5-6a).

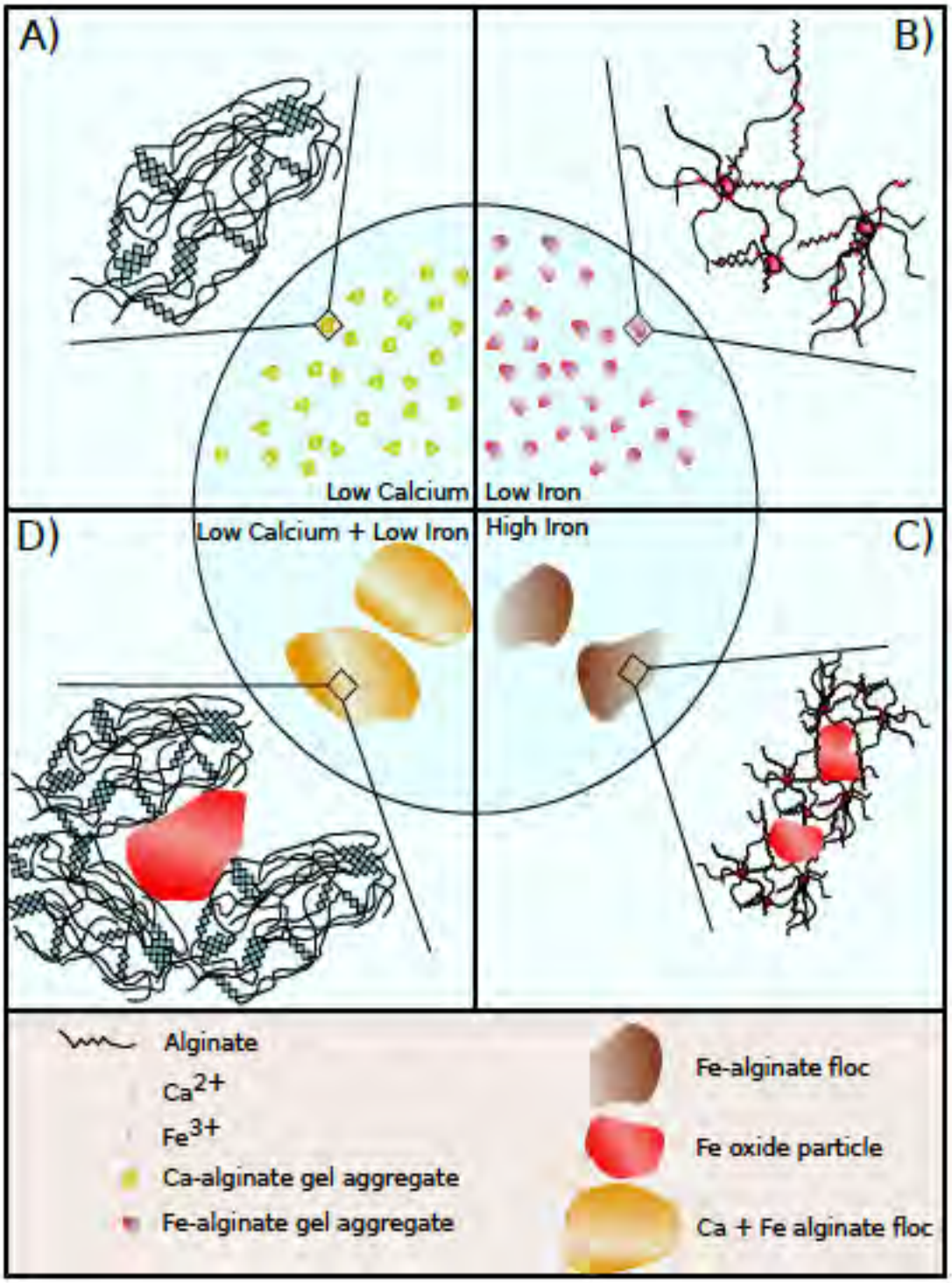

Figure 5-9. Schematic of proposed bulk solution assemblages following the addition to 0.1 g/L alginate of A) 2 - 5 mM calcium (equilibrated overnight) resulting in Ca-alginate gel aggregates of <1 µm, B) ~0.2 mM iron resulting in Fe-alginate aggregates <1 µm comprising both complexed Fe^{3+} and stabilized nanosized colloids , C) ~1 mM iron resulting Fe-alginate flocs of ~100 µm, and D) ~0.2 mM iron to the Ca-alginate system of A) resulting flocs of ~200 µm.

To summarize, in the case of lower alginate concentrations (0.1 $g.L^{-1}$) where alginate is not able to stabilize large amounts of iron oxide, biphasic fouling behaviour was still observed (Figure 5-6a). These high specific resistance fouling layers were formed at iron concentrations up to ~ 0.6 mM. At higher Fe(III) concentrations, the specific resistance of the fouling layer on the membrane was observed to decrease, due to the increased aggregate size and syneresis. Such biphasic fouling behaviour has also been reported in Ca-alginate systems where calcium induces gelation of 0.1, 0.4 and 1 $g.L^{-1}$ alginate solutions at calcium concentrations up to 6 mM. Beyond 6 mM Ca addition, the highly impermeable gel assemblages become substantially more permeable, an observation attributed to gel collapse associated with the enhanced calcium binding by MG blocks [159].

5.5. Conclusions

This study provides an in-depth understanding of the properties of the fouling layers formed upon membrane filtration of alginate solutions to which ferric iron salts are added both in the absence and presence of calcium. Fe-alginate gels (in the absence of calcium in the system) possess higher cake resistance than Ca-alginate gels and require substantially lower concentrations of iron to induce gelation, due to both the higher binding affinity of Fe(III) compared to Ca for alginate functional groups and the difference in gelation mechanism. In addition to the direct Fe-induced cross-linking of alginate as previously observed in Ca-alginate systems, fouling is likely to be aggravated through the formation of randomly-oriented independent nanosized FeOOH-alginate aggregates within the Fe-alginate gel (Figure 5-9). However, once sufficient iron is present that cannot be stabilized by alginate, extensive FeOOH

precipitation occurs with the subsequent formation of large aggregates in suspension and permeable assemblages on the membrane surface. Further, unlike Ca-alginate assemblages, the properties of the Fe-alginate fouling layers are strongly dependent on alginate concentration with this effect most likely related to the ability (or inability) of alginate to prevent the aggregation of iron oxide particles that are formed on Fe(III) addition to alginate solutions.

Another significant finding is the major impact of calcium on the fouling layer properties in the Fe-alginate system with the resulting Fe-Ca-alginate gel containing substantially less water and exhibiting lower resistance than gels formed in the absence of calcium. The results obtained suggest that the presence of calcium in the Fe-alginate system renders "internal" alginate binding sites inaccessible to iron and thus promotes FeOOH precipitation and aggregation resulting in the formation of much larger FeOOH aggregates and accompanying relatively permeable membrane fouling layers.

Chapter 6. Effect of Iron(III) and Calcium on Membrane Fouling by Soluble Microbial Products

6.1. Introduction

The shortage of potable water around the world and more stringent effluent quality requirement of receiving body have promoted the development of wastewater treatment and reuse technology. Membrane bioreactors (MBRs), which involve a combination of membrane separation and the activated sludge process, have gained considerable attention due to their potential advantages over conventional biological treatment processes. Besides advantages such as reduced footprint and superior effluent quality over the conventional activated sludge treatment process, the efficiency of MBRs is also independent of sludge-settling (which is important for conventional activated sludge performance) due to the complete retention of sludge by the membranes [176]. However, the separation process is inevitably plagued by critical membrane fouling issues as a result of its ability to reject most of the particles present. The main forms of fouling include deposition of solids as a cake layer, pore blocking by colloidal particles, adsorption of soluble compounds and biofouling. Although routine operating procedures such as aeration coupled with intermittent filtration and subcritical flux operation could reasonably alleviate the deposition of sludge particulates onto the membrane surface, they do little to prevent the accumulation of colloidal material or, more catastrophically, the formation of thin but

dense and highly impermeable gel layers on the membrane surface by soluble microbial products (SMPs) [6, 20].

The SMPs in MBR are far from homogeneous in terms of particle size, gelling propensity and chemical components (mainly composed by polysaccharides, proteins, nucleic, and a certain amount of humic substances) [4, 10]. Although the proteins also play an important role in gelling process [75], the major component of SMPs directly responsible for membrane fouling in gel formation appears to be the polysaccharides due to the presence of carboxylic acid sites which associate strongly with divalent or multi-valent metal ions [3, 20, 127]. Polysaccharides typically constitutes around 35% of the dissolved organic carbon (DOC) present in MBR supernatants [25] with the membrane fouling rate found to be linearly related to the the polysaccharide content of the supernatant [177]. Alginate, a polysaccharide derived from either algae or bacteria, has been used widely as a surrogate of the polysaccharides present in MBR supernatants with a variety of investigations of the role of divalent and/or multivalent metal ions in alginate gel formation [134, 178].

In addition to membrane fouling, another disadvantage of MBR technology is its well-recognized poor performance with regard to phosphorus removal. The most common solution involves the addition of iron salts such as ferric chloride to wastewater to aid phosphorus removal [152], but addition of such coagulants is recognized to aggravate membrane fouling due to the increase in particle load present. For example, the North Head MBR plant in Sydney with capacity of 2 ML/day achieves satisfactory effluent quality for the intended on-site reuse but suffers from a greater degree of membrane fouling than desired, in part as a result of the dosing of iron into the sewer as an aid for odor control. Similarly, high concentrations of either

iron or aluminum salts are added to the submerged MBR plant at Brooklyn in the northern suburbs of Sydney in order to ensure that the phosphorus content of effluent discharged to the Hawkesbury River stays within required limits but result in severe membrane fouling. Despite the importance of the issue, limited research has been undertaken either on the effect of iron salt addition on membrane fouling or on approaches to optimization of the process such that phosphorus removal and membrane fouling are managed satisfactorily.

A variety of factors are recognized to strongly influence the fouling behaviour of SMP in the presence of metal-based coagulants. In particular, the presence of calcium, a ubiquitous element in wastewaters, may influence the extent and severity of membrane fouling with SMPs due to its ability to form impermeable gels with polysaccharide. Calcium is typically present in wastewaters at concentrations of 1.5 to 11 mM [80] with the actual content determined particularly by the hardness of the source drinking waters. Additionally, lime ($Ca(OH)_2$) is widely used for pH adjustment in wastewater treatment with the required lime dosage depending primarily on the alkalinity of the wastewater [96].

While the binding behaviour between alginate and calcium/iron, and importance of alginate and calcium/iron content to cake filtration performance have been well-recognized in previous chapters, the objective of this chapter is to elucidate (i) the variation in properties of the fouling layer resulting from filtration of SMP containing a range of concentrations of iron and calcium, (ii) the difference in gel layer properties and fouling mechanism between Fe-SMPs and Ca-SMPs, and (iii) the change in cake layer properties and fouling mechanism when both iron and calcium coexist in the MBR supernatant. I will address the above issues in this chapter by

examining the characteristics of the fouling layer formed by SMPs in the presence of calcium or/and iron in dead-end filtration at constant applied pressure.

6.2. Materials and methods

6.2.1. Raw supernatant

Sludge was collected from the return activated sludge pumping line before secondary biological treatment at the St Marys wastewater treatment plant in the western suburbs of Sydney. Iron salts were not dosed to this plant for the purposes of either odour control or phosphorus removal and, as such, the sludge was well suited to investigation of the impact of Fe and Ca dosage on metal binding and cake layer properties. The sludge supernatant rather than the sludge itself was used for each filtration study in view of our interest in SMP-mediated fouling. The mixed liquor was centrifuged at 5000 rpm for 5 minutes, and the supernatant then filtered through 1.2 μm glass microfiber filter using a Millipore suction pump.

The main characteristics of activated sludge and SMP are listed in Table 6-1 and were obtained by following the Standard Methods for the Examination of Water & Wastewater [179]. The concentrations of total organic carbon (TOC) of SMP were determined using a Shimadzu TOC-5000 analyzer with ozone generator for total nitrogen (TN) measurement. The protein content was determined following the modified Lowry method using BSA as the standard [180], while the polysaccharide content was measured according to the phenol method using glucose as the standard [181]. The pH of the supernatant used for dead-end constant filtration experiments was determined to be 7.6 using an Orion 5 Star multifunctional meter (Thermo

Electro Corporation, USA). No pH adjustment was performed upon addition of calcium or/and iron because the strong buffering ability of the raw supernatant resulted in insignificant pH change.

6.2.2. Analytical methods

6.2.2.1. Bulk solution

The concentrations of metals present in the supernatant were measured using inductively coupled plasma optical emission spectrometry (Optima 3000 ICP-emission spectrometry, Perkin-Elmer). The size and zeta-potential of SMP aggregates after addition of calcium and/or iron to the supernatant were measured by laser Doppler micro-electrophoresis and dynamic light scattering (DLS) respectively using a Malvern Zetasizer Nano ZS. A Malvern 2000 Mastersizer was used when the sizes were too large for DLS measurement.

6.2.2.2. Cake characterization

Fourier transform infrared (FTIR) spectra of the formed SMP gel were obtained using a PerkinElmer Spectrum 100 FTIR spectrophotometer with scanning undertaken from 4000 to 650 cm^{-1} at 1.0 cm^{-1} interval. The morphology of SMP gel was observed using an Hitachi S3400 scanning electron microscope (SEM) with elemental analysis of the gel layer undertaken using a Bruker Silicon Drift Energy Dispersive X-ray (EDX) analyzer. Before imaging analysis, the specimen was placed in a Labec GWD115 drying cupboard at a set temperature of ~35 ^{o}C to dry and outgas overnight prior to being inserted in the EM chamber.

To determine the crystal phase composition of the gel samples, X-ray diffraction (XRD) measurements were carried out at room temperature using an X'Pert PRO Muti-purpose X-ray Diffraction System (MPD system) with Cu Kα radiation (λ = 0.15418 nm). The phases were identified by comparing diffraction patterns with those on the standard powder XRD cards compiled by the Joint Committee on Powder Diffraction Standards (JCPDS). An accelerating voltage of 45 kV and emission current of 40 mA were used.

6.2.3. Determination of material properties

Constant pressure dead-end filtration reaches a steady state condition when the deposited cake layer is fully consolidated and there exists a linear relationship between the cumulative permeate volume (V) and the filtration time (t) to volume ratio (t/V) according to

$$\frac{t}{V} = kV + b \tag{6-1}$$

where k and b are the slope and intercept respectively of the linear regression. The specific resistance to filtration (SRF) is expressed by [182]

$$\frac{t}{V} = \frac{\mu}{P}[\frac{SRF}{2}CV + R_m] \tag{6-2}$$

and so

$$SRF = \frac{2Pk}{\mu C} \tag{6-3}$$

where P is the applied pressure, u is the viscosity of filtrate and C is deposited mass of cake solids on the membrane surface per unit filtrate volume and per cross-sectional area. SRF is commonly expressed in the units of length/mass (e.g. m/kg).

At the end of the constant pressure filtration, the consolidated gel layer was peeled from the membrane with its wet weight (W_g) determined using a high precision (0.001 g) electronic balance. Therefore, the average solid fraction ($\varnothing_{av}$) of the gel layer can then be related to the initial solid fraction ($\varnothing_i$) and filtration volume (AV) according to

$$\phi_{av} = \frac{\phi_i AV}{W_g} \tag{6-4}$$

where A is the effective filtration area, and ϕ_i is the initial solid fraction and determined from triplicate experiments by measuring the retained dry mass of SMP (by placing the wet SMP gel in a desiccator) over the filtration volume, and thus the average porosity (ε_{av}) is

$$\varepsilon_{av} = 1 - \phi_{av} \tag{6-5}$$

6.3. Results and discussions

6.3.1. Effects of iron(III) and calcium on the properties of SMP in bulk solution

6.3.1.1. Characteristics of SMP

The main characteristics of activated sludge and extracted SMP have been summarized in Table 6-1. The elemental contents of SMP are represented in Figure 6-1 and show that SMP contains about 0.84 mM Ca and negligible iron before further calcium and iron addition.

Table 6-1. The main characteristics of activated sludge and extracted SMP.

Parameters	Concentrations (mg/L)
MLSS	10930
TP	15.49
TN	6.23
TOC	26.03
Protein	14.78
Polysaccharide	12.77

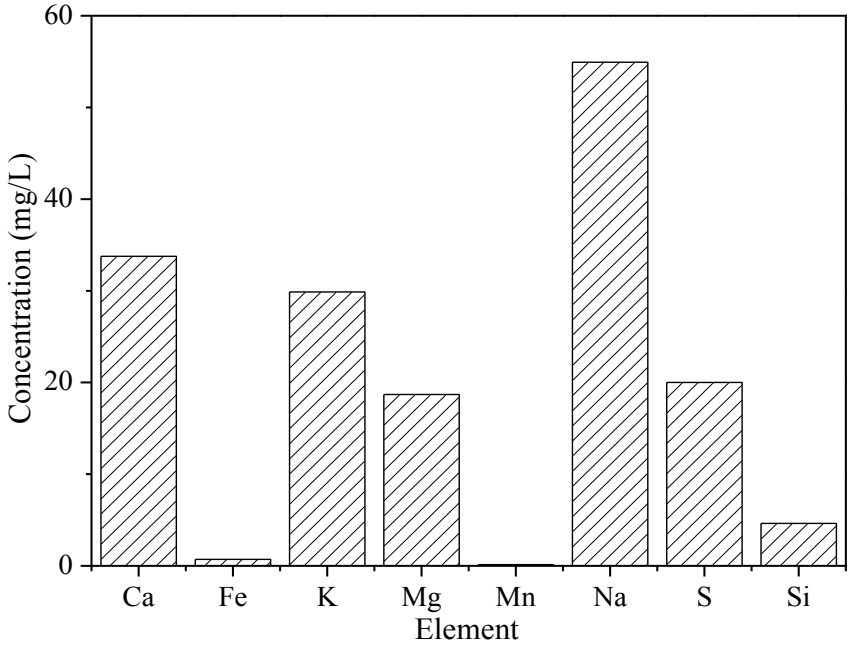

Figure 6-1. The concentrations of elements in the activated sludge supernatant.

6.3.1.2. Size

The particle sizes of SMP in the bulk solution were measured on addition of 0 - 0.15 mM Fe(III) or 0 - 6 mM Ca. Results presented in Figure 6-2 indicate that the addition of 1 mM Ca to SMP resulted in a decrease in measured size, likely due to the formation of more compact egg-box structures of the polysaccharides present in the SMP [103]. Further calcium addition resulted in an increase in size with the rate of size increase per unit of added calcium increasing for calcium concentrations > 5 mM with this increase in size most likely a result of calcium bridging of polysaccharides present in the SMP. The change in size of Ca-SMP is consistent with our observation on the variation of size of Ca-alginate assemblages in Chapter 3. In the Fe-SMP

system, the size increased slightly at low iron dosages (0-0.04 mM), but was then followed by a dramatic increase with further addition of iron (Figure 6-2). Based on the results of Fe-alginate in Chapter 5, the size increase from relatively low Fe concentration (0.05 mM) is probably due to the role of pre-existing calcium (0.84 mM) that may assist in the particle aggregation to form larger Fe-SMP clusters. SMP may interact with iron in the same way as the alginate that is coordinating with iron to form water-soluble Fe-SMP complexes and stabilizes FeOOH nanoparticles at low iron concentration. However, once the binding sites of SMP for iron are saturated or pre-occupied by calcium, these nanoparticles tend to agglomerate and form macroscopic precipitates. Therefore, in the presence of calcium, SMP is unable to either complex added iron or to stabilize freshly formed iron oxyhydroxides by adsorbing to the iron oxyhydroxide surfaces, leading to dramatic size increase.

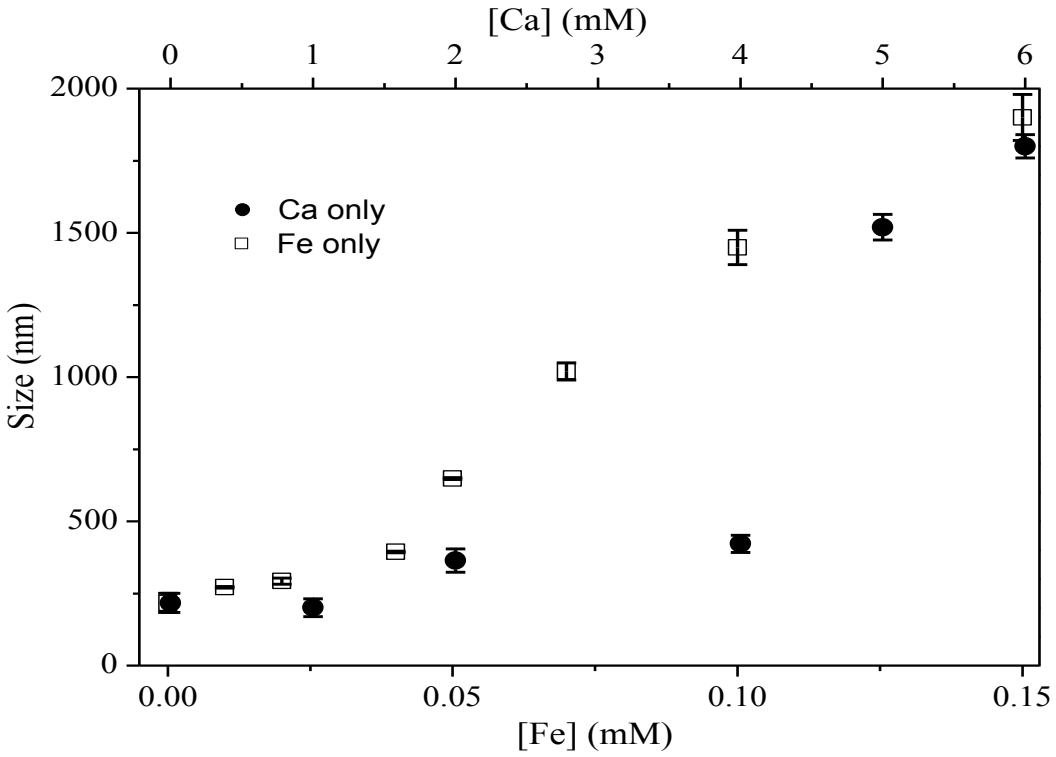

Figure 6-2. Sizes of SMP clusters at different calcium and iron concentrations. Error bars are the standard error of the mean from duplicate experiments.

6.3.1.3. Zeta-potential

The zeta potentials of SMP in bulk solution were measured on addition of 0 - 0.15 mM Fe(III) and 0 - 6 mM Ca (Figure 6-3). The zeta potentials of Ca-SMP assemblages increased on increasing calcium concentration while the zeta potentials of Fe-SMP assemblages were nearly independent of the level of iron addition, indicating the dominant interaction between SMP and iron interaction is probably the stabilization of iron oxyhydroxide particles (FeOOH) by SMP rather than formation of dissolved complexes. However, despite the different zeta potential behaviour, significant aggregation occurred in both cases as discussed in the previous section, which further indicated that surface charge reduction was not necessary in flocculation of these biologically produced organic compounds [145].

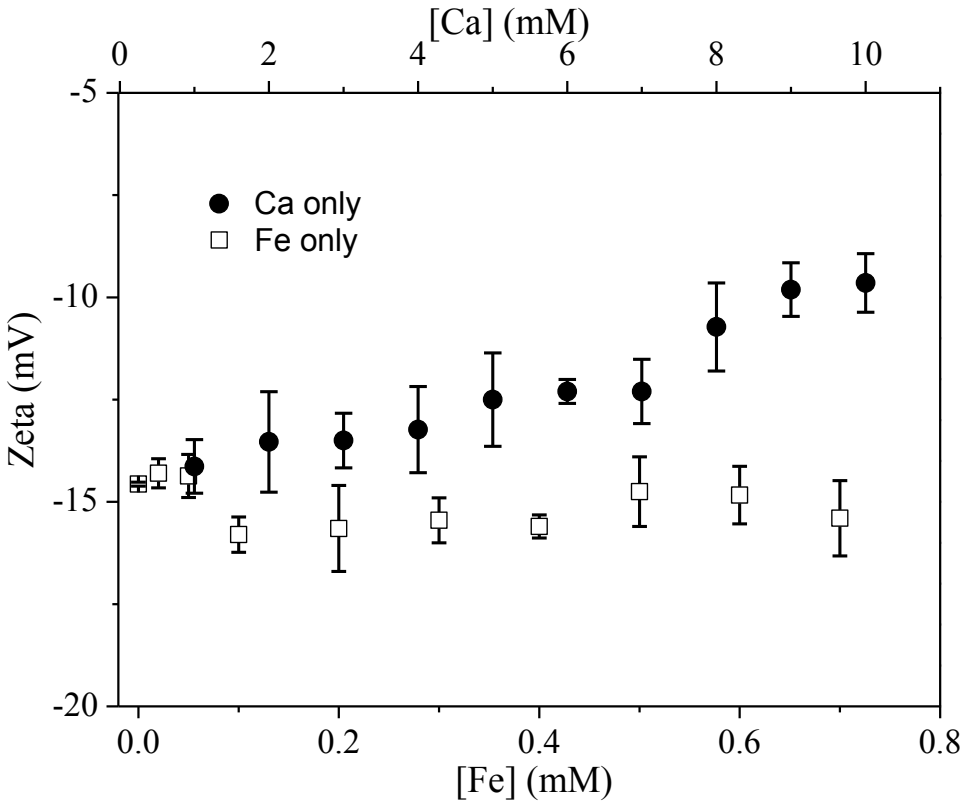

Figure 6-3. Zeta potential of SMP at different calcium and iron concentrations. Error bars are the standard error of the mean from duplicate experiments.

6.3.2. Effects of iron(III) and calcium on the properties of SMP cake layer

6.3.2.1. Cake resistance and porosity

To illustrate the effects of iron and calcium on the properties of the SMP cake layer, the cake resistance and porosity were examined at a TMP of 135 kPa. In the absence of calcium or iron addition, the cake layer is most likely made up of a network of polysaccharides with other SMP components potentially trapped within the network. Even low concentrations of metals in the supernatant such as Mg, Al, Si and especially Ca and Fe are recognized to have a significant impact on the formation and properties of the cake layer, resulting in high cake resistance (Figure 6-4, at point 0) [183]. Indeed, the principal cause of severe fouling in membrane filtration is understood to be due to the multivalent cations either present initially in or added to the sludge supernatant with these cations bridging polysaccharides through metal-ligand complexation [133, 176]. As can be seen from Figure 6-4, the cake resistance increased slightly upon calcium addition to SMP and reached a peak at 2 mM calcium, but then started to decrease with further addition of calcium with the most dramatic change occurring at around 5 mM Ca.

In the Fe-SMP system, the cake resistance decreased at even low concentrations of added iron, which differs from the previously studied Fe-alginate system. This may well be due to the presence of ~0.8 mM calcium in the raw supernatant with this hypothesis supported by the observation that a further addition of 2 mM calcium resulted in lower cake resistance in the presence of iron, indicating the large synergistic effects of calcium and iron in the SMP system.

The increase in iron concentration may increase the adsorption of SMP/Ca-SMP to the surface of iron oxides in a similar manner to that in the Fe-alginate system (with stronger adsorption in the presence of calcium) resulting in fouling mitigation. However, the improved cake filterability in Ca-SMP and Fe-SMP systems are possibly mainly attributed to (i) particle size increase in bulk solution, and (ii) gel network collapse during aggregation and syneresis.

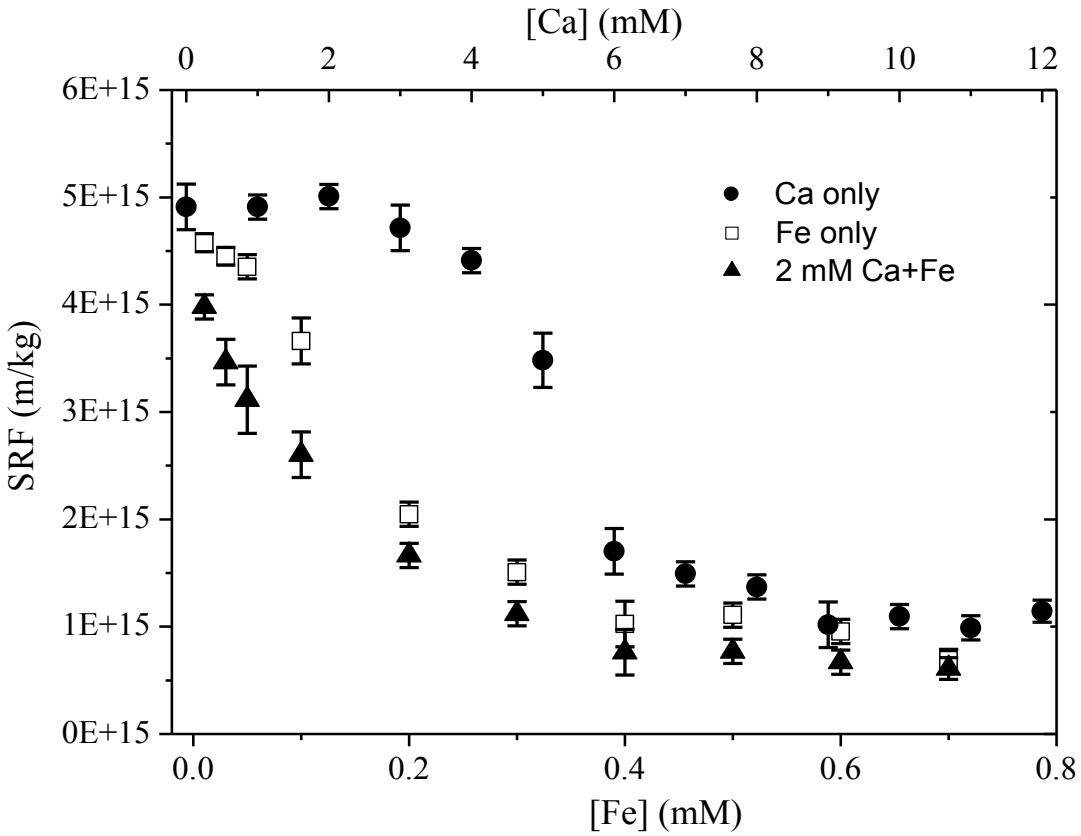

Figure 6-4. Specific resistance to filtration (SRF) varies as calcium and iron concentrations in SMP solution.

On further addition of calcium and iron beyond 5 and 0.05 mM respectively, dramatic increases in size were observed (Figure 6-2). Large SMP aggregates have little capability to participate in the gel formation since the binding sites of the polysaccharides or/and proteins present are likely saturated and incapable of binding

with other groups. The colloid size also plays a role in whether the deposit formed on the membrane surface is a gel or cake deposit. The physico–chemical properties of the filtered media changed on increasing calcium and iron concentrations with the deposit passing from a gel-type structure to a cake deposit [184]. Larger particles in general form a more open cake fouling layer than small particles, with the larger particles creating a relatively compact, ordered cake deposit on the membrane surface of higher permeability than the deposits formed by small particles [84]. Another key indication of transfer from gelation to the more permeable cake deposit is the significant porosity reduction (and therefore water content) of Ca-SMP and Fe-SMP (Figure 6-5). The gel structure collapse probably occurred during syneresis as a result of the formation of relatively large sizes enabling water flow between the pores in these assemblages.

In the case of addition of both calcium and iron to SMP solution, large amounts of Fe/Ca-SMP clusters precipitated on the membrane surface which cracked easily during the peeling process, leading to difficulty in quantifying the wet cake mass (and thus porosity).

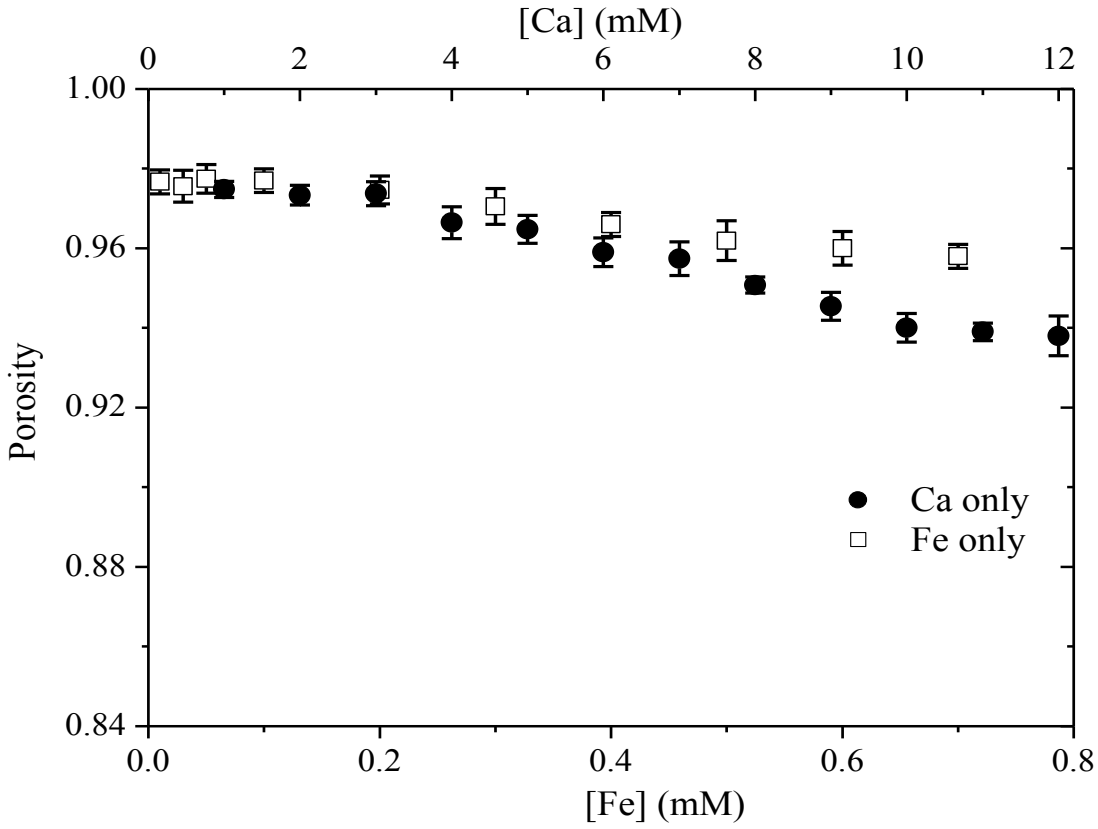

Figure 6-5. Cake porosity varies as calcium and iron concentrations in SMP solution.

6.3.2.2. SEM-EDX analysis

To further illustrate the effects of iron and calcium on the properties of the fouling layer, the morphology of the assemblage was observed by SEM. As can be seen from the electron micrographs of the Ca-SMP system shown in Figure 6-6, it is evident that the gel surface was dramatically altered by the presence of increasing calcium, transforming from a smooth looking gel to much rougher surface indicative of a cake structure. In the Fe-SMP micrographs (Figure 6-7), "black spots" similar to those formed in the Fe-alginate system were observed at high iron concentration with these spots likely to be iron oxides that have aggregated as a result of the inability of the organics in supernatant to prevent particle-particle interactions [164].

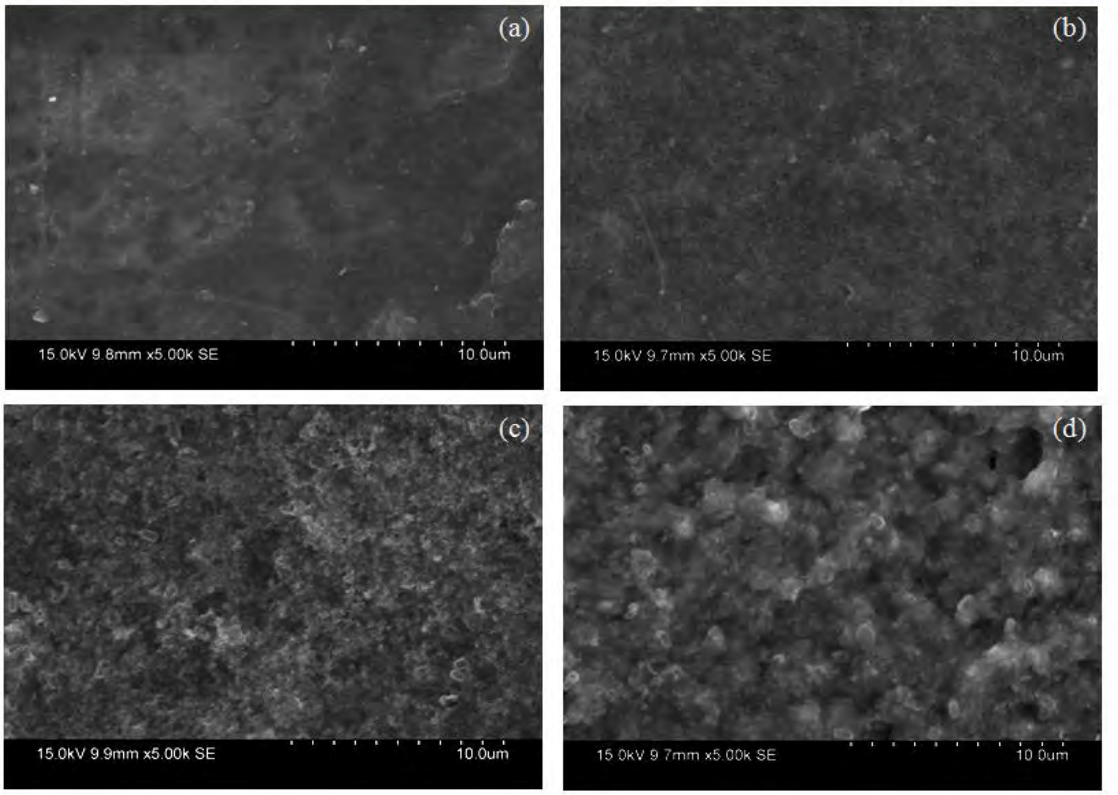

Figure 6-6. Images of deposits formed on the membrane from (a) raw SMP, and in the presence of (b) 2 mM Ca, (c) 4 mM Ca and (d) 10 mM Ca.

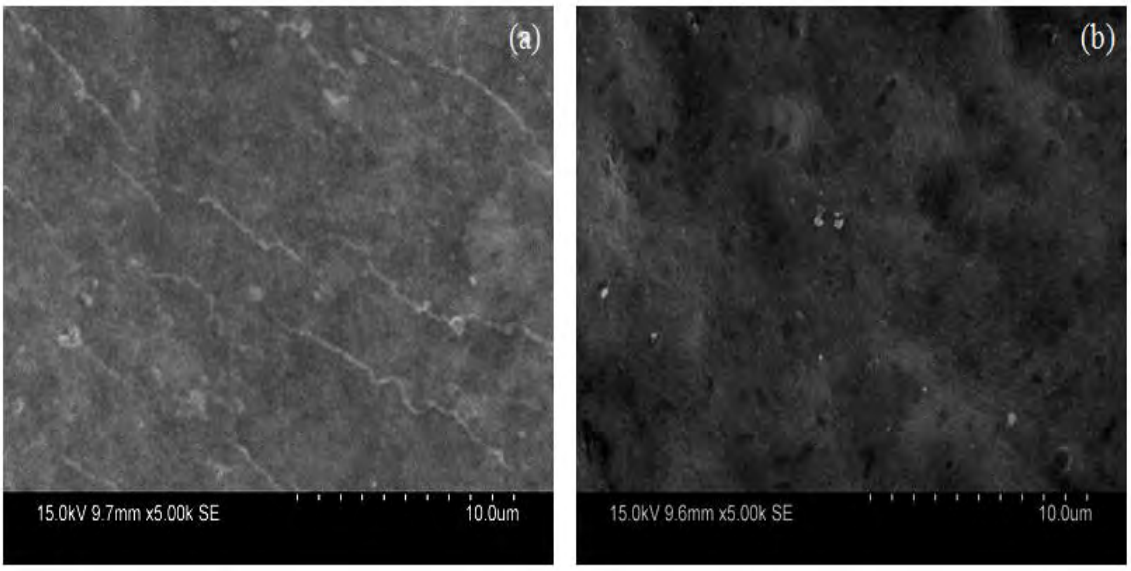

Figure 6-7. SMP images in the presence of (a) 0.02 mM Fe and (b) 0.7 mM Fe.

In order to verify the major chemical components of the fouling layer, elemental analyses was performed to determining the relative concentration of Na, Mg, P, K, Ca, and Fe by SEM-EDX (Figure 6-8). Together with the results of ICP showing metal concentrations in the supernatant (Figure 6-1), EDX analysis indicates that the membrane retains a higher portion of Ca and Fe than Mg, Na and K. This complies with the results of Wang and Waite who showed that the concentration of calcium and iron in the MBR supernatant is higher than that in the MBR effluent [20]. In addition, on increase in the extent of calcium and/or iron addition, the retention ratio of calcium and iron also increased (Table 6-2).

Table 6-2. EDX analysis of retained metal on the membrane (mass weight percentage, %).

		Ca (mM)				Fe (mM)	
	Raw	2	4	10	12	0.02	0.6
Fe (%)	**16.4**	15.5	12.7	3.2	2.1	18.8	30.4
Ca (%)	**13.2**	17.4	24.6	34.0	35.0	13.0	8.9

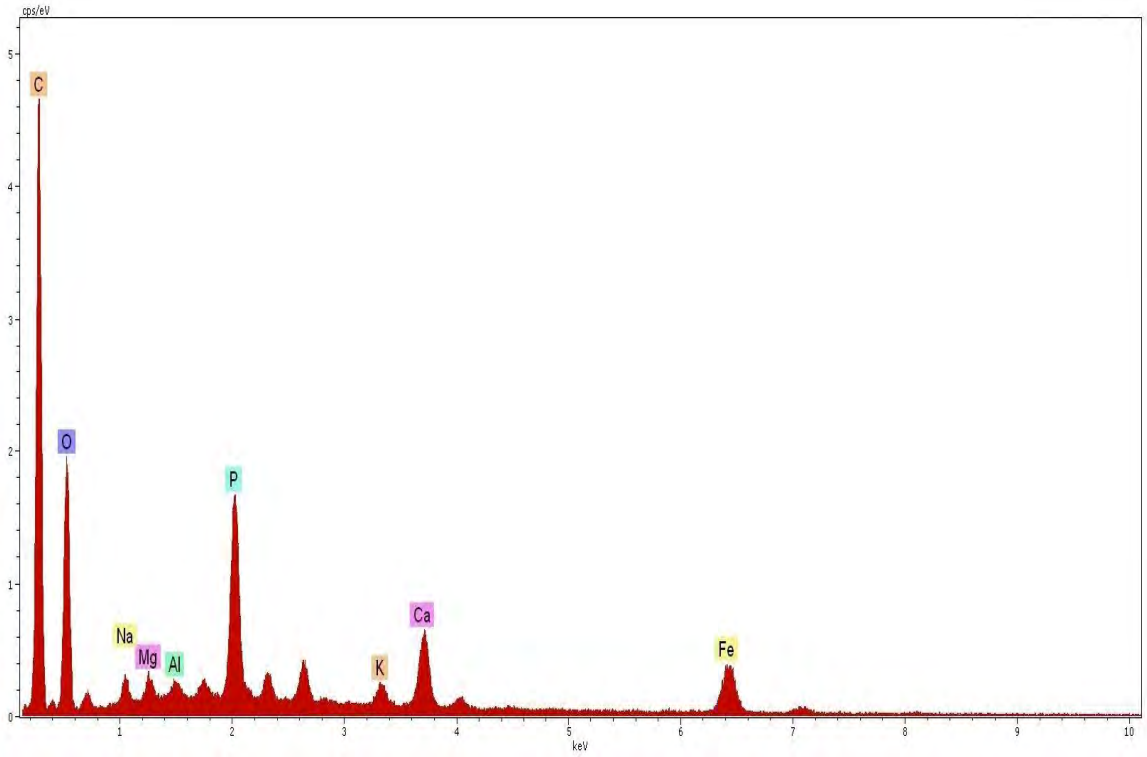

Figure 6-8. EDX analysis of SMP gel layer

6.3.2.3. FTIR and XRD

The FTIR spectrum of the foulants obtained from filtering the sludge supernatant are illustrated in Figure 6-9 (a). The spectrum shows a broad region of absorption between 3600 and 3000 cm^{-1} due to stretching of the O-H bond in hydroxyl functional groups, while the sharper peaks at 2926 and 2848cm^{-1} are due to the stretching of C-H bonds [185]. The foulants should also include protein and polysaccharides. There are two peaks (1648 and 1544 cm^{-1}) in the spectrum unique to the protein secondary structure, assigned as amides I and II [186]. The broad peak of 1040 cm^{-1} exhibits the presence of polysaccharides [183]. The FTIR results indicate that the major components of foulants contain expected protein and polysaccharide materials. Besides these groups membrane foulants also include other organic substances featured by functional groups. Another major peak is evident at a wave

number of 1720 cm^{-1},which is associated with carboxylic groups, and which represents a functionality typical of humic and fulvic acids [8, 187]. The band near 1250 cm^{-1} is from the asymmetric stretching vibration of the C-O-C ester, which means the membrane foulants contained a medium amount of lipids [17]. The peaks at 1450 cm^{-1} and 1385 cm^{-1} are mainly from asymmetric bending and symmetric deformations of methyl groups [188]. The presence of proteins, polysaccharides and lipids illustrates that the organic substances in membrane foulants are very complicated.

At low concentrations of calcium (and iron) addition to SMP solution where the fouling is still considered severe, the peaks of the FTIR spectra are essentially unchanged (Figure 6-9 (b) at 2 mM Ca, and (c) 0.01 mM Fe). However, in the case of overdosing when the cake resistance was significantly reduced, peaks between 1040 and 1540 cm^{-1} disappeared together with a shift in the polysaccharide peak of 1040 cm^{-1}. Interestingly, a small calcium addition (2 mM) to the Fe-SMP system does not have significant impact on the FTIR results (Figure 6-9 (d)) even though this small addition improved filtration performance markedly.

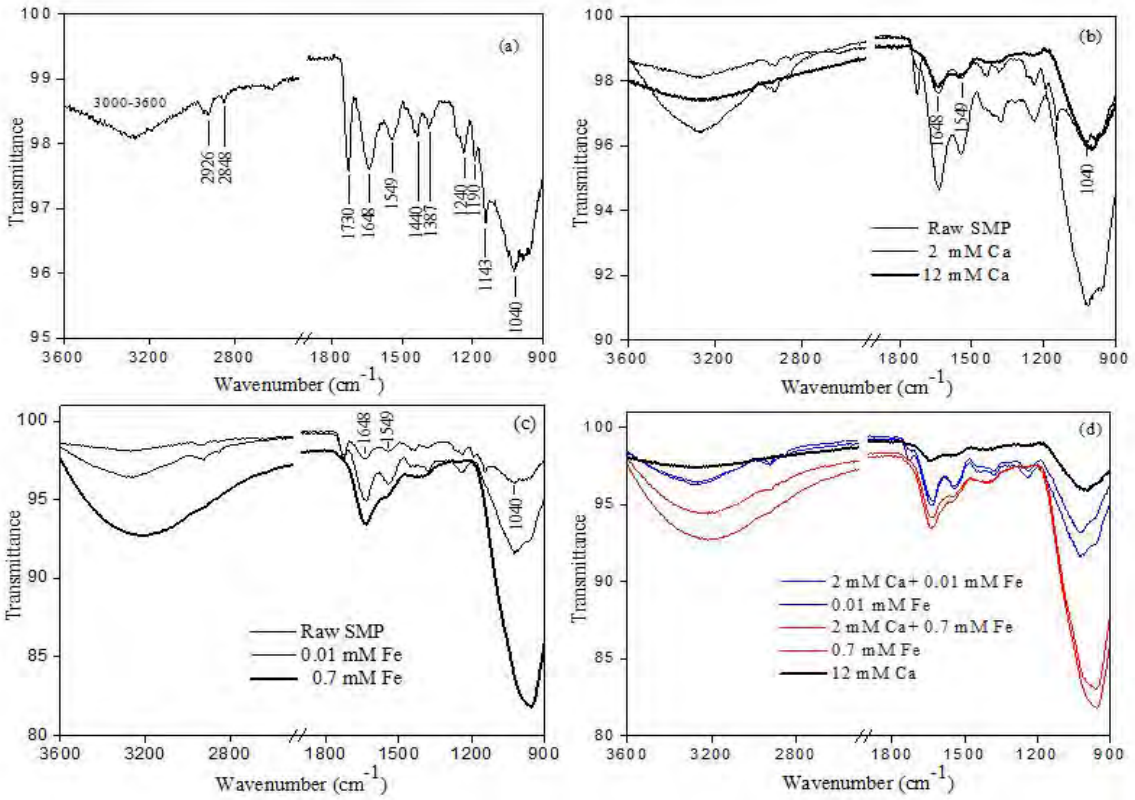

Figure 6-9. FTIR spectra of SMP (a) in the absence of calcium and iron addition, (b) with 2 and 12 mM calcium presence, (c) with 0.01 and 0.7 mM Fe, and (d) in the presence of both calcium and iron.

The change in the FTIR spectra at high calcium (and iron) concentrations is considered to be due to the formation of inorganic oxides on the membrane surface. To further characterize the cake layer, XRD was performed with results shown in Figure 6-10. XRD patterns showed calcite was the main crystal form present in the cake layer of the SMP control. After addition of calcium, the patterns did not change much but the peak intensity decreased to some extent, especially for the treatment with high calcium addition (6 mM). However, it was noted that even a small amount of iron (0.4 mM) lead to the disappearance of all the calcite peaks no matter whether calcium was present or not, indicating that calcite formation was readily inhibited by the presence of iron. While not confirmed, this effect of iron addition was most likely

attributable to the adsorption of calcium to iron oxyhydroxide surfaces with the resultant removal of calcium from solution preventing calcite formation,

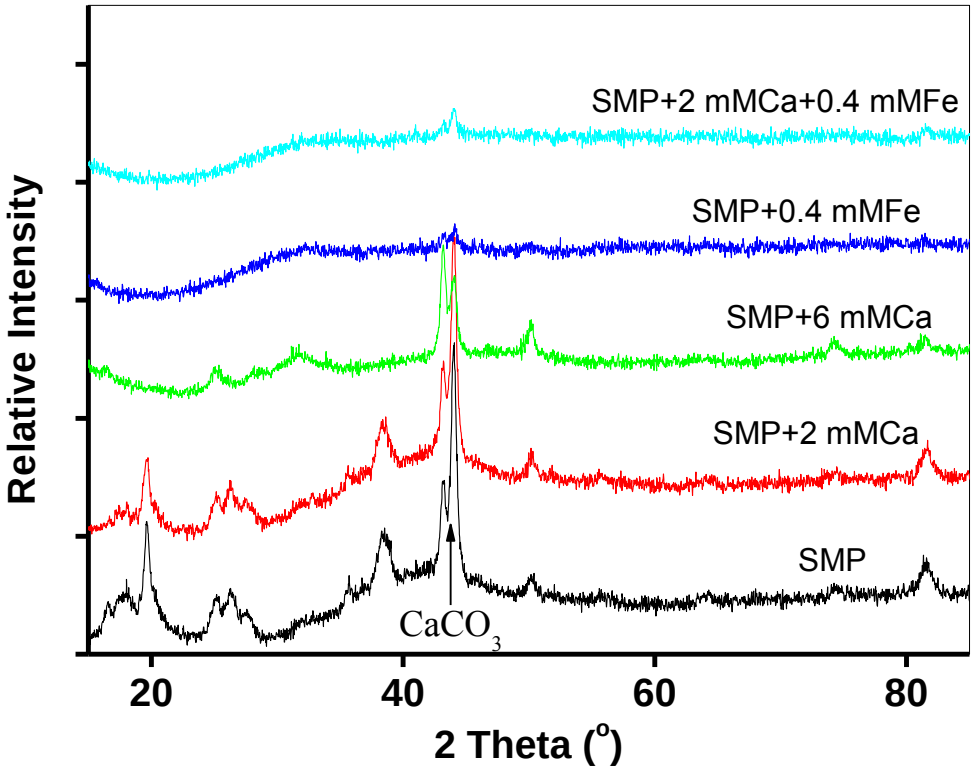

Figure 6-10. XRD spectra of SMP cake layer

6.4. Conclusions

Real supernatant from centrifuged activated sludge was used in constant pressure dead-end filtration to study the fouling behaviour of the SMP gel layer formed on the membrane surface in a range of concentrations of calcium and iron. The filtration behaviour, as well as the particle size distribution and zeta-potential of Ca-SMP and Fe-SMP, are similar to the results obtained when using alginate as a surrogate. As found for alginate, severe fouling was observed at low calcium or iron concentrations, and decreased significantly once over dosed. In addition, calcium plays an important role in reducing the severity of the fouling caused by Fe-SMP with this effect

possibly attributable to the ability of the presence of calcium to induce particle aggregation. Further characterization of the SMP gel by SEM coupled EDX analysis found significant change in morphology at high calcium or iron dosage. On increasing calcium or iron addition, the membrane retained more calcium and iron though the formation of calcite was no longer observed with this effect either due to removal of calcium from solution by adsorption to iron oxyhydroxides formed on the membrane or (less likely) as a result of the formation of more amorphous precipitates.

Chapter 7. Summary and conclusions

An overview of the results from each of the preceding chapters is presented in this chapter. These results are then examined in light of the stated questions in the introduction of the thesis. Finally, some implications of the work are discussed and future avenues for research are suggested.

7.1. Overview of results

The overall objective of this thesis has been to elucidate the role of calcium and iron in membrane fouling caused by soluble microbial products (SMP) and alginate, a polysaccharide widely used as a model for SMP. These issues were investigated through a series of laboratory experiments where constant-pressure dead-end filtration was used as a primary method to identify the fouling behaviour of alginate and SMP in the presence of calcium and iron (both separately and together).

Chapter 3 provided evidence that the effect of calcium on alginate fouling is biphasic through a series of experiments in which the characteristics of Ca-alginate in bulk solution such as binding behaviour and size, as well as the subsequent formed cake properties under a range of calcium and alginate concentrations were obtained. At higher applied calcium concentrations, a second phase of enhanced calcium uptake following alginate binding sites saturation was observed, providing evidence of an extension of previously recognized cooperative binding behaviour of calcium and alginate at lower calcium concentrations. This enhanced uptake of calcium was also shown to have marked impact on filtration behaviour with the cake resistance of the gel layer decreasing dramatically once enhanced uptake of calcium in bulk solution

occurred. In addition, the properties of both the bulk solution Ca-alginate and the Ca-alginate layer formed on the membrane depended more on the calcium concentration than the alginate concentration, indicating the dominant role of calcium in Ca-alginate fouling.

Chapter 4 reported filtration behaviour of Ca-alginate aggregates over a range of sodium and calcium concentrations. Although, as reported by other investigators, there was a strong relationship between calcium concentration and membrane fouling, the fouling was also affected strongly by the monovalent ion concentration. Ca-alginate binding/gelation could be prevented by sodium competing for carboxyl groups on the alginate at high sodium concentration, while at the same time, the calcium concentration required to induce gel formation also increased as sodium concentration increased. Further, it was pointed out in this chapter that it is the amount of bound calcium rather than the total calcium present that drives the onset of enhanced calcium uptake and gel breakdown. In addition, the DCB theory rather than DLVO theory was better able to describe the binding behaviour between calcium and alginate.

Chapter 5 illustrated the interaction between iron and alginate, and concluded that the dominant mechanism in this case involves alginate stabilization of FeOOH nanoparticles rather than the direct formation of Fe-alginate complexes. Increasing iron concentration could also lead eventually to reduced fouling (as found for the Ca-alginate system), though this effect could be mitigated by increasing alginate concentration. This means that Fe-alginate fouling is alginate concentration dependent in contrast to the Ca-alginate system that is driven by calcium concentration only. Further comparison of fouling in the Fe-alginate and Ca-alginate

systems led to the conclusion that substantially lower concentrations of iron (than calcium) were required to induce gelation Most importantly, the presence of calcium prior to iron addition influences the gel properties significantly resulting in the formation of assemblages that were substantially less fouling.

Chapter 6 built on the results of previous chapters and provides an overview of the fouling behaviour of solutions containing SMP for a range of calcium and iron concentrations. The results obtained are consistent with those obtained in the alginate system and provided further evidence of the role of calcium and iron in membrane fouling with real wastewaters.

7.2. Objectives

Six main objectives of this thesis represented in section 1.6 of the Introduction are reiterated below with discussion of how they have been achieved and the new knowledge that has been generated from these investigations.

- How does the presence of calcium influence polysaccharide gelation and does this increase or decrease fouling? Does the gelling propensity of polysaccharides increase linearly with increase in calcium or polysaccharides concentration?
- Once the calcium binding capacity of the polysaccharide is reached, does the resistance of the gel layer formed on the membrane plateau or keep increasing in excess of the polysaccharide binding capacity?

Calcium has been shown to either increase or decrease cake resistance during the filtration of alginate, while biphasic behaviour was reported where progressive

addition of calcium initially reduced filtrate flux but then improved it. Investigations in chapter 3 further demonstrated that the effect of calcium on alginate fouling was biphasic with two distinct regimes delineated through linking the binding behaviour in bulk solution to gel formation on the membrane surface. At low calcium concentrations, high cake resistance was apparent with the resistance plateauing as calcium concentration increased. Once the calcium-binding capacity of the polysaccharide was reached, enhanced calcium uptake occurred, hypothesized to be due to collapse of the low permeability gel structure, and cake resistance decreased almost linearly. In addition, on increasing alginate concentration by a factor of 10 (from 0.1 to 1 $g.L^{-1}$), the cake resistance of the Ca-alginate gel layer remained very similar, which indicates that gelation depends more on the calcium rather than the alginate concentration.

- How do monovalent cations such as sodium influence the binding behaviour of alginate for calcium?

As discussed in Chapter 4, although the relationship between calcium concentration and membrane fouling is very important and has been studied widely, the fouling was also strongly influenced by the monovalent ion concentration. In the case of low calcium addition, a small amount of calcium was sufficient to induce gel formation at low sodium concentration with resultant severe fouling whereas, at high sodium concentration, gelation was prevented by the sodium competing for alginate carboxyl groups leading to reduced fouling due to incomplete Ca-alginate gel formation. However, at calcium concentrations high enough to overcome the sodium screening effect, cake resistance at high sodium concentration was very high. Meanwhile, for low sodium concentrations, the calcium concentration was already

high enough to result in significant aggregate size increase and improved cake properties. Therefore, the effect of sodium on alginate fouling depends on the concentrations of both sodium and calcium if present.

- Does the gelling propensity of polysaccharides increase linearly with increase of iron or polysaccharide concentration? Once iron is added in excess of the polysaccharide binding capacity, does the resistance of the gel layer formed on the membrane plateau or keep increasing?

The fouling behaviour of Fe-alginate also displays a biphasic pattern as shown in Chapter 5, with increasing iron concentration leading to reduced fouling eventually, possibly as a result of the adsorption of alginate on iron oxyhydroxide surfaces with resultant formation of large aggregates. However, the improved filtration performance could be impeded by increasing alginate concentration with the higher alginate concentrations presumably preventing iron oxide from precipitating out of alginate solution thereby resulting in more severe fouling. As such, Fe-alginate fouling is alginate concentration dependent which is different from the Ca-alginate system where the fouling was driven by the calcium concentration only.

- Does the addition of ferric chloride render the fouling in MBRs more or less severe?
- Does the presence of calcium in wastewater influence the interaction of SMP with added Fe? What happens if both calcium and iron are present in the system?

These last two questions were investigated in Chapters 5 and 6. Calcium, a ubiquitous metal in water and wastewater systems, has a significant effect on the

interaction of Fe with alginate or SMP. Whether the addition of iron renders fouling more severe or assists in fouling mitigation seems to depend largely on the presence of calcium. If calcium is absent, severe membrane fouling upon iron dosage is expected. However, in the presence of calcium, it is much easier to form larger aggregates upon iron addition presumably because calcium occupies iron binding sites and makes iron oxyhydroxide precipitation easier to occur. As a result, the fouling properties of the cake are improved significantly.

7.3. Implications

Our findings support the conclusion that all the cations present in wastewater, whether they are monovalent, divalent or multi-valent cations, are interacting with each other and have significant impact on the wastewater treatment system, especially in MBR plants where membrane fouling may be severe. Therefore, the coagulant choice and dosage should be considered based on influent wastewater characteristics.

The material properties of Ca-alginate for different NaCl and calcium concentrations presented here may be used as a reference in wastewater treatment for dosing coagulant based on metal composition of the influent. Traditionally, plants with high M/D ratios may benefit from reducing this ratio by reducing the monovalent cation concentration, increasing the divalent cation concentration, or doing both. My research results may provide an alternative way to optimize coagulant dosing method and dosage, and so minimize membrane fouling through trying to avoid severe the gelation period. If there is high concentration of monovalent ions in raw wastewater, low calcium dosage may help to retard fouling layer build-up although this may have a potential adverse effect on floc formation. In the case of low

or medium monovalent concentration, trying to overdose calcium to pass the severe fouling period may be beneficial. However, for any case, jar test is suggested to optimize the coagulation process.

The research also has significant implications for membrane filtration where the membrane fouling caused by iron is severe. As described in the Fe-alginate and Fe-SMP systems, the presence of calcium seems vital to reduction of severe fouling.

7.4. Future work

While the effect of sodium on Ca-alginate binding and fouling by Ca-alginate assemblages has been examined in this thesis, its impact on Fe-alginate and Fe-Ca-alginate should also be investigated in future. I have obtained initial results in Fe-alginate system, and found that the cake resistance decreases as the sodium concentration increases which is opposite to the phenomenon in the Ca-alginate system. This is probably because the phenomenon is different from the bridging mechanism of calcium with the interaction between iron and alginate occurring as a result of the adsorption of alginate to the iron oxyhydroxide surface. Since increasing ionic strength would enhance iron oxide precipitation, it is reasonable to see reduced cake resistance as the sodium concentration in Fe-alginate system increases. Future work could also be undertaken regarding the effect of pH on fouling behaviour of Fe-alginate. As more iron oxyhydroxide will be formed at higher pH, I expect smaller iron concentrations to induce gelation, but the transition to reduced cake resistance may also occur at relatively lower iron concentrations than observed at lower pH.

Further, future work should also investigate whether the sodium concentration has the same influence to the fouling behaviour of Ca-SMP and Fe-SMP as that in the alginate system.

References

[1] B. Teychene, C. Guigui, C. Cabassud, G. Amy, Toward a better identification of foulant species in MBR processes, Desalination, 231 (2008) 27-34.

[2] S. Judd, Fouling control in submerged membrane bioreactors, Water Sci. and Technol., 51 (2005) 27-34.

[3] S. Judd, A review of fouling of membrane bioreactors in sewage treatment, Water. Sci. Technol. , 49 (2004) 229-235.

[4] A. Drews, C.-H. Lee, M. Kraume, Membrane fouling - a review on the role of EPS, Desalination, 200 (2006) 186-188.

[5] J. Wu, X. Huang, Effect of mixed liquor properties on fouling propensity in membrane bioreactors, J. Membr. Sci., 342 (2009) 88-96.

[6] Q. Wang, Z. Wang, Z. Wu, J. Ma, Z. Jiang, Insights into membrane fouling of submerged membrane bioreactors by characterizing different fouling layers formed on membrane surfaces, Chem. Eng. J., 179 (2012) 169-177.

[7] Q. Li, M. Elimelech, Organic fouling and chemical cleaning of nanofiltration membranes: measurements and mechanisms, Environ. Sci. Technol., 38 (2004) 4683-4693.

[8] C. Jarusutthirak, G. Amy, J.-P. Croué, Fouling characteristics of wastewater effluent organic matter (EfOM) isolates on NF and UF membranes, Desalination, 145 (2002) 247-255.

[9] M. Into, A.-S. Jönsson, G. Lengdén, Reuse of industrial wastewater following treatment with reverse osmosis, J. Membr. Sci., 242 (2004) 21-25.

[10] D.J. Barker, D.C. Stuckey, A review of soluble microbial products (SMP) in wastewater treatment systems, Water Res., 33 (1999) 3063-3082.

[11] H.K. Shon, S. Vigneswaran, S.A. Snyder, Effluent Organic Matter (EfOM) in Wastewater: Constituents, Effects, and Treatment, Critical Reviews in Environ. Sci. Technol., 36 (2006) 327-374.

[12] G. Amy, Fundamental understanding of organic matter fouling of membranes, Desalination, 231 (2008) 44-51.

[13] A. Drews, M. Vocks, U. Bracklow, V. Iversen, M. Kraume, Does fouling in MBRs depend on SMP?, Desalination, 231 (2008) 141-149.

[14] S. Rosenberger, M. Kraume, Filterability of activated sludge in membrane bioreactors, Desalination, 151 (2003) 195-200.

[15] S. Rosenberger, H. Evenblij, S. te Poele, T. Wintgens, C. Laabs, The importance of liquid phase analyses to understand fouling in membrane assisted activated sludge processes—six case studies of different European research groups, J. Membr. Sci., 263 (2005) 113-126.

[16] C.S. Laspidou, B.E. Rittmann, A unified theory for extracellular polymeric substances, soluble microbial products, and active and inert biomass, Water Res., 36 (2002) 2711-2720.

[17] A. Ramesh, D. Lee, J. Lai, Membrane biofouling by extracellular polymeric substances or soluble microbial products from membrane bioreactor sludge, Appl Microbiol Biotechnol, 74 (2007) 699-707.

[18] E.H. Bouhabila, R. Ben Aïm, H. Buisson, Microfiltration of activated sludge using submerged membrane with air bubbling (application to wastewater treatment), Desalination, 118 (1998) 315-322.

[19] C. Wisniewski, A. Grasmick, Floc size distribution in a membrane bioreactor and consequences for membrane fouling, Colloids and Surfaces A: Physicochemical and Engineering Aspects, 138 (1998) 403-411.

[20] X.M. Wang, T.D. Waite, Role of gelling soluble and colloidal microbial products in membrane fouling, Environ. Sci. Technol., 43 (2009) 9341-9347.

[21] B.P. Frank, G. Belfort, Polysaccharides and sticky membrane surfaces: critical ionic effects, J. Membr. Sci., 212 (2003) 205-212.

[22] P. Le-Clech, V. Chen, T.A.G. Fane, Fouling in membrane bioreactors used in wastewater treatment, Journal of Membrane Science, 284 (2006) 17-53.

[23] K.J. Wilkinson, A. Joz-Roland, J. Buffle, Different roles of pedogenic fulvic acids and aquagenic biopolymers on colloid aggregation and stability in freshwaters, Limnol. Oceanogr., 42 (1997) 1714-1724.

[24] M.L. Wells, Marine colloids: a neglected dimension, Nature, 391 (1998) 530-531.

[25] A.C. Fonseca, R.S. Summers, A.R. Greenberg, M.T. Hernandez, Extra-cellular polysaccharides, soluble microbial products, and natural organic matter impact on nanofiltration membranes flux decline, Environ. Sci. Technol., 41 (2007) 2491-2497.

[26] Y.M. Lin, L. Wang, Z.M. Chi, X.Y. Liu, Bacterial alginate role in aerobic granular bio-particles formation and settleability improvement, Sep. Sci. Technol., 43 (2008) 1642-1652.

[27] Y. Lin, M. de Kreuk, M.C.M. van Loosdrecht, A. Adin, Characterization of alginate-like exopolysaccharides isolated from aerobic granular sludge in pilot-plant, Water Res., 44 (2010) 3355-3364.

[28] P.C. Carman, Fundamental principles of industrial filtration, Trans. Inst. Chem. Eng., 16 (1938) 168-183.

[29] X.M. Wang, T.D. Waite, Gel layer formation and hollow fiber membrane filterability of polysaccharide dispersions, J. Membr. Sci., 322 (2008) 204-213.

[30] B. Mi, M. Elimelech, Organic fouling of forward osmosis membranes: Fouling reversibility and cleaning without chemical reagents, J. Membr. Sci., 348 (2010) 337-345.

[31] I. Donati, S. Paoletti, Material properties of alginates, in: B.H.A. Rehm (Ed.) Alginates: Biology and Applications, Springer Berlin Heidelberg, 2009, pp. 1-53.

[32] P.A.J. Gorin, J.F.T. Spencer, Exocellular alginic acid from Azotobacter Vinelandii, Can. J. Phys, 44 (1966) 993-998.

[33] J.R.W. Govan, J.A.M. FyeeE, T.R. Jarman, Isolation of alginate-producing mutants of Pseudomonas fluorescens, Pseudomonas putida and Pseudomonas mendocina, Microbiology, 125 (1981) 217-220.

[34] O. Smidsrød, G. Skjåk-Braek, Alginate as immobilization matrix for cells, Trends Biotechnol., 8 (1990) 71-78.

[35] A. Martinsen, G. Skjåk-Braek, O. Smidsrød, Alginate as immobilization material: I. Correlation between chemical and physical properties of alginate gel beads, Biotechnol. Bioeng., 33 (1989) 79-89.

[36] K.I. Draget, O. Gåserød, I. Aune, P.O. Andersen, B. Storbakken, B.T. Stokke, O. Smidsrød, Effects of molecular weight and elastic segment flexibility on syneresis in Ca-alginate gels, Food Hydrocoll., 15 (2001) 485-490.

[37] O. Smidsrød, R.M. Glover, S.G. Whittington, The relative extension of alginates having different chemical composition, Carbohyd. Res., 27 (1973) 107-118.

[38] M.B. Stewart, S.R. Gray, T. Vasiljevic, J.D. Orbell, The role of poly-M and poly-GM sequences in the metal-mediated assembly of alginate gels, Carbohydrate Polymers, 112 (2014) 486-493.

[39] G.T. Grant, E.R. Morris, D.A. Rees, P.J.C. Smith, D. Thom, Biological interactions between polysaccharides and divalent cations: the egg-box model, FEBS Lett., 32 (1973) 195-198.

[40] G. Orive, S.K. Tam, J.L. Pedraz, J.-P. Halle, Biocompatibility of alginate-poly-l-lysine microcapsules for cell therapy, Biomaterials, 27 (2006) 3691-3700.

[41] L. Wang, E. Khor, A. Wee, L.Y. Lim, Chitosan-alginate PEC membrane as a wound dressing: Assessment of incisional wound healing, J. Biomed. Mater. Res., 63 (2002) 610-618.

[42] J.W. Doyle, T.P. Roth, R.M. Smith, Y.-Q. Li, R.M. Dunn, Effect of calcium alginate on cellular wound healing processes modeled in vitro, J. Biomed. Mater. Res., 32 (1996) 561-568.

[43] B. Thu, P. Bruheim, T. Espevik, O. Smidsrød, P. Soon-Shiong, G. Skjåk-Bræk, Alginate polycation microcapsules : I. Interaction between alginate and polycation, Biomaterials, 17 (1996) 1031-1040.

[44] S.R. Gray, N. Dow, J.D. Orbell, T. Tran, B.A. Bolto, The significance of interactions between organic compounds on low pressure membrane fouling, Water Science and Technology, 64 (2011) 632-639.

[45] H.-Y. Yu, M.-X. Hu, Z.-K. Xu, J.-L. Wang, S.-Y. Wang, Surface modification of polypropylene microporous membranes to improve their antifouling property in MBR: NH3 plasma treatment, Separation and Purification Technology, 45 (2005) 8-15.

[46] H.-Y. Yu, Y.-J. Xie, M.-X. Hu, J.-L. Wang, S.-Y. Wang, Z.-K. Xu, Surface modification of polypropylene microporous membrane to improve its antifouling property in MBR: CO2 plasma treatment, J. Membr. Sci., 254 (2005) 219-227.

[47] T.-H. Bae, I.-C. Kim, T.-M. Tak, Preparation and characterization of fouling-resistant TiO2 self-assembled nanocomposite membranes, J. Membr. Sci., 275 (2006) 1-5.

[48] R.W. Field, D. Wu, J.A. Howell, B.B. Gupta, Critical flux concept for microfiltration fouling, J. Membr. Sci., 100 (1995) 259-272.

[49] S. Judd, H. Alvarez‐Vazquez, B. Jefferson, The impact of intermittent aeration on the operation of air‐lift tubular membrane bioreactors under sub‐critical conditions, Sep. Sci. Technol., 41 (2006) 1293-1302.

[50] T. Ueda, K. Hata, Y. Kikuoka, O. Seino, Effects of aeration on suction pressure in a submerged membrane bioreactor, Water Res., 31 (1997) 489-494.

[51] C. Psoch, S. Schiewer, Critical flux aspect of air sparging and backflushing on membrane bioreactors, Desalination, 175 (2005) 61-71.

[52] E.H. Bouhabila, R. Ben Aïm, H. Buisson, Fouling characterisation in membrane bioreactors, Separation and Purification Technology, 22-23 (2001) 123-132.

[53] P. Le-Clech, V. Chen, T.A.G. Fane, Fouling in membrane bioreactors used in wastewater treatment, J. Membr. Sci., 284 (2006) 17-53.

[54] Z. Geng, E.R. Hall, P.R. Bérubé, Membrane fouling mechanisms of a membrane enhanced biological phosphorus removal process, J. Memb. Sci., 296 (2007) 93-101.

[55] B. Frølund, R. Palmgren, K. Keiding, P.H. Nielsen, Extraction of extracellular polymers from activated sludge using a cation exchange resin, Water Res., 30 (1996) 1749-1758.

[56] S.-H. Kim, S.-Y. Moon, C.-H. Yoon, S.-K. Yim, J.-W. Cho, Role of coagulation in membrane filtration of wastewater for reuse, Desalination, 173 (2005) 301-307.

[57] F. Fan, H. Zhou, H. Husain, Use of chemical coagulants to control fouling potential for wastewater membrane bioreactor processes, Water Environ. Res., 79 (2007) 952-957.

[58] V. Lahoussine-Turcaud, M.R. Wiesner, J.-Y. Bottero, Fouling in tangential-flow ultrafiltration: The effect of colloid size and coagulation pretreatment, J. Membr. Sci., 52 (1990) 173-190.

[59] J. Wu, F. Chen, X. Huang, W. Geng, X. Wen, Using inorganic coagulants to control membrane fouling in a submerged membrane bioreactor, Desalination, 197 (2006) 124-136.

[60] J. Wu, X. Huang, Effect of dosing polymeric ferric sulfate on fouling characteristics, mixed liquor properties and performance in a long-term running membrane bioreactor, Separation and Purification Technology, 63 (2008) 45-52.

[61] H.-f. Zhang, B.-s. Sun, X.-h. Zhao, Z.-h. Gao, Effect of ferric chloride on fouling in membrane bioreactor, Separation and Purification Technology, 63 (2008) 341-347.

[62] K.-J. Hwang, H.-C. Liu, Cross-flow microfiltration of aggregated submicron particles, J. Membr. Sci., 201 (2002) 137-148.

[63] I. Ivanovic, T. Leiknes, H. Ødegaard, Fouling control by reduction of submicron particles in a BF‐MBR with an integrated flocculation zone in the membrane reactor, Sep. Sci. Technol., 43 (2008) 1871-1883.

[64] T. Leiknes, The effect of coupling coagulation and flocculation with membrane filtration in water treatment: A review, J. Environ. Sci., 21 (2009) 8-12.

[65] S. Yeoman, T. Stephenson, J.N. Lester, R. Perry, The removal of phosphorus during wastewater treatment: A review, Environmental Pollution, 49 (1988) 183-233.

[66] T. Clark, T. Stephenson, A. Pearce, Phosphorus removal by chemical precipitation in a biological aerated filter, Water Res., 31 (1997) 2557-2563.

[67] J. Li, Effects of Fe(III) on floc characteristics of activated sludge, Journal of Chemical Technology & Biotechnology, 80 (2005) 313-319.

[68] K. Keiding, P.H. Nielsen, Desorption of organic macromolecules from activated sludge: Effect of ionic composition, Water Res., 31 (1997) 1665-1672.

[69] J.H. Bruus, P.H. Nielsen, K. Keiding, On the stability of activated sludge flocs with implications to dewatering, Water Res., 26 (1992) 1597-1604.

[70] K. Kakii, S. Kitamura, T. Shirakashi, M. Kuriyama, Effect of calcium ion on sludge characteristics, J. Ferment. Technol., 63 (1985) 263-270.

[71] A. Zita, M. Hermansson, Effects of ionic strength on bacterial adhesion and stability of flocs in a wastewater activated sludge system, Appl. Environ. Microb., 60 (1994) 3041-3048.

[72] C. CP, G. JJ, Effects of salinity on physical characteristics of activated sludge flocs, Water Qual Res J Can, 33 (1998).

[73] D.C. Sobeck, M.J. Higgins, Examination of three theories for mechanisms of cation-induced bioflocculation, Water Res., 36 (2002) 527-538.

[74] Higgins MJ, Miller LA, S. DC, Improving industrial wastewater treatment using divalent cation addition, Proceedings of the 72nd AnnualConference on Water Environment Fed, New Orleans (1999).

[75] M.J. Higgins, J.T. Novak, The effect of cations on the settling and dewatering of activated sludges: Laboratory results, Water Environ. Res., 69 (1997) 215-224.

[76] J.T. Novak, G.L. Goodman, A. Pariroo, J.-C. Huang, The blinding of sludges during filtration, J. Water Pollut. Con. F., 60 (1988) 206-214.

[77] M.J. Higgins, D. Sobeck, S.J. Owens, L.M. Szabo, For your floc's sake: choosing alternatives to sodium based chemicals, Proceedings of the Water Environment Federation, 2000 (2000) 22-35.

[78] J.T. Novak, N.G. Love, M.L. Smith, E.R. Wheeler, The effect of cationic salt addition on the settling and dewatering properties of an industrial activated sludge, Water Environ. Res., 70 (1998) 984-996.

[79] S.N. Murthy, J.T. Novak, R.D. De Haas, Monitoring cations to predict and improve activated sludge settling and dewatering properties of industrial wastewaters, Water Science and Technology, 38 (1998) 119-126.

[80] P. Drechsel, C.A. Scott, L. Raschid-Sally, M. Redwood, A. Bahri, Wastewater Irrigation and Health: Assessing and Mitigating Risk in Low-Income Countries, International Water Management Institute-Intrenational Development Research Centre, Ottawa, Canada, (2010).

[81] X.M. Wang, T.D. Waite, Gel layer formation and hollow fiber membrane filterability of polysaccharide dispersions, J. Membr. Sci., 322 (2008) 204-213.

[82] S. Lee, M. Elimelech, Relating organic fouling of reverse osmosis membranes to intermolecular adhesion forces, Environ. Sci. Technol., 40 (2006) 980-987.

[83] P. van den Brink, A. Zwijnenburg, G. Smith, H. Temmink, M. van Loosdrecht, Effect of free calcium concentration and ionic strength on alginate fouling in cross-flow membrane filtration, J. Membr. Sci., 345 (2009) 207-216.

[84] W.J.C. van de Ven, K.v.t. Sant, I.G.M. Pünt, A. Zwijnenburg, A.J.B. Kemperman, W.G.J. van der Meer, M. Wessling, Hollow fiber dead-end ultrafiltration: Influence of ionic environment on filtration of alginates, J. Membr. Sci., 308 (2008) 218-229.

[85] K. Listiarini, W. Chun, D.D. Sun, J.O. Leckie, Fouling mechanism and resistance analyses of systems containing sodium alginate, calcium, alum and their

combination in dead-end fouling of nanofiltration membranes, J. Membr. Sci., 344 (2009) 244-251.

[86] K. Listiarini, L. Tan, D.D. Sun, J.O. Leckie, Systematic study on calcium–alginate interaction in a hybrid coagulation-nanofiltration system, J. Membr. Sci., 370 (2011) 109-115.

[87] Y. Mo, K. Xiao, Y. Shen, X. Huang, A new perspective on the effect of complexation between calcium and alginate on fouling during nanofiltration, Sep. Purif. Technol., 82 (2011) 121-127.

[88] P.R. Bérubé, E. Lei, The effect of hydrodynamic conditions and system configurations on the permeate flux in a submerged hollow fiber membrane system, J. Membr. Sci., 271 (2006) 29-37.

[89] P. Kovalsky, G. Bushell, T.D. Waite, Prediction of transmembrane pressure build-up in constant flux microfiltration of compressible materials in the absence and presence of shear, J. Membr. Sci. , 344 (2009) 204-210.

[90] F.M. Tiller, J.R. Crump, Recent advances in compressible cake filtration theory, Mathematical Models and Design Methods in Solid-Liquid Separation, 88 (1985) 3-24.

[91] F.M. Tiller, R. Lu, J.H. Kwon, D.J. Lee, Variable flow rate in compactible filter cakes, Water Res., 33 (1999) 15-22.

[92] S. Judd, Fouling control in submerged membrane bioreactors, in: Water Science and Technology, 2005, pp. 27-34.

[93] B.S. McSwain, R.L. Irvine, M. Hausner, P.A. Wilderer, Composition and distribution of extracellular polymeric substances in aerobic flocs and granular sludge, Appl. Environ. Microbiol., 71 (2005) 1051-1057.

[94] T. Seviour, M. Pijuan, T. Nicholson, J. Keller, Z.G. Yuan, Gel-forming exopolysaccharides explain basic differences between structures of aerobic sludge granules and floccular sludges, Water Res., 43 (2009) 4469-4478.

[95] O. SmidsrÃ¸d, G. SkjaËšk-BrË¦k, Alginate as immobilization matrix for cells, Trends in Biotechnology, 8 (1990) 71-78.

[96] Metcalf&Eddy, Wastewater Engineering:, Treatment and Reuse, McGraw-Hill, (2004).

[97] S.R. Santiwong, J. Guan, T.D. Waite, Effect of ionic strength and pH on hydraulic properties and structure of accumulating solid assemblages during microfiltration of montmorillonite suspensions, J. Colloid Interface Sci., 317 (2008) 214-227.

[98] O. Smidsrod, Molecular basis for some physical properties of alginates in the gel state, Faraday Discuss. Chem. Soc., 57 (1974) 263-274.

[99] Y.P. Fang, S. Al-Assaf, G.O. Phillips, K. Nishinari, T. Funami, P.A. Williams, L.B. Li, Multiple steps and critical behaviours of the binding of calcium to alginate, J. Phys. Chem. B, 111 (2007) 2456-2462.

[100] Z.Y. Wang, Q.Z. Zhang, M. Konno, S. Saito, Sol-gel transition of algiante solution by the addition of various divalent-cations : a rheological study, Biopolymers, 34 (1994) 737-746.

[101] T.R. Laaman, Hydrocolloids in Food Processing, Wiley-Blackwell, Oxford, UK (2010).

[102] O. Smidsrod, A. Haug, Effect of divalent metals on properties of alginate solutions I. calcium ions, Acta Chem. Scand., 19 (1965) 329-340.

[103] M. Rajaonarivony, C. Vauthier, G. Couarraze, F. Puisieux, P. Couvreur, Development of a new drug carrier made from alginate, J. Pharm. Sci., 82 (1993) 912-917.

[104] J.O. You, Y.C. Liu, C.A. Peng, Efficient gene transfection using chitosan-alginate core-shell nanoparticles, Int. J. Nanome. , 1 (2006) 173-180.

[105] O. Smidsrød, G. Skjak-Brk, Alginate as immobilization matrix for cells, Trends in Biotechnology, 8 (1990) 71-78.

[106] R. Kohn, Ion binding on polyuronates - alginate and pectin, Pure Appl. Chem., 42 (1975) 371-397.

[107] I. Donati, S.v. Holtan, Y.A. MÃ¸rch, M. Borgogna, M. Dentini, G. Skjåk-Bræk, New hypothesis on the role of alternating sequences in calcium-alginate gels, Biomacromolecules, 6 (2005) 1031-1040.

[108] M. Dittrich, S. Sibler, Calcium Carbonate Precipitation by Cyanobacterial Polysaccharides, Geological Society, London, 336 (2010) 51-63.

[109] M. Obst, M. Dittrich, H. Kuehn, Calcium adsorption and changes of the surface microtopography of cyanobacteria studied by AFM, CFM, and TEM with respect to biogenic calcite nucleation, Geochem. Geophys., Geosyst., 7 (2006) Q06011.

[110] M. Obst, B. Wehrli, M. Dittrich, $CaCO_3$ nucleation by cyanobacteria: laboratory evidence for a passive, surface-induced mechanism, Geobiology, 7 (2009) 324-347.

[111] M. Obst, J.J. Dynes, J.R. Lawrence, G.D.W. Swerhone, K. Benzerara, C. Karunakaran, K. Kaznatcheev, T. Tyliszczak, A.P. Hitchcock, Precipitation of amorphous CaCO3 (aragonite-like) by cyanobacteria: a STXM study of the influence of EPS on the nucleation process, Geochim. Cosmochim. Acta, 73 (2009) 4180-4198.

[112] C. Dupraz, P.T. Visscher, Microbial lithification in marine stromatolites and hypersaline mats, Trends Microbiol., 13 (2005) 429-438.

[113] G. Arp, A. Reimer, J. Reitner, Microbialite formation in seawater of increased alkalinity, Satonda Crater Lake, Indonesia, J. Sediment. Res., 73 (2003) 105-127.

[114] I.-S. Chang, P.L. Clech, B. Jefferson, S. Judd, Membrane fouling in membrane bioreactors for wastewater treatment, J. Environ. Eng., 128 (2002) 1018-1029.

[115] W.J.C. van de Ven, K. van't Sant, I.G.M. Pünt, A. Zwijnenburg, A.J.B. Kemperman, W.G.J. van der Meer, M. Wessling, Hollow fiber dead-end ultrafiltration: influence of ionic environment on filtration of alginates, J. Membr. Sci., 308 (2008) 218-229.

[116] A. Haug, O. Smidsrod, The effect of divalent metals on the properties of alginate solutions 2. Compasion of different metal ions, Acta Chem. Scand. , 19 (1965) 341-351.

[117] K.L. Chen, S.E. Mylon, M. Elimelech, Enhanced aggregation of alginate-coated iron oxide (hematite) nanoparticles in the presence of calcium, strontium, and barium cations, Langmuir, 23 (2007) 5920-5928.

[118] K.L. Chen, S.E. Mylon, M. Elimelech, Aggregation kinetics of alginate-coated hematite nanoparticles in monovalent and divalent electrolytes, Environ. Sci. Technol., 40 (2006) 1516-1523.

[119] P. Aslani, R.A. Kennedy, Studies on diffusion in alginate gels. I. Effect of cross-linking with calcium or zinc ions on diffusion of acetaminophen, J. Control. Release, 42 (1996) 75-82.

[120] B.T. Stokke, K.I. Draget, O. Smidsrod, Y. Yuguchi, H. Urakawa, K. Kajiwara, Small-angle X-ray scattering and rheological characterization of alginate gels. 1. Ca-alginate gels, Macromolecules, 33 (2000) 1853-1863.

[121] N.M. Velings, M.M. Mestdagh, Physico-chemical properties of alginate gel beads, Polym. Gels Netw., 3 (1995) 311-330.

[122] B.T. Stokke, O. Smidsrød, D.A. Brant, Predicted influence of monomer sequence distribution and acetylation on the extension of naturally occurring alginates, Carbohydr. Polym., 22 (1993) 57-66.

[123] L.B. Li, Y.P. Fang, R. Vreeker, I. Appelqvist, Reexamining the egg-box model in calcium-alginate gels with X-ray diffraction, Biomacromolecules, 8 (2007) 464-468.

[124] A.S. Kinsela, A. Tjitradjaja, R.N. Collins, T.D. Waite, T.E. Payne, B.C.T. Macdonald, I. White, Influence of calcium and silica on hydraulic properties of sodium montmorillonite assemblages under alkaline conditions, J. Colloid and Interface Sci., 343 (2010) 366-373.

[125] N. Yang, X. Wen, T.D. Waite, X. Wang, X. Huang, Natural organic matter fouling of microfiltration membranes: prediction of constant flux behaviour from constant pressure materials properties determination, J. Membr. Sci., 366 (2011) 192-202.

[126] M. Sheintuch, O. Lev, P. Einav, E. Rubin, Role of exocellular polymer in the design of activated sludge, Biotechnol. Bioeng. , 28 (1986) 1564-1576.

[127] V. Urbain, J.C. Block, J. Manem, Bioflocculation in activated sludge: an analytic approach, Water Res., 27 (1993) 829-838.

[128] F.D. Sanin, P.A. Vesilind, Synthetic sludge: A physical/chemical model in understanding bioflocculation, Water Environ. Res., 68 (1996) 927-933.

[129] M.C.M. van Loosdrecht, J. Lyklema, W. Norde, A.J.B. Zehnder, Bacterial adhesion: a physicochemical approach, Microb. Ecol., 17 (1989) 1-15.

[130] C.L. Grady, G.T. Daigger, H.C. Lim, Biological Wastewater Treatment, Marcel Dekker, 1999.

[131] S. Arabi, G. Nakhla, Impact of calcium on the membrane fouling in membrane bioreactors, J. Membr. Sci., 314 (2008) 134-142.

[132] L.K. Wang, Y.T. Hung, Membrane and desalination technologies, Humana Press, 2010.

[133] R. Lapasin, S. Pricl, Rheology of industrial polysaccharides: theory and applications, Aspen Publishers, 1999.

[134] Y. Xin, M.W. Bligh, Y. Wang, T.D. Waite, Effect of calcium on membrane fouling by alginate gels, Journal of Membrane Science, Submitted (2014).

[135] C.K. Siew, P.A. Williams, N.W.G. Young, New insights into the mechanism of gelation of alginate and pectin: charge annihilation and reversal mechanism, Biomacromolecules, 6 (2005) 963-969.

[136] C. Garnier, M.A.V. Axelos, J.-F. Thibault, Selectivity and cooperativity in the binding of calcium ions by pectins, Carbohyd. Res., 256 (1994) 71-81.

[137] E.E. Braudo, A.A. Soshinsky, V.P. Yuryev, V.B. Tolstoguzov, The interaction of polyuronides with calcium ions. 1: binding isotherms of calcium ions with pectic substances, Carbohydr. Polym., 18 (1992) 165-169.

[138] J. Mattai, J.C.T. Kwak, Mg and Ca binding to heparin in the presence of added univalent salt, Biochimica et Biophysica Acta (BBA) - General Subjects, 677 (1981) 303-312.

[139] C. Ouwerx, N. Velings, M.M. Mestdagh, M.A.V. Axelos, Physico-chemical properties and rheology of alginate gel beads formed with various divalent cations, Polym. Gels Netw., 6 (1998) 393-408.

[140] C.H. Goh, P.W.S. Heng, L.W. Chan, Cross-linker and non-gelling Na^+ effects on multi-functional alginate dressings, Carbohydr. Polym., 87 (2012) 1796-1802.

[141] T.A. Davis, F. Llanes, B. Volesky, A. Mucci, Metal selectivity of sargassum spp. and their alginates in relation to their α-l-guluronic acid content and conformation, Environ. Sci. Technol., 37 (2002) 261-267.

[142] A.J. de Kerchove, M. Elimelech, Structural growth and viscoelastic properties of adsorbed alginate layers in monovalent and divalent salts, Macromolecules, 39 (2006) 6558-6564.

[143] K.I. Draget, K. Steinsvåg, E. Onsøyen, O. Smidsrød, Na- and K-alginate; effect on Ca^{2+}-gelation, Carbohydr. Polym., 35 (1998) 1-6.

[144] F.M.M. Morel, J.G. Hering, Principles and applications of aquatic chemistry, Wiley, 1993.

[145] J.L. Pavoni, M.W. Tenney, W.F. Echelberger, Jr., Bacterial exocellular polymers and biological flocculation, J. Water Pollut. Con. F., 44 (1972) 414-431.

[146] K.L. Chen, S.E. Mylon, M. Elimelech, Aggregation kinetics of alginate-coated hematite nanoparticles in monovalent and divalent electrolytes, Environ. Sci. Technol., 40 (2006) 1516-1523.

[147] S. Lee, J. Cho, M. Elimelech, Combined influence of natural organic matter (NOM) and colloidal particles on nanofiltration membrane fouling, J. Membr. Sci., 262 (2005) 27-41.

[148] A.M.T.R. Committee, Committee Report: Recent advances and research needs in membrane fouling, J. Am. Water Works Ass., 97 (2005) 79-89.

[149] H.-C. Kim, B.A. Dempsey, Membrane fouling due to alginate, SMP, EfOM, humic acid, and NOM, J. Membr. Sci., 428 (2013) 190-197.

[150] A.J.M. Segeren, J.V. Boskamp, M. van den Tempel, Rheological and swelling properties of alginate gels, Faraday Discussions of the Chemical Society, 57 (1974) 255-262.

[151] M.A. LeRoux, F. Guilak, L.A. Setton, Compressive and shear properties of alginate gel: effects of sodium ions and alginate concentration, J. Biomed. Mater. Res., 47 (1999) 46-53.

[152] R.I. Sedlak, Phosphorus and nitrogen removal from municipal wastewater: principles and practice, Lewis Publishers, (1991).

[153] P. Xu, F. Guo, J. Huang, S. Zhou, D. Wang, J. Yu, J. Chen, Alginate-based ferrofluid and magnetic microsphere thereof, International Journal of Biological Macromolecules, 47 (2010) 654-660.

[154] I. Machida-Sano, Y. Matsuda, H. Namiki, In vitro adhesion of human dermal fibroblasts on iron cross-linked alginate films, Biomed. Mater., 4 (2009) 025008.

[155] I. Machida-Sano, Y. Matsuda, H. Namiki, A novel harvesting method for cultured cells using iron-cross-linked alginate films as culture substrates, Biotechnol. App. Biochem., 55 (2009) 1-8.

[156] X.-W. Shi, Y.-M. Du, L.-P. Sun, J.-H. Yang, X.-H. Wang, X.-L. Su, Ionically crosslinked alginate/carboxymethyl chitin beads for oral delivery of protein drugs, Macromolecular Bioscience, 5 (2005) 881-889.

[157] P. Degen, S. Leick, H. Rehage, Mechanical stability of ionotropic alginate beads, Z. Phys. Chemie-Int. J. Res. Phys. Chem. Chem. Phys., 223 (2009) 1079-1090.

[158] R. Hernandez, J. Sacristan, C. Mijangos, Sol/Gel transition of aqueous alginate solutions induced by Fe^{2+} cations, Macromol. Chem. Phys., 211 (2010) 1254-1260.

[159] Y. Xin, M.W. Bligh, A.S. Kinsela, Y. Wang, T.D. Waite, Calcium-mediated polysaccharide gel formation and breakage: Impact on membrane foulant hydraulic properties, J. Membr. Sci., 475 (2015) 395-405.

[160] A.L. Rose, T.D. Waite, Kinetics of iron complexation by dissolved natural organic matter in coastal waters, Mar. Chem., 84 (2003) 85-103.

[161] A.N. Pham, A.L. Rose, A.J. Feitz, T.D. Waite, Kinetics of Fe(III) precipitation in aqueous solutions at pH 6.0–9.5 and 25°C, Geochim. Cosmochim. Acta, 70 (2006) 640-650.

[162] M.W. Bligh, T.D. Waite, Role of heterogeneous precipitation in determining the nature of products formed on oxidation of Fe(II) in seawater containing natural organic matter, Environ. Sci. Technol., 44 (2010) 6667-6673.

[163] M.W. Bligh, T.D. Waite, Formation, aggregation and reactivity of amorphous ferric oxyhydroxides on dissociation of Fe(III)-organic complexes in dilute aqueous suspensions, Geochim. Cosmochim. Acta, 74 (2010) 5746-5762.

[164] P.l. Sipos, O. Berkesi, E. TombÃ¡cz, T.G. St. Pierre, J. Webb, Formation of spherical iron(III) oxyhydroxide nanoparticles sterically stabilized by chitosan in aqueous solutions, J. Inorg. Biochem., 95 (2003) 55-63.

[165] E. Chiessi, G. Paradossi, M. Venanzi, B. Pispisa, Copper complexes immobilized to chitosan, J. Inorg. Biochem., 46 (1992) 109-118.

[166] J.M. Nieto, C. Peniche-Covas, J. Del Bosque, Preparation and characterization of a chitosan-Fe(III) complex, Carbohydr. Polym., 18 (1992) 221-224.

[167] S.C. Bhatia, N. Ravi, A magnetic study of an Fe−chitosan complex and its relevance to other biomolecules, Biomacromolecules, 1 (2000) 413-417.

[168] F. Jones, H. Cölfen, M. Antonietti, Interaction of κ-carrageenan with nickel, cobalt, and iron hydroxides, Biomacromolecules, 1 (2000) 556-563.

[169] F. Jones, H. Cölfen, M. Antonietti, Iron oxyhydroxide colloids stabilized with polysaccharides, Colloid Polym. Sci. , 278 (2000) 491-501.

[170] E.M. Coe, L.H. Bowen, J.A. Speer, Z. Wang, D.E. Sayers, R.D. Bereman, The recharacterization of a polysaccharide iron complex (Niferex), J. Inorg. Biochem., 58 (1995) 269-278.

[171] E.M. Coe, R.D. Bereman, W.T. Monte, An investigation into the size of an iron dextran complex, J. Inorg. Biochem., 60 (1995) 149-153.

[172] J.G. Hering, F.M.M. Morel, Slow coordination reactions in seawater, Geochim. Cosmochim. Acta, 53 (1989) 611-618.

[173] R.J.M. Hudson, D.T. Covault, F.M.M. Morel, Investigations of iron coordination and redox reactions in seawater using 59Fe radiometry and ion-pair solvent extraction of amphiphilic iron complexes, Mar. Chem., 38 (1992) 209-235.

[174] K.J. Sreeram, H.Y. Shrivastava, B.U. Nair, Studies on the nature of interaction of iron(III) with alginates, Biochim. Biophys. Acta-Gen. Subj., 1670 (2004) 121-125.

[175] I. Machida-Sano, S. Ogawa, H. Ueda, Y. Kimura, N. Satoh, H. Namiki, Effects of composition of iron-cross-linked alginate hydrogels for cultivation of human dermal fibroblasts, Int. J. Biomater., 2012 (2012) 820513.

[176] S. Judd, The MBR book: principles and applications of membrane bioreactors for water and wastewater treatment, Elsevier Science, 2011.

[177] S. Rosenberger, C. Laabs, B. Lesjean, R. Gnirss, G. Amy, M. Jekel, J.C. Schrotter, Impact of colloidal and soluble organic material on membrane performance in membrane bioreactors for municipal wastewater treatment, Water Res., 40 (2006) 710-720.

[178] Y. Xin, M.W. Bligh, T. Liu, T.D. Waite, Effect of iron on membrane fouling by alginate and the influence of presenting calcium, J. Membr. Sci., submitted (2014).

[179] A.D. Eaton, M.A.H. Franson, A.P.H. Association, A.W.W. Association, W.E. Federation, Standard methods for the examination of water & wastewater, American Public Health Association, 2005.

[180] O. Lowry, N. Rosebrough, A. Farr, R. Randall, Protein measurement with the folin phenol reagent., J. Biolog. Chem, 193 (1951) 265-275.

[181] M. DuBois, K.A. Gilles, J.K. Hamilton, P.A. Rebers, F. Smith, Colorimetric method for determination of sugars and related substances, Analytical Chemistry, 28 (1956) 350-356.

[182] P.B. Sorensen, J.R. Christensen, J.H. Bruus, Effect of small scale solids migration in filter cakes during filtration of wastewater solids suspensions, Water Environ. Res., 67 (1995) 25-32.

[183] F. Meng, H. Zhang, F. Yang, L. Liu, Characterization of cake layer in submerged membrane bioreactor, Environ. Sci. Technol., 41 (2007) 4065-4070.

[184] P. Bacchin, D. Si-Hassen, V. Starov, M.J. Clifton, P. Aimar, A unifying model for concentration polarization, gel-layer formation and particle deposition in cross-flow membrane filtration of colloidal suspensions, Chemical Engineering Science, 57 (2002) 77-91.

[185] M. Kumar, S.S. Adham, W.R. Pearce, Investigation of seawater reverse osmosis fouling and its relationship to pretreatment type, Environ. Sci. Technol., 40 (2006) 2037-2044.

[186] T. Maruyama, S. Katoh, M. Nakajima, H. Nabetani, T.P. Abbott, A. Shono, K. Satoh, FT-IR analysis of BSA fouled on ultrafiltration and microfiltration membranes, J. Membr. Sci., 192 (2001) 201-207.

[187] A. Leenheer Jerry, J.-P. Croué, M. Benjamin, V. Korshin Gregory, J. Hwang Cordelia, A. Bruchet, R. Aiken George, Comprehensive isolation of natural organic matter from water for spectral characterizations and reactivity testing, in: Natural Organic Matter and Disinfection By-Products, American Chemical Society, 2000, pp. 68-83.

[188] A.R. Badireddy, S. Chellam, P.L. Gassman, M.H. Engelhard, A.S. Lea, K.M. Rosso, Role of extracellular polymeric substances in bioflocculation of activated sludge microorganisms under glucose-controlled conditions, Water Res., 44 (2010) 4505-4516.

[189] A.N. Pham, Kinetics and mechanism of various iron transformations in natural waters at circumneutral pH, The University of New South Wales, PhD Thesis, (2007).

Appendix to Chapter 2

	C_1	C_2	C_3	C_4
1 mM Ca	23.72%	4.26%	2.37%	11.76%
6 mM Ca	15.86%	3.04%	4.68%	3.18%
7 mM Ca	4.71%	1.90%	9.27%	15.45%
9 mM Ca	8.28%	0.83%	12.20%	13.04%
10 mM Ca	6.41%	0.69%	6.31%	9.63%
12 mM Ca	7.14%	0.52%	10.19%	9.17%

Tabel A1. Average absolute deviations for fitting parameters C_1 to C_4 in Equations (2-12) and (2-13).

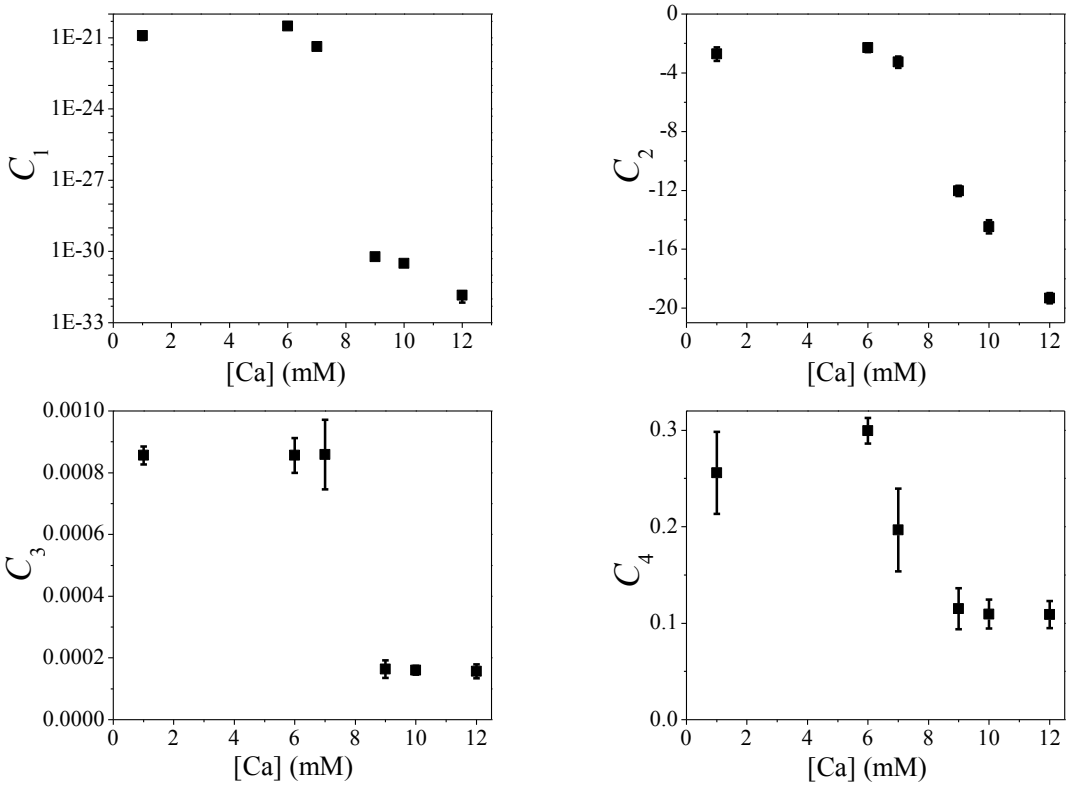

Figure A1. Variation with calcium concentration of model parameters C_1 - C_4 used in Equations (2-12) and (2-13) resulting from the modelling procedure.

Appendix to Chapter 5

Calculation of reaction rate using competitive ligand method and comparison with the rate of iron oxyhydroxide precipitation

Complexation of Fe(III) by organic ligands often occurs so rapidly that it is not easy to measure the rate of reaction directly. However, it is possible to measure the relative rate of reaction of iron with two ligands by determining the relative amounts of two products formed competitively. If one of the rate constants is known then it is easy to determine the other. The validity of this method relies on two following assumptions: a) the kinetics of dissociation of two complex of Fe-ligand is slow, and b) no intermediate complex would present at significant concentration. Precipitation of ferric ion is assumed to be negligible at low iron dosage and high concentrations of two ligands.

In this study, sulfosalicylic (SSA), with known rate constant of k_{SSA} =3.5×10^4 M^{-1}S^{-1} for formation of a ferric complex [160], was chosen as a competitive ligand. When ferric ion (hereafter abbreviated as Fe') is added to a solution containing both alginate (presented as L) and sulfosalicylic (SSA), I hypothesize the occurrence of two simultaneous competing irreversible reactions with formation rate constants k_{Alg} and k_{SSA} respectively, and they could be related by [189]

$$\frac{[\mathrm{Fe'}]_T}{[\mathrm{FeSSA}]_{eq}} = \frac{k_L}{k_{SSA}} \times \frac{[L]_T}{[\mathrm{SSA}]_T} + 1 \qquad \text{(A1)}$$

Where,

$[Fe]_T$: total amount of Fe(III) added (1.5 uM)

$[FeSSA]_{eq}$: concentration of FeSSA complex at equilibrium (and determined by UV-spectrum)

$[L]_T$: total alginate concentration used during the measurement (from 0.2 to 2 g/L)

$[SSA]_T$: total SSA concentration in solution (2 mM)

By plotting Eq (A1) in Figure A2 could get the value of $\frac{k_L}{k_{SSA}}$ from the slope, and obtain the k_L= 17.22 $(g/L)^{-1}S^{-1}$ based on known $k_{SSA.}$

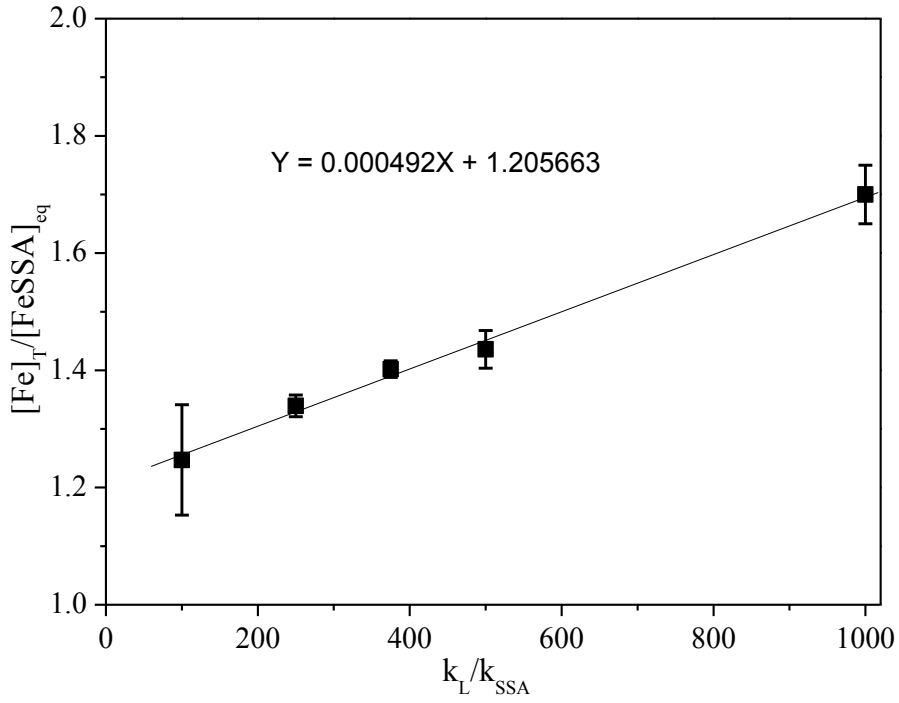

Figure A2. Linearised data for calculation of k_L

In Fe-alginate solution, reaction rate of forming Fe-alginate complex is

$$R_C = k_L[\mathrm{Fe'}][\mathrm{L}] \tag{A2}$$

while the rate of iron precipitation is [161]:

$$R_P = k_f[\mathrm{Fe'}][\mathrm{Fe_I}] \tag{A3}$$

where k_f is the ratio of the precipitation rate constant, Fe' is the concentration of the sum of dissolved inorganic Fe species, and Fe_I is the sum of all dissolved and precipitated species (total inorganic Fe(III)).

The molecular weight of alginate used ranges between 12,000 and 19,000 $g.mol^{-1}$, which is about 2.1~3.3 uM at 0.4 $g.L^{-1}$ alginate. Considering that the minimum applied iron concentration in this study is 0.05 mM (50 uM) and one iron could provide multiple sites for alginate binding, it is reasonable to conclude that $[Fe_I]=[Fe]_T - [FeL] \approx [Fe]_T$.

Given $k_f = 5\times10^6$ $M^{-1}S^{-1}$ at pH 7.5 [161], in the case of [L]= 0.4 $g.L^{-1}$ and $[Fe]_T$= 0.05 mM, the ratio of

$$\frac{R_p}{R_c} = \frac{k_f[\mathrm{Fe'}][\mathrm{Fe_I}]}{k_L[\mathrm{Fe'}][\mathrm{L}]} = \frac{k_f[\mathrm{Fe_I}]}{k_L[\mathrm{L}]} = \frac{5\times10^6\times0.00005}{17.22\times0.4} = 36.29 \tag{A4}$$

Values of R_p/R_c over a range of Fe concentrations and for two alginate concentrations are shown in Table A2.

[Fe] (mM)	0.05	0.1	0.2	0.3	0.4	0.5	0.6	0.7	0.8	0.9	1.0
0.1 g.L^{-1} Alg	145.2	290.4	580.7	871.1	1161	1453	1742	2032	2323	2613	2903
0.4 g.L^{-1} Alg	36.29	72.59	145.2	217.8	290.4	362.9	435.5	508.1	580.7	653.3	725.9

Tabel A2. R_p/R_c ratios at different alginate and Fe concentration.

Scanning electron microscopy (SEM): Cake surface morphology

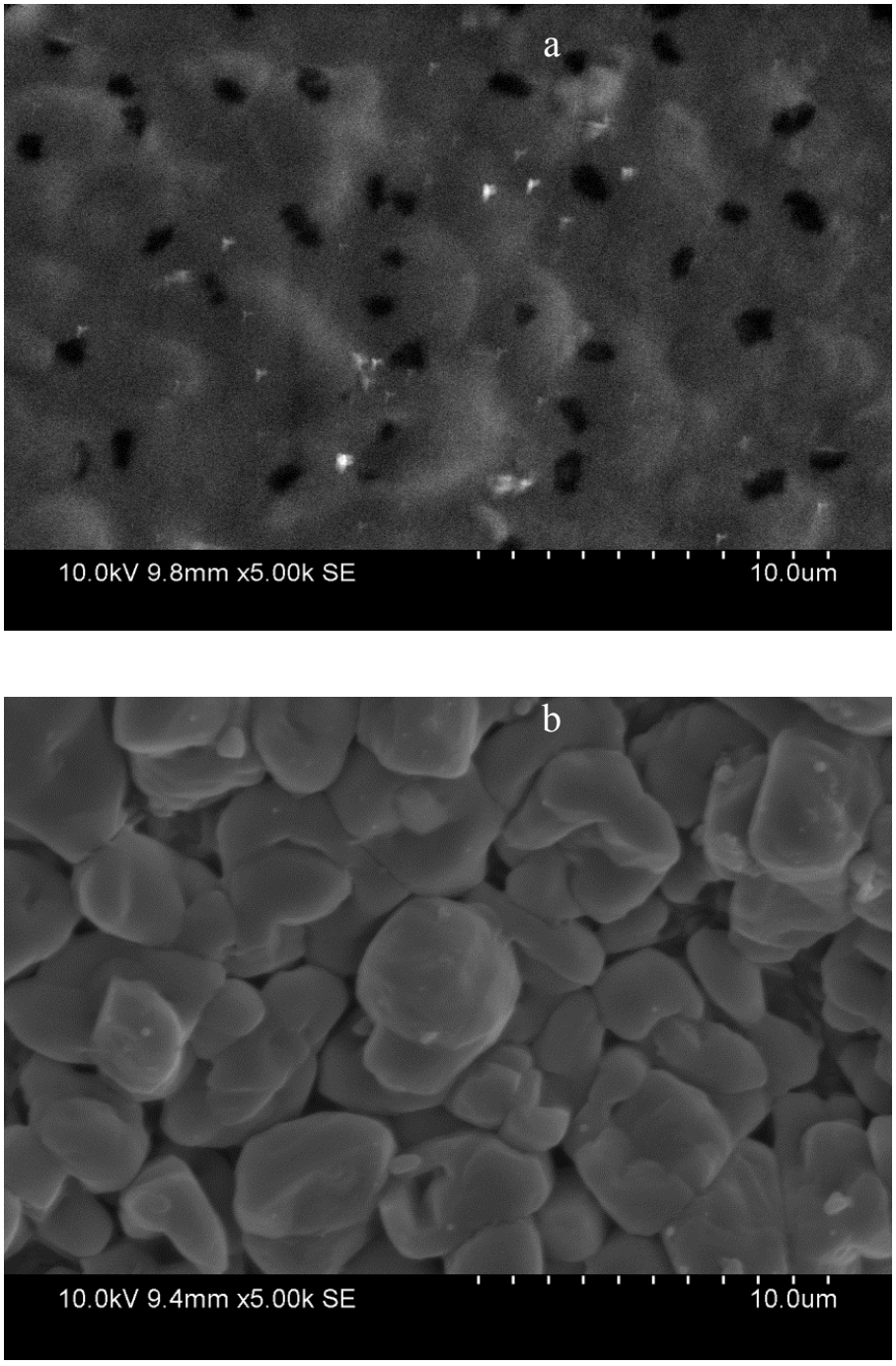

Figure A3. Scanning electron microscopy (SEM) image of gel formed under constant pressure dead-end filtration in 0.1 $g.L^{-1}$ alginate solution with 0.4 mM Fe (a) Fe-alginate (b) Fe-Ca-alginate (with 5 mM calcium). Samples were placed in a drying cupboard (set to ~35 °C) to dry and outgas prior to imaging.

Free calcium concentration measurement

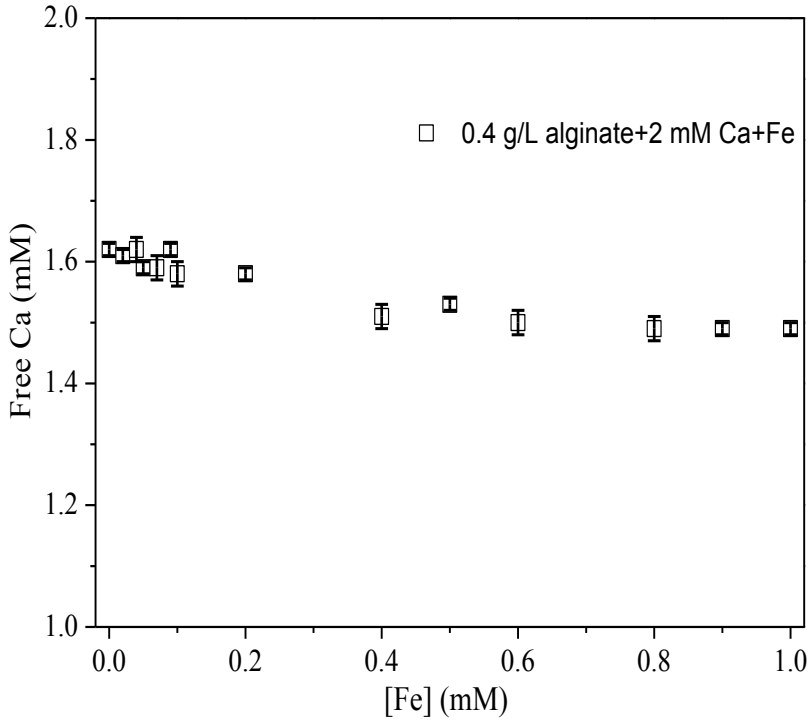

Figure A4. Free calcium concentrations as increasing iron concentration in 0.4 $g.L^{-1}$ alginate solution. Standard errors bars are from duplicates.

Optical Microscopy

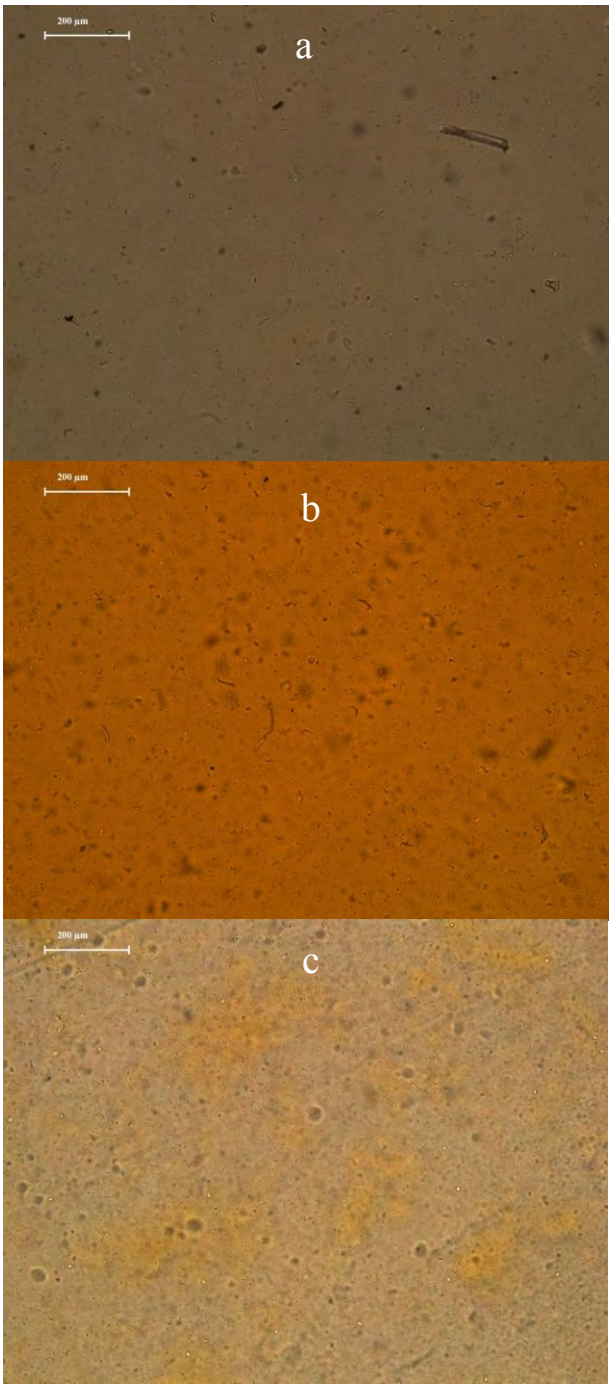

Figure A5. Optical microscopy images of gel formed under constant pressure dead-end filtration in 0.1 $g.L^{-1}$ alginate solution under 22.5 kPa at (a) 0.1 mM iron, (b) 0.5 mM iron, and (c) 5 mM calcium + 0.2 mM iron. (Scale bar = 200 µm). Note: large specs and lines are imperfections on the glass slides and not part of the alginate assemblages.